AD-A148 057 AN OPTICALLY COUPLED SAMPLING SYSTEM WITH 4 GHZ BANDWIDTH(U) MISSISSIPPI UNIV UNIVERSITY DEPT OF ELECTRICAL ENGINEERING S B SAMAAN ET AL. 30 OCT 84 1/2

UNCLASSIFIED N00014-81-K-0256 F/G 20/6 NL

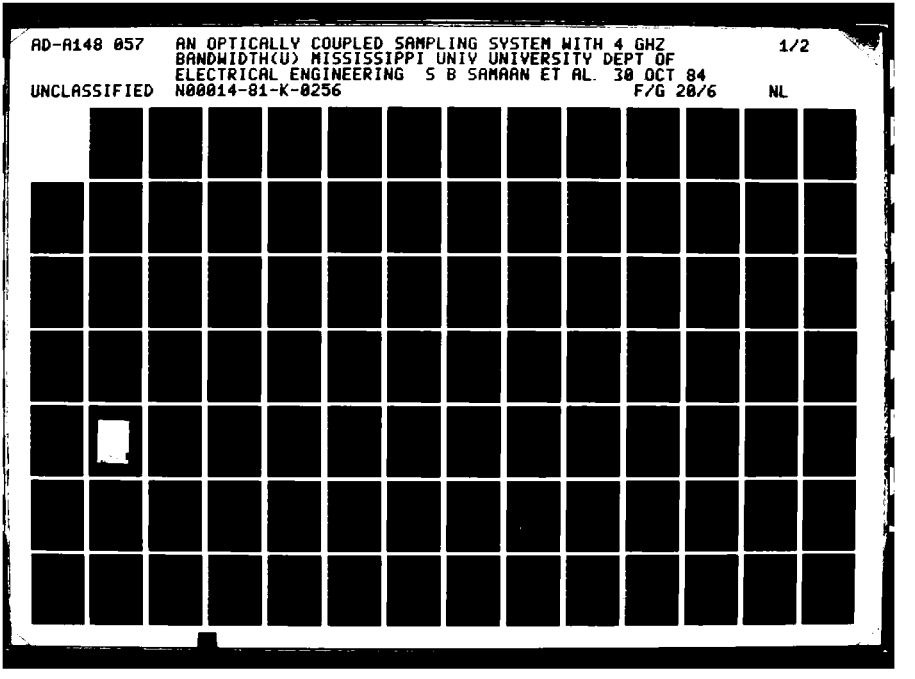

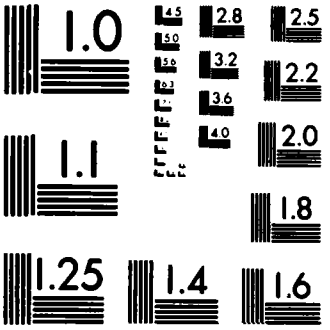

AD-A148 057

DTIC FILE COPY

REPORT DOCUMENTATION PAGE

READ INSTRUCTIONS BEFORE COMPLETING FORM

1. REPORT NUMBER	2. GOVT ACCESSION NO.
3. RECIPIENT'S CATALOG NUMBER	
4. TITLE (and Subtitle)	5. TYPE OF REPORT & PERIOD COVERED
AN OPTICALLY COUPLED SAMPLING SYSTEM WITH 4 GHz BANDWIDTH	1/1/81-9/30/84
	6. PERFORMING ORG. REPORT NUMBER
7. AUTHOR(s)	8. CONTRACT OR GRANT NUMBER(s)
S.B. Samaan L. Wilson Pearson Charles E. Smith	N00014-81-K-0256
9. PERFORMING ORGANIZATION NAME AND ADDRESS	10. PROGRAM ELEMENT, PROJECT, TASK AREA & WORK UNIT NUMBERS
Department of Electrical Engineering University of Mississippi University, MS 38677	
11. CONTROLLING OFFICE NAME AND ADDRESS	12. REPORT DATE
Office of Naval Research Attn: Richard G. Brandt 800 North Quincy Street; Arlington, VA 22217	October 30, 1984
	13. NUMBER OF PAGES 159
14. MONITORING AGENCY NAME & ADDRESS(if different from Controlling Office)	15. SECURITY CLASS. (of this report)
Contract Administrator ONR Resident Representative GA Institute of Technology 206 O'Keefe Bldg.; Atlanta, GA 30332	Unclassified
	15a. DECLASSIFICATION/DOWNGRADING SCHEDULE

16. DISTRIBUTION STATEMENT (of this Report)

Approved for public release; distribution unlimited

17. DISTRIBUTION STATEMENT (of the abstract entered in Block 20, if different from Report)

18. SUPPLEMENTARY NOTES

19. KEY WORDS (Continue on reverse side if necessary and identify by block number)

Optically Coupled Sampling Head
Sampling Oscilloscope Systems (High Frequency)
Optically Transmitted Sampling Oscilloscope Signals
Sampling Strobe Jitter
Optically Triggered Avalanche Transistors
Time Domain Scattering Measurements

20. ABSTRACT (Continue on reverse side if necessary and identify by block number)

A new approach to the design of an optically coupled multi-gigahertz sampling system with improved bandwidth is reported. The system utilizes the Tektronix S-6 sampling head, the Tektronix 7S12 TDR/Sampler plug-in unit, and a Tektronix 7000 series oscilloscope mainframe. Three fiber optic links replace existing hardwired conductors which convey the vertical error and feedback signals and the horizontal sampling command signal between the sampling head and the oscilloscope sampling plug-in.

DD FORM 1 JAN 73 1473 EDITION OF 1 NOV 65 IS OBSOLETE
S/N 0102-014-6601 |

SECURITY CLASSIFICATION OF THIS PAGE (When Data Entered)

20. Abstract cont'd.

The remote sampling head and its associated fiber optic interfacing circuits are powered using a rechargeable battery pack. The dielectric fiber pigtails allow placing the sampling head in an electromagnetic test environment without the distortion of the electromagnetic fields usually caused by metallic connecting conductors. Replacing the metallic conductors by the fiber pigtails also eliminates electromagnetic interference (EMI) with the sampling system operation.

Two commercial fiber optic links are used in the analog mode to convey the error and feedback signals. The sampling command signal issued by the 7S12 sampler is used to trigger a pulsed laser diode driver circuit. The laser diode produces a fast-rise infrared laser pulse of several hundred milliwatts. This laser pulse is used to trigger the avalanche transistor in the sampling head strobe generator circuit by coupling the optical energy directly to the reverse biased collector-base junction of the transistor.

Qualitative and quantitative tests were carried out to evaluate the optically coupled system performance. The test results show that the error and feedback links cause only a small distortion of acquired waveforms. The noise introduced by these links is significant only for small sampled signals on the order of 10 millivolts. The sampling command link is shown to cause the strobe jitter to have a standard deviation of only 28 ps. The overall system bandwidth is shown to be 4 GHz. Improvements in the noise and bandwidth performance of the system are possible, and recommendations are made to this effect for implementation in a future version of the system.

ACKNOWLEDGEMENT

The authors wish to acknowledge the University of Mississippi for partially supporting this work.

TABLE OF CONTENTS

LIST OF TABLES

LIST OF FIGURES

Figure Page

Figure Page

Figure | Page

CHAPTER 1

INTRODUCTION

1.1. The Optically Coupled Sampling System, Motivation, and Previous Work

In some high frequency sampling measurements, the presence of the sampling head, which is used to acquire the high frequency signal and the cables which connect the sampling head to a mainframe oscilloscope, causes a modification in the parameters of the test environment. The high frequency electromagnetic fields associated with the test set-up may, also, cause an interference with the internal functioning of the sampling system due to unwanted voltages induced in the cables interconnecting the sampling head to the mainframe oscilloscope.

An example of such a situation is one where the induced current on the surface of a scatterer is being probed using a loop probe and a sampling head. The sampling head and its associated cable connections cause a distortion in the incident field. On the other hand, the high frequency electromagnetic fields may induce noise voltages in the sampling head extender cable which connects it to the sampling oscilloscope, thus rendering the measurement results useless.

In order to eliminate the problems mentioned above. Holbrook [1] constructed a sampling system in which the sampling head is coupled to the mainframe sampling unit via fiber optic links. By replacing the

metallic cables with the very thin dielectric fiber pigtails (Fig. 1.1), the problem of incident field distortion and electromagnetic interference could be essentially eliminated.

Before reviewing the work in [1], the reader is referred to Appendix B for a review of the operation of high frequency sampling oscilloscopes specialized to the Tektronix (7S12)-(S-6) system used both in the system of reference [1] and the present work.

The system constructed by Holbrook employed two analog fiber optic links (built using discrete components) in order to deliver the error and feedback signals between the remote sampling head and the mainframe oscilloscope. The bandwidth of these links was limited to about one-tenth of the original (7S12)-(S-6) design. This bandwidth-limiting was imposed in order to combat the noise introduced to the system as a result of using the fiber optic links. The sampling command signal in Holbrook's system was delivered from the mainframe sampling unit via a laser pulse generated by a low power CW laser diode and was detected at the sampling head with an avalanche photodiode. The output of the photodiode was used to drive an avalanche buffer stage, that in turn triggered the avalanche transistor (Q70, Figure B.2) in the S-6 strobe generator circuit. This arrangement required that the strobe generator board of the S-6 be rebuilt to accomodate the avalanche photodetector and the buffer stage. For this reason, the sampling head had to be removed from the manufacturers casing and placed in a metallic shielding cylinder.

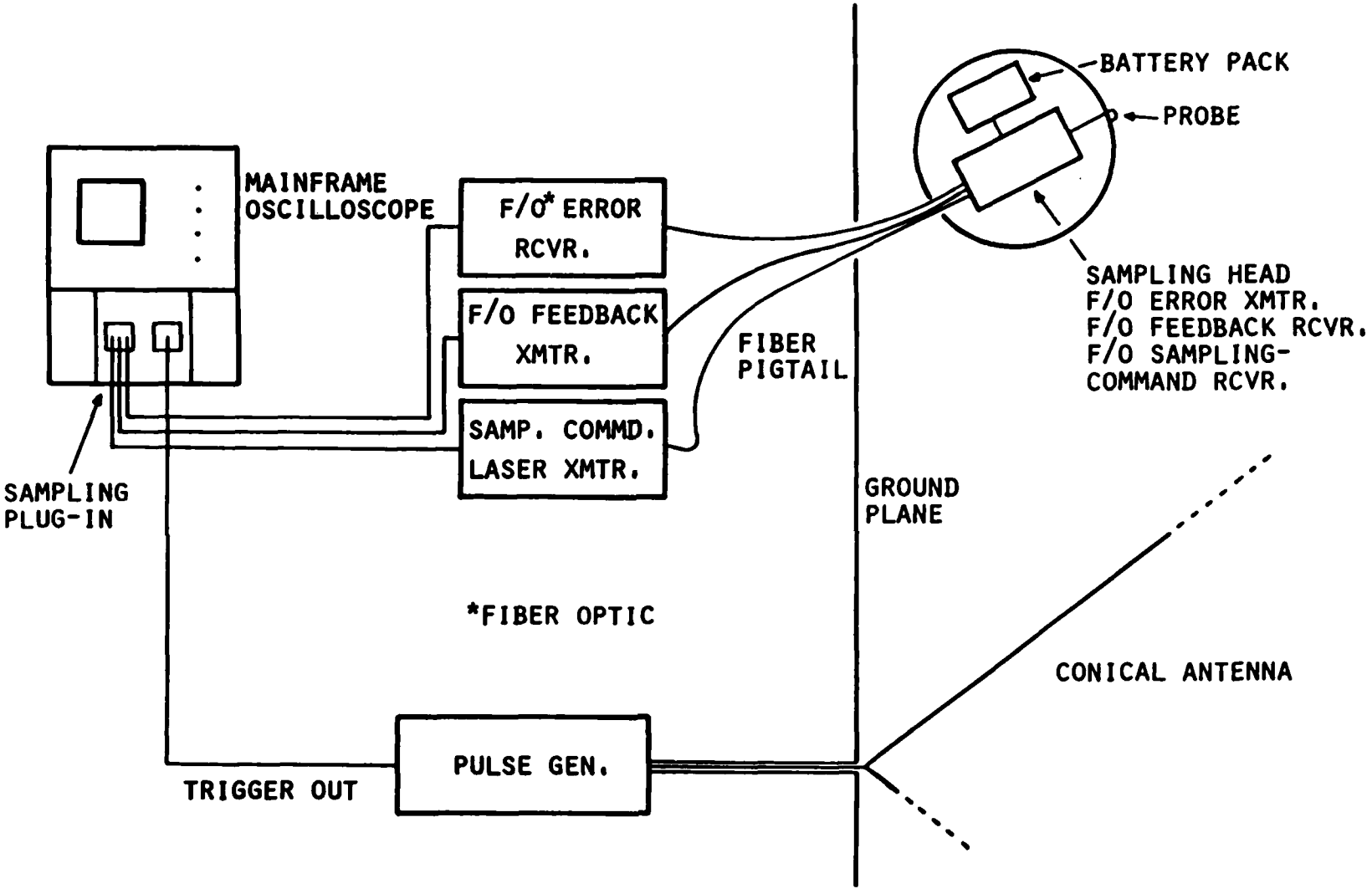

Figure 1.1 The Optically Coupled Sampling System. An application to probe the surface current induced on a metallic scatterer.

The system of [1] suffered from distortion of the acquired waveforms and manifested a bandwidth of only 1 GHz. The bandwidth was limited mainly by the relatively large time jitter present in the sampling command signal. It is believed that this jitter resulted from the noise introduced by the avalanche photodetector and the scintillation of the optical intensity of the laser pulses produced by the semiconductor laser diode. The distortion in the acquired waveforms was caused by both the sampling command jitter and the limited bandwidth of the error and feedback links, as well as through self-induced electromagnetic interference.

Before reviewing the present work, it is worthwhile mentioning that Lawton and Andrews [2], [3], [4] have patented a dual mode sampling system for sampling fast electrical or optical signals. In this system, the sampling gate which is built around two GaAs photoconductors is strobed with narrow optical pulses to acquire an electrical waveform. To acquire optical waveforms, the optical signal is focused on one photoconductor and the gate is strobed with electrical pulses. This system was implemented in order to eliminate the problems of strobe kick-out[1], waveform distortion, and limited dynamic range associated with conventional electrically strobed diode-gate sampling systems. In the Lawton-Andrews system, the error and feedback signals are conveyed between the sampling head and the mainframe sampling oscilloscope using

---

[1] "Kick-out" pertains to the leakage of some strobe signal energy through the signal input connector to the outside probed signal source.

hardwired links. However, if those signals along with the optical strobes are coupled using fiber optic pigtails, a system which performs the function of the Holbrook [1] system could perhaps be realized.

1.2. Optically Coupled Sampling System, Present Work

The present work adopts the Holbrook configuration to obtain an improved performance. This configuration was chosen in order to avoid having to build a specialized GaAs sampling head as is the case with the Lawton-Andrews system, and, also, due to the availability of the Tektronix (7S12)-(S-6) sampling system to the author. In this approach, the error and feedback links are designed around a pair of commercially available modular fiber optic transmitter/receiver sets. The bandwidth of the feedback link is set to a value higher than the minimum required by the 7S12 in order to ensure unhampered operation of the link. The bandwidth of the error link is set to the maximum allowed by the fiber optic receiver used, which is about one-half the bandwidth required by the 7S12 sampler. The increased bandwidth of the error and feedback links over the values reported in [1] permits the acquisition of waveforms with reduced distortion.

The sampling command signal is delivered from the sampling unit to the sampling head via a fast-rise laser pulse. The laser pulse is generated by a high power pulsed GaAs laser diode and launched into a high quality glass fiber pigtail. At the S-6 the laser pulse is detected by the avalanche transistor (Q70, Figure B.2) in the strobe

generator circuit. With this scheme, the intervening avalanche photodetector and buffer stage reported in [1] are eliminated, thus reducing the noise and consequently the time jitter in the strobe pulses which open the sampling gate. The high power of the laser used (about 700 mW) compared to that of [1] (about 1 mW) improves the signal to noise ratio and reduces the strobe jitter introduced by the scintillation of the optical laser pulse. The reduction of strobe jitter achieved with this scheme was necessary for achieving a higher bandwidth for the optically coupled sampling system.

1.3. Survey of Present Work

Chapter two, after this introduction, is concerned with the design details of the error, feedback, and sampling command links. The results of the performance tests on each separate link are also presented.

In Chapter three the results of the qualitative and quantitative tests which were performed on the optically coupled sampling system are reported. Also reported are the results of tests on the system when only certain links are optical while others are hardwired. From these results observations are made regarding the system's characteristics such as waveform distortion, noise level, and bandwidth.

In the last chapter, conclusions are drawn regarding the performance of the optically coupled sampling system and recommendations for future work are made.

Appendix A contains details of system construction, first-time operation, and calibration.

Appendix B presents the concepts of the operation of sampling oscilloscopes specialized to the case of the Tektronix (7S12)-(S-6) system.

Appendix C contains a note on some aspects of random errors in sampling measurements.

CHAPTER 2

DESIGN OF FIBER OPTIC LINKS

2.1. Introduction

In this chapter the details of the electronic design of the fiber optic links used in this investigation are presented. Three links were designed, namely, an error link, a feedback link, and a sampling command link.

2.2. Requirements of the Fiber Optic Links

The fiber optic links must satisfy certain requirements before they can optimally replace the coaxial cables used to transmit the error, feedback, and sampling command signals between the sampling unit and the sampling head. These requirements can be assessed from a knowledge of the principle of operation of sampling oscilloscopes and the inter-circuit parameters of the (7S12)-(S-6) system used. This knowledge is presented in Appendix B of this work, and in a more detailed form in [5] and [6].

2.2.1. Requirements of the Error Link

The input impedance of the fiber optic error trasmitter must be larger than a few kilohms in order to cause no voltage drop in the S-6

preamplifier output impedance which is on the order of 100 ohms. The output impedance of the fiber optic error receiver must approximate that of the S-6 preamplifier, which is the output impedance of an operational amplifier and a series capacitor.

The required bandwidth for the error link can be inferred from the time interval of approximately 0.4 μs for which the memory gate stays open. As a conservative estimate, this duration is assumed to be twice the link risetime. From this and using the approximate relation,

$$\text{rise time} \times \text{bandwidth} = 0.35 \qquad (2.1)$$

a bandwidth of 1.8 MHz is obtained for the error link.

2.2.2. Requirements of the Feedback Link

The input impedance of the feedback transmitter must be several tens of kilohms in order to avoid loading the 7S12 feedback attenuator whose output impedance is on the order of a few kilohms. The output impedance of the feedback receiver can have a maximum value of only a few kilohms.

The bandwidth that the feedback link must have can be computed from knowing that the 7S12 acquires a maximum of 60,000 samples per second. Hence, the minimum time per sample is 16.7 μs. Subtracting from this the time that it takes the sample signal to propagate from the sampling head to the memory output, namely, 0.4 μs, leaves 16.3 μs as the time allowed for the feedback link to deliver the signal to the S-6. If this duration is assumed to be twice the link risetime and equation 2.1 is used, one obtains a bandwidth of 43 KHz for the feedback link.

In addition to the above, the feedback link must be a DC coupled link with a dynamic range of ±1 volt in order to facilitate transmitting the DC offest voltage.

2.2.3. Requirements of the Sampling Command Link

The sampling command link should be able to deliver the information corresponding to the instant of occurance of the falling edge of the negative going sampling command pulse, to transistor Q70 in the S-6 sampling head (see Figure B.2), and to cause it to avalanche. This must be accomplished with minimal introduction of time jitter.

2.3. Choice of Analog Fiber Optic Transmitter and Receiver

Two sets of commercially available analog/digital fiber optic transmitter-receiver pairs were selected for use in the error and feedback links. The choice was a compromise between electrical characteristics, physical size, and cost. Both transmitter and receiver are hybrid units placed in a small package which is mountable on a printed circuit board.

The relevant specifications of the transmitter and the receiver in the analog mode of operation are listed in Table 2.1 along with the specifications of the fiber pigtail used. These specifications will be referred to when presenting link designs. For more detailed specifications, the reader is referred to [7].

A rough estimate of the voltage gain between the receiver output and the transmitter input can be computed from the manufacturer's data [7].

Table 2.1. Electrical Specifications of the Fiber Optic Transmitter and Receiver Used for the Error and Feedback Links

Fiber Optic Transmitter	
Make and Model	Burr-Brown, FOT110KG
Modes of Operation	Digital/Analog
Input Impedance	100 ohms (analog input)
Linear Range of Operation*	1.8-3.2 volts at analog input
AM Bandwidth (3 dB)	2.5 MHz (typ.)
Total Harmonic Distortion	<2%(inferred from manufacturer's specifications)
Propagation Delay (100 KHz, Square Wave at 50% points)	120 ns (typ.)
Output Optical Power Launched into Fiber of Diam.=200μm, N.A.=0.48, with Digital NRZ input.	10 μw (nominal) (adjustable with external resistor)

*This value was measured for the particular device used.

Table 2.1 (cont'd.)

Fiber Optic Receiver

Make and Model	Burr-Brown
Responsivity, (Light Received from Fiber with Diam.=200μm, N.A. < 0.5)	1 V/μW (typ.)
Bandwidth	1 MHz (typ.)
Output Noise (with 47 pf cap. on Load, and BW = 10 Hz to 2 MHz)	0.8 mV, rms (typ.)
Propagation Delay, (50% points, in/out)	0.8 μs (typ.)

Fiber Pigtail Used

Make and Model	Math QSF-400
Length	10 m
Core Diam	0.4 mm
N.A.	0.22
Attenuation	10 dB/Km
Bandwidth	15 MHz-Km

However, for the sake of avoiding design errors, the gain was experimentally measured and found to be approximately 3.4 for a receiver load resistance of 47 kilohms. This gain was obtained after reducing the transmitter output power to 10% of its nominal value by an external power adjustment resistance (set to 47 ohms).

As can be seen from the specifications of the fiber optic transmitter and receiver, the direct use of these devices to deliver the error and feedback signals is not feasible. For this reason, interfacing circuits between the 7S12 and the S-6 modules and the fiber optic transmitters and receivers were designed.

2.4. Design of the Fiber Optic Error Transmitter

Figure 2.1 shows the complete circuit diagram of the error link that was designed around the fiber optic transmitter and receiver described in the previous section. On the transmitter side, R1 and R2 serve to elevate the quiescent DC voltage at the analog input of the transmitter from 1.89 volts to the middle of the linear range of operation, namely, 2.5 volts. C1 protects the input from the accidental creation of external DC loops which can permanently damage the transmitter.

R3 is the power adjustment resistor which determines the optical intensity level of the transmitter's LED. The value chosen for R3 reduces the optical power to 10% of its nominal value. This reduction was necessary in order to reduce the supply current furnished by the battery pack on the sampling head side of the system. R4 puts pins 3 and 28 at

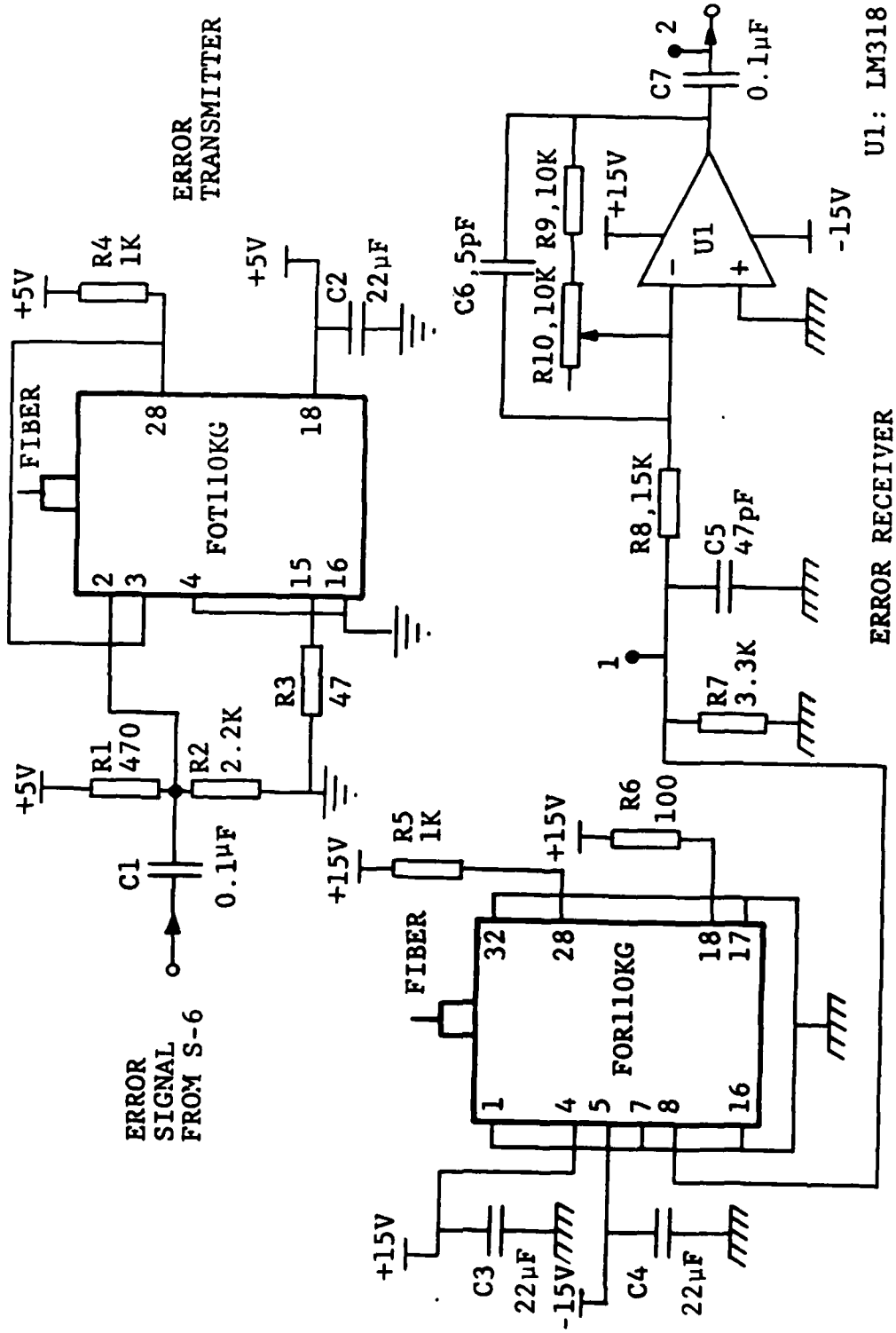

Figure 2.1. Circuit diagram of the fiber optic error transmitter and error receiver.

logic 1 in order to enable AM modulation of the LED. C2 is a power supply bypass capacitor.

2.5. Design of the Fiber Optic Error Receiver

Referring to Figure 2.1, R7 at the receiver output was chosen to be much smaller than the 47 kilohms for which the transmitter-receiver gain was found to be 3.4. This small value of R7 reduces the gain of the link to about 1.5 and, thus, enhances its bandwidth, consequently lowering its overall delay time to about 0.35 μs. Reducing the delay is necessary in order to deliver the error signal to the memory circuit in the mininmum time possible. C5 prevents high frequency oscillations at the output of the receiver.

Because the fiber optic receiver inverts the output electrical signal with respect to the input optical signal, an inverting amplifier was incorporated. The gain of the inverting amplifier is adjustable by varying R10. The approximate gain of this stage can be computed from the ratio (R9 + R10)/R8. The operational amplifier chosen for this stage has a unity gain bandwidth of 15 MHz. This high value of bandwidth was necessary in order to make the added signal delay as small as possible (less than 0.05 μs in the case of the LM318).

C6 prevents the inverting amplifier from oscillation at high frequencies, and C7 prevents DC coupling between the Op-Amp output and the 7S12 post amplifier input. R6 provides reverse bias for the receiver's PIN diode detector. R5 disables the squelch feature in the receiver [7]. C3 and C4 are power supply bypass capacitors.

2.6. Design of the Fiber Optic Feedback Transmitter

Figure 2.2 depicts the circuit diagram of the fiber optic feedback transmitter. The first stage of the feedback transmitter is a noninverting DC amplifier which utilizes a BiFET operational amplifier as the active element. The input impedance of this stage is solely determined by R1, which simulates the impedance seen by the feedback signal at the sampling head. The gain of this stage can be chosen by selecting one of the resistors R5, R2, or "open" in the negative feedback voltage divider. This allows the gain to be switchable between 5, 2, or 1, respectively. The values of R5 and R2 required to acheive the gains of 5 and 2 are determined from the following relationship:

$$\text{gain} = 1 + \frac{R3}{R}$$

where R can be either R5, R2, or infinity.

The reason behind providing selectable gain at the input of the feedback transmitter is to enable enhancing the signal to noise ratio of small and medium amplitude feedback signals. This is achieved by cancelling the gain of the transmitter with the proper attenuation at the receiver. This process brings the feedback signal down to its original amplitude while at the same time attenuating any noise introduced to it by the intervening fiber optic channel. The gain can be set to 5 only when the sampled signal amplitude is less than 100 mV, and can be set to 2 when the sampled signal is smaller than 250 mV. And

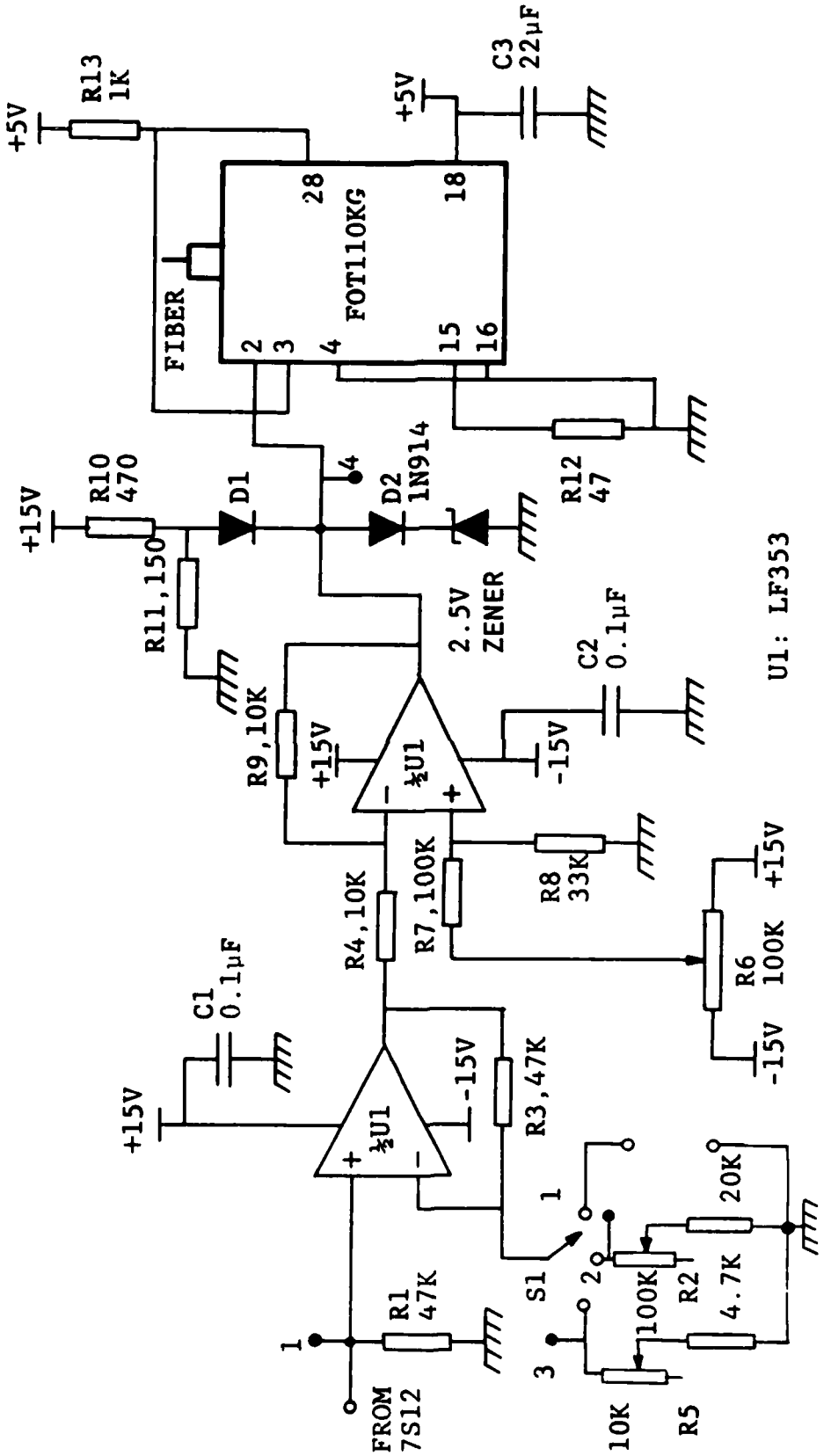

Figure 2.2. Circuit diagram of the fiber optic feedback transmitter.

finally, the gain must be set to 1 when signals whose amplitudes exceed 250 mV are sampled. These voltage limitations ensure that the fiber optic transmitter operates within its linear region.

The second stage is an inverting amplifier whose gain is set to unity by the ratio R9/R4. This stage is used to shift the DC level of the feedback signal by varying the voltage supplied by the potentiometer R6. This shift is necessary in order to compensate for any amplification of the DC offset voltage by the preceeding stage. R6 is set during system calibration in such a manner as to maintain the no-signal DC level at the input of the fiber optic transmitter at 2.5 volts, which is the center of its linear region of operation.

In order to avoid the accidental application of very large, or very small DC voltages to the input of the transmitter, when R6 is being adjusted, two voltage clipping circuits are provided. R10, R11, and D1 prevent the DC level at the input of the transmitter from falling below 0 volts, while D2 and D3 prevent it from exceeding 3.6 volts.

The optical power adjustment resistance, R12, was chosen to have the relatively high value of 47 Ohms which lowers the optical power output of the transmitter to 10% of its nominal value. Lowering the optical power was found necessary in order to combat a thermally introduced distortion effect on the falling edge of large and fast transmitted signals. This distortion is produced when the input signal to the link decreases suddenly causing a current surge in the LED. The optical power output follows the current rise, but starts to drop slightly after.

a very brief period of time. This drop is beleived to be due to the warm-up of the LED which follows the current rise. By choosing R12 to be relatively large, the current in the LED was kept at a relatively small value at all times. R13 sets pins 3 and 28 of the transmitter at logic 1 in order to permit modulation of the LED's optical power. C1, C2, and C3 are supply bypass capacitors.

2.7. Design of the Fiber Optic Feedback Receiver

Figure 2.3 depicts the complete circuit diagram of the fiber optic feedback receiver. The output of the fiber optic receiver is connected to the input of an inverting amplifier whose gain can be set to approximately: 1/5, 1/2, or 1, by respectively selecting one of the three feedback resistors R17, R18, or R19. The criterion for selecting any one of these three gains is to make its product with the gain of the first stage of the feedback transmitter equal to unity.

The 500 ohm potentiometer (R20) at the output of the first amplifier is used to deliver a fraction of its output voltage to the next stage. The attenuation introduced by this potentiometer compensates for the gain inherent in the fiber optic transmitter-receiver link which was measured to be approximately 3.4 (see Section 2.3). The final stage of the feedback receiver is a first order lowpass filter whose DC gain is unity and whose cutoff frequency f_c is determined by the following relationship:

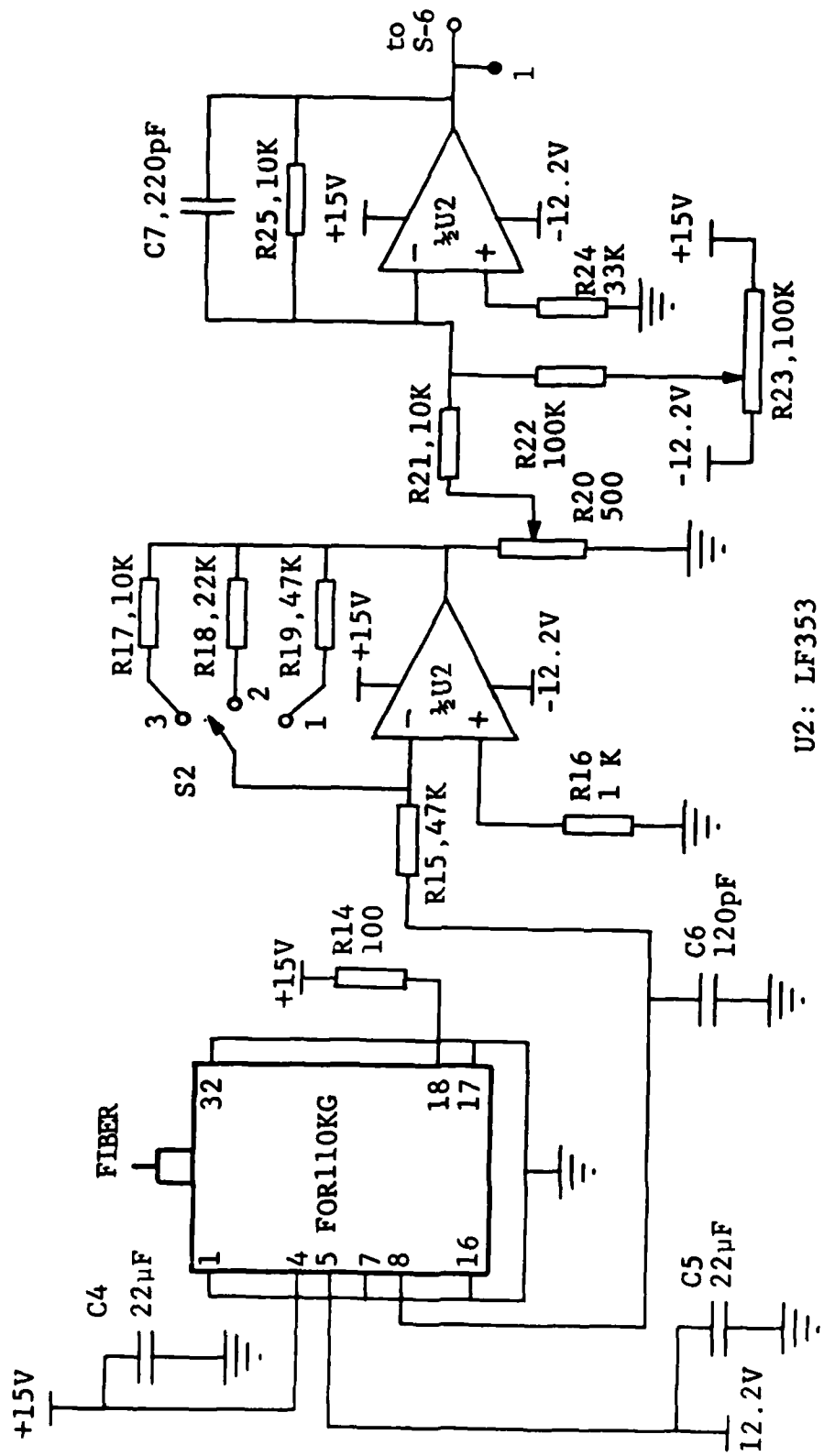

Figure 2.3. Circuit diagram of the fiber optic feedback receiver.

$$f_c = \frac{1}{2\pi(C7)(R25)}$$

Substituting the values of C7 and R25 into the above equation gives 72.3 KHz. This frequency is much smaller than the cutoff frequencies of all other parts of this link and, hence, it is the effective bandwidth for the feedback link.

Potentiometer R23 is used to adjust the DC level at the output stage. DC level adjustment is necessary in order to compensate for the DC shift introduced by the fiber optic receiver.

R14 provides the reverse bias required for the receiver's PIN diode detector. C6 prevents the output amplifier inside the fiber optic detector from oscillating at a very high frequency. C4 and C5 are supply bypass capacitors.

It should be noted that the total number of phase inverting stages in the feedback link (including the fiber optic receiver itself) is even. Hence, the output changes in the same direction as the input.

2.8. Design of the Sampling Command Link

Guided by the requirements that must be satisfied by the sampling command link as detailed in Subsection 2.2.3, and taking into account the previous experience in designing this link as reported in [1], the following objectives were set for the design of the sampling comand link in this work:

1. To keep the total number of stages in the link at a minimum. This minimizes the noise in the signal path, ensuring as small a time jitter as possible in the strobe pulse.

2. To make the circuits immune to external noise by maintaining very high signal levels throughout the link.

3. To facilitate the use of the S-6 sampling head without the need for major modifications or the rebuilding of any of its circuits.

In order to fulfill those design objectives, a high power, pulsed semiconductor laser is used to generate a fast-rise infrared laser pulse every time a sampling command is issued. This pulse is guided by a high quality fiber pigtail to the sampling head end of the system. At the sampling head, the laser is used to trigger the avalanche of transistor Q70 (see Figure B.2) by directly coupling the laser energy to its chip [8]. This technique is discussed further in a later section. In what follows, the laser source used and the circuit to drive it are presented.

2.8.1. The Pulsed Laser Diode

The source of laser energy used to deliver the sampling command signal is a commercially obtainable gallium arsenide injection laser diode designed for pulsed operation. This laser source has a hetro-junction structure consisting of three semiconductor layers: N-type GaAs, P-type GaAs, and P-type GaAlAs. Recombination of the charge carriers occurs in the vicinity of the P-type GaAs region. Infrared photons are released as a result of recombination, and the radiation is confined in a perpendicular direction to the junction by waveguiding action. The reader is referred to [9] concerning the detailed operation of these diodes.

It should be noted that the diode produces a low intensity non-coherent radiation at small forward currents. Lasing action does not start until a minimum value of forward current is exceeded, this is termed the threshold current of the diode, I_{th}. Beyond this current, the diode generates a laser whose intensity is proportional to the current amplitude. The forward current can be increased above threshold up to a maximum value (I_{fm}) beyond which permanent damage of the diode may result. Permanent damage to the diode or a severe degradation of its performance can also be caused by reverse voltages in excess of a few volts depending on diode type.

Commercially available pulsed laser diodes can produce several watts of laser energy for a very brief period of time, and the currents required for their operation can be as high as 100 amperes. Due to the large forward currents required, the repetition rate of the current pulses through these diodes must be kept small to avoid overheating the junction and melting the diode. Duty cycles of less than 1% are typical. The relevant specifications of the particular laser diode used in this work are listed in Table 2.2.

The circuit that was designed and used to drive the laser diode makes use of avalanche transistor action for generating very fast large amplitude current impulses. Before indulging into the details of the design of this circuit, a word about avalanche transistors is in order.

Table 2.2. Pulsed Laser Diode Specifications

Make	M/A COM Laser Diode, Inc.
Type	LD-60 FR (F, for fiber pigtail, and, R for reverse polarity)
Case:	Positive
Peak Radiated Flux at I_{fm}	2 W (min)
Flux Coupled into Fiber Pigtail*	1.2 W (at 27°C)
Fiber Pigtail	100 μm glass core
Wavelength (λ)	904 nm
I_{fm}	10 A
I_{th}*	4.4 A
10%-90% Risetime of Optical Flux	< 0.5 ns
Duty Factor	0.1% (max) at I_{fm}
Pulse Width at 50% Points	200 ns (max)
Maximum Reverse Voltage	3 V

* The values of parameters marked with an asterisk apply to the particular diode used. Unmarked parameters were obtained from the manufacturers data sheets.

2.8.2. Avalanche in Transistors

The maximum reverse bias that can be applied between the collector and the base of a transistor before breakdown occurs is symbolized by BV_{CBO} [10]. The electrons making up the reverse saturation current I_{CO} which flows between the collector and the base are accelerated more and more when an increasing reverse voltage is applied, thus, knocking off other electrons from the semiconductor lattice. The new electron-hole pairs generated from this action cause I_{CO} to increase to a new value, say MI_{CO}, where M is a multiplication factor. A certain voltage may be reached where M becomes virtually infinite, causing a large current to flow through the collector-base junction. At this point, breakdown is said to have occured. The variation of collector current I_C versus V_{CE}, before breakdown, is shown in Figure 2.4, marked $I_E = 0$.

When the base is open circuited (or connected to a constant current source) breakdown may still occur, and the breakdown voltage in this case is designated by BV_{CEO}. This voltage can be as small as a half of BV_{CBO}. The breakdown voltage may be made to lie between BV_{CEO} and BV_{CBO} by connecting a resistor between the base and the emitter. The breakdown voltage under such a circumstance is termed BV_{CER}. Notice that now the $I_C - V_{CE}$ characteristic curves exhibit a negative resistance region.[1] After breakdown, the collector voltage decreases to a value on

---

[1]According to [10], the $I_C - V_{CE}$ characteristic curves for certain types of transistors show a negative resistance behavior even for the case when the emitter is open.

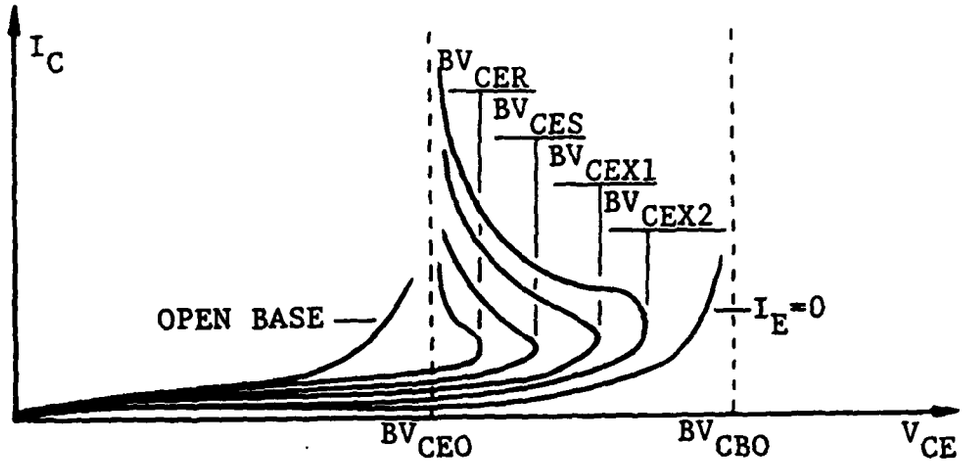

Figure 2.4. Avalanche transistor breakdown characteristics.

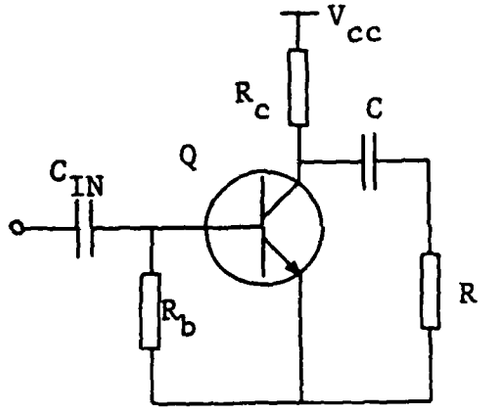

Figure 2.5. Typical avalanche transistor circuit.

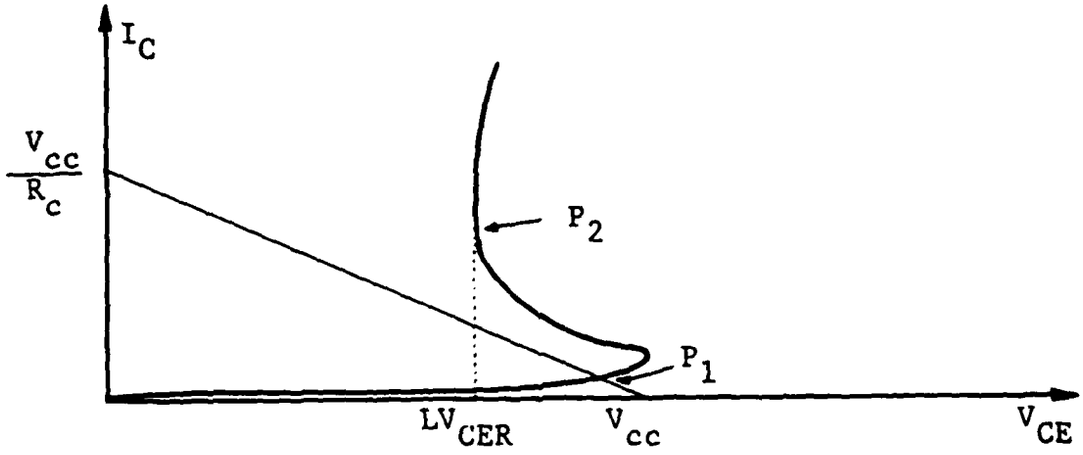

Figure 2.6. Load line and operating points of the avalanche transistor.

the negative resistance part close to BV_{CEO} and a large current passes through the transistor. If the base-emitter resistance is made zero when, for example, a pulse transformer secondary is connected to the base, the breakdown voltage becomes BV_{CES} which is seen to be larger than BV_{CER}. A still larger breakdown voltage can be obtained if a small reverse bias is applied to the base, and this is indicated in Figure 2.4 by BV_{CEX}. A positive bias, however, usually lowers the breakdown voltage of the transistor.

Before describing the typical circuit operation of an avalanche transistor, it is worthwhile mentioning that nondestructive avalanche may occur in many types of transistors, even those that were not designed for avalanche operation. An example of those are most mesa transistors.

To use an avalanche transistor for generating a fast pulse, it is usually connected in a circuit configuration like that of Figure 2.5. In this circuit, the base resistance R_b can be replaced by the secondary of a pulse transformer, in which case its value becomes zero.

When a reverse voltage which is slightly lower than BV_{CER} is applied to the collector of the transistor, a very small collector current (I_{CO}) flows causing the operating point to be P1 in Figure 2.6. If a positive current pulse is now injected into the base, the breakdown voltage is lowered momentarily to a value below the applied collector voltage. When this happens the transistor avalanches instantly, and the operating point moves up the negative slope of the new and momentary $I_C - V_{CE}$

characteristic (not shown), causing the collector voltage to latch at a value LV_{CER} lower than the applied reverse voltage. This transition happens very quickly and the resulting negative step at the collector can have a falltime of only a few nanoseconds. This falltime is usually much smaller than the normal OFF-ON switching time of the transistor. The relatively large current (up to several amperes) required by the transistor during breakdown is supplied by the capacitor C connected to its collector. This capacitor and the resistance R connected in series with it provide a low impedance for the collector current and cause the load line to appear temporarily as being much steeper than the one determined by R_c. This temporary load line intersects the breakdown characteristic curve at a point of elevated current. After all the charge on C has been dissipated, the breakdown current is forced down to a very small value, and the transistor starts moving slowly back to a stable quiescent point, dictated by the original load line of R_c. This point is the same point at which the transistor was before avalanche, namely, P1. This return to P1 is normally much slower than the breakdown time and is determined by the time constant R_cC. It should be noted that after breakdown the transistor spends a brief recovery time which is a small fraction of a microsecond before starting its climb toward P1 [10]. After reaching P1, the transistor is ready for another avalanche cycle.

2.8.3. Principle of Operation of the Pulsed Laser Diode Driver

The principle of operation of the driver circuit that was implemented in this work relies on the phenomenon of avalanche in transistors described in the last subsection. The basic building block of this circuit is shown in Figure 2.7. This simplified circuit features all the important characteristics of the more complicated circuit that was actually used, and which is presented later in subsection 2.8.4.

The transistor Q is reverse biased with a supply voltage V_{cc} that is slightly smaller than the breakdown voltage BV_{CBS}. The capacitor C charges to the voltage of the collector, V_{cc}. The voltage drop across R_c caused by the reverse saturation current (I_{CO}) of the transistor is very small and will be neglected in the present treatment. With this set of conditions, the circuit is triggered by applying a negative pulse at the primary of transformer T. A positive current pulse is developed in the secondary of T and is injected into the base of Q. This pulse causes Q to avalanche instantly and its collector voltage drops several tens of volts from V_{cc} down to LV_{CES} in a few nanoseconds. The charge stored in C is very quickly dissipated through the transistor, resulting in a large current surge through the laser diode LD. The small resistance R_m connected in series with LD can be used to monitor the current surge with the aid of an oscilloscope.

After spending a small fraction of a microsecond at LV_{CES}, the collector voltage starts to climb exponentially toward V_{cc}. The rate of this voltage climb depends on the time constant R_cC.

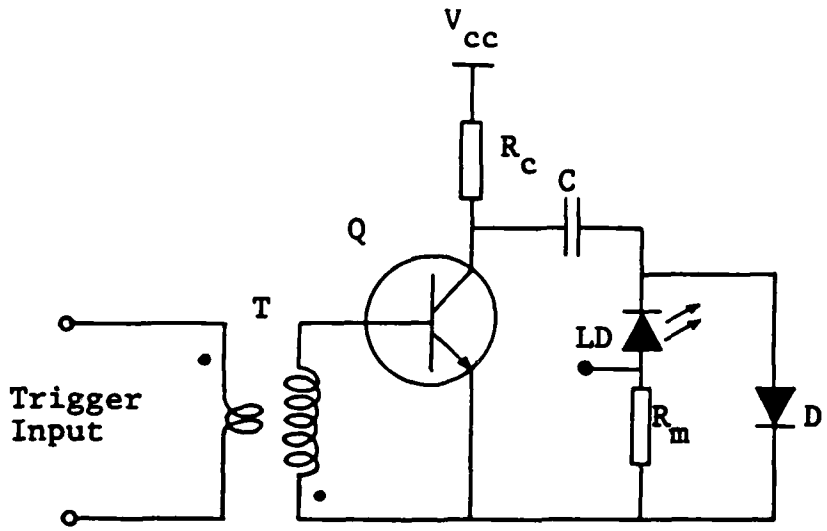

Figure 2.7. Basic pulsed laser diode driver.

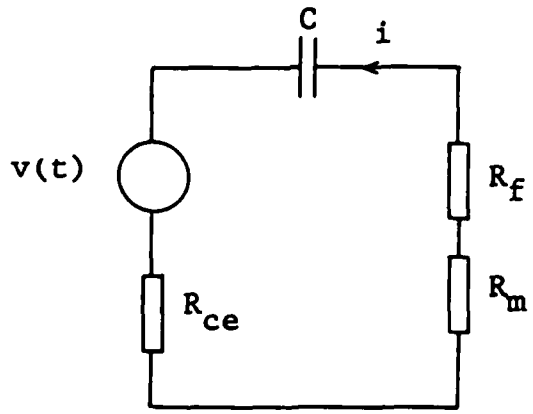

Figure 2.8. Transient model of the basic pulsed laser diode driver.

The diode D provides a path to ground for the charging current of C. Without this diode a large reverse voltage would develop across the laser diode causing its instant damage.

In order to determine the effect of the different circuit parameters on the amplitude of the current pulse through the laser diode and its time duration, transient modeling of the simplified driver circuit was carried out.

Figure 2.8 depicts the transient model corresponding to the circuit of Figure 2.7. R_f is the forward resistance of the laser diode. R_{ce} is the resistance between the collector and emitter of Q during avalanche, and v(t) is a time dependent voltage source which represents the variation of V_{CE} with time during breakdown.

Kirchoff's voltage law for the circuit gives,

$$\frac{q}{C} + R \frac{dq}{dt} = v(t) \qquad (2.2)$$

where q is the charge stored in C at any instant of time t. R is the total resistance in the circuit, and is equal to the sum of R_m, R_f, and R_{ce}. Dividing both sides of Equation 2.2. by R and multiplying by an integrating factor $e^{t/RC}$, we obtain

$$e^{t/RC} \frac{q}{RC} + e^{t/RC} \frac{dq}{dt} = e^{t/RC} \frac{v(t)}{R}$$

integrating both sides of the above equation with respect to t, and solving for q, we obtain

$$q = e^{-t/RC} \int_0^t e^{t/RC} \frac{v(t)}{R} dt + K e^{-t/RC} \qquad (2.3)$$

where K is a constant of integration.

To find K, we impose the initial condition $q = CV_o$ at $t=0$, where $V_o=v(0)$. Substituting in Equation 2.3, we obtain

$$CV_o = 0 + K$$

Therefore,

$$q = e^{-t/RC} \int_0^t e^{t/RC} \frac{v(t)}{R} dt + CV_o e^{-t/RC}$$

The current in the circuit can be found by differentiating the above equation. This gives

$$i = \frac{v(t)}{R} - \frac{V_o}{R} e^{-t/RC} - \frac{e^{-t/RC}}{RC} \int_0^t e^{t/RC} \frac{v(t)}{R} dt \qquad (2.4)$$

From the above equation, it can be seen that the amplitude of the current pulse is inversely proportional to the total resistance in the circuit, R, and that as C is increased the amplitude of the impulse increases up to the maximum determined by R.

For the sake of illustration, the voltage breakdown profile was approximated roughly by setting

$$v(t) = \frac{50}{1+t^3 \times 10^{27}} \quad \text{volts} \qquad t \geq 0 \qquad (2.5)$$

in equation 2.4, and numerical integration was used to solve for i as a function of time, for the case R = 10 ohms, and for several values of C. The results are shown in Figure 2.9. It can be inferred from this figure that the width of the current pulse, for a given value of R, is determined by C. The breakdown profile function v(t) is not shown in Figure 2.9, however, if the curve of i versus t for the case C = 200 nf is scaled by multiplying it by 10 Ohms, it yields a voltage function which resembles v(t) for values of t smaller than about 15 nanoseconds.

It is worthwhile mentioning that v(t) was assumed to be independent of external circuit parameters. Experiment has shown that this is true only for values of C, R_m and R_f such that the maximum current pulse amplitude is smaller than roughly $V_o/5R_{ce}$.

When the value of C becomes small enough such that $q/C \gg R\, dq/dt$ in equation 2.2., the value of the current pulse i approaches $C\, dv(t)/dt$. In other words, the current pulse becomes proportional to the derivative of v(t). Under such a circumstance a current pulse risetime smaller than the falltime of v(t) may be obtained.

An interesting feature offered by the circuit of Figure 2.7 is its capability to automatically limit the energy imparted to the laser diode

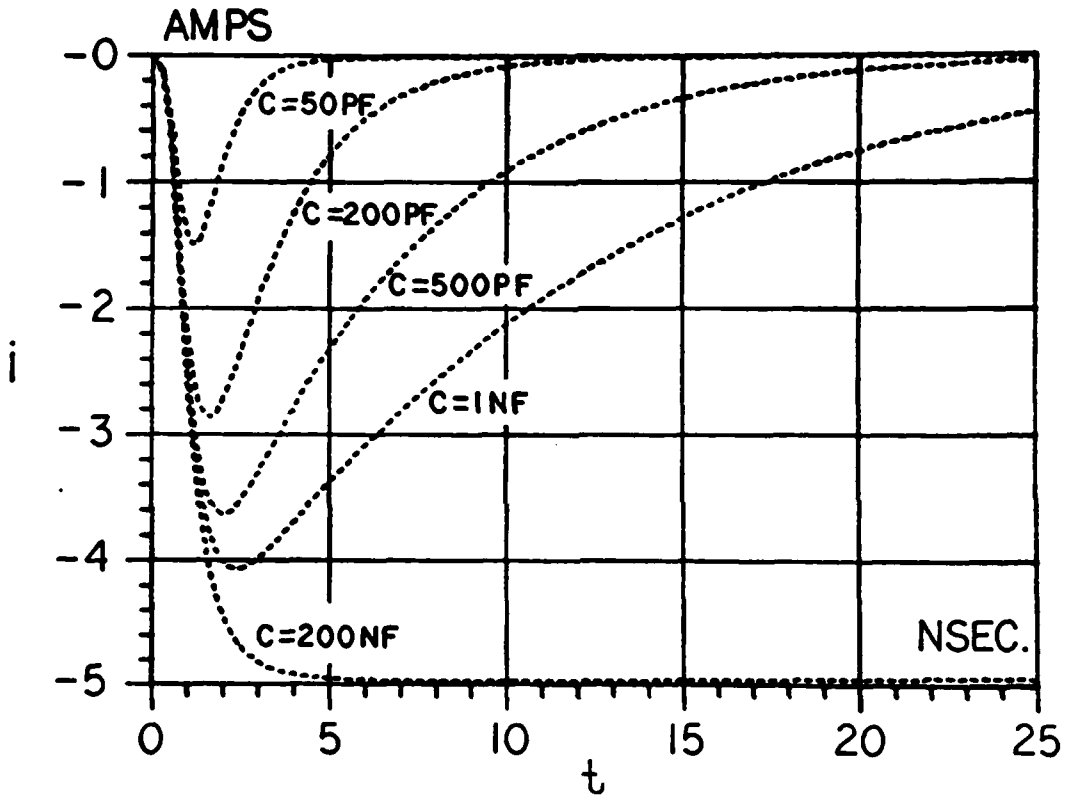

Figure 2.9. Solution of eq. 2.4. showing the current (i) versus time (t) through the pulsed laser diode, for R=10 ohms, and several values of the collector discharge capacitor (C).

when the pulse repetition rate increases to what would appear at first as a value that might cause the duty factor of the diode to be exceeded. This happens due to the fact that the capacitor C has to recharge before the next avalanche breakdown could occur. The time constant $R_c C$ determines the final voltage V_o attained by C before the next pulse is issued. Simple RC-circuit analysis yields the following equation for computing V_o:

$$V_o = V_{cc} - (V_{cc} - LV_{CES})\, e^{-\Delta T/R_c C} \qquad (2.6)$$

where ΔT is the time between two trigger pulses and is equal to the inverse of the repetition frequency (f_{rep}) at which the circuit is operated.

By properly choosing R_c, the time constant $R_c C$ can be made such that as the repetition frequency is increased, C has less and less time to recharge and the voltage V_o becomes smaller and smaller, automatically decreasing the amplitude of the current pulse passing through the laser diode, hence, maintaining the total power dissipation in the diode below its maximum rating.

If the repetition rate is increased further a situation is reached where the voltage to which C can charge (V_o) is equal to the minimum voltage necessary for breakdown to occur, and which is denoted here by V_{Bmin}. Beyond this repetition rate the circuit starts to skip trigger pulses avalanching only every other pulse. This mechanism also acts to ensure that the maximum duty factor of the laser diode is not exceeded.

2.8.4. Practical Pulsed Laser Diode Driver

Figure 2.10 shows the circuit that was used in the fiber optically coupled sampling system to drive the laser diode.

Four avalanche transistors Q1, Q2, Q3, and Q4 are operated in a parallel mode to supply the current pulse of several amperes required by the laser diode. Four transistors were required since one transistor (of the types available to the author) could not supply a current significantly higher than the 4.4 ampere threshold current of the laser diode used (Table 2.2). It was determined experimentally that the effective collector-emitter resistance of each transistor during avalanche is higher than the total external resistance in the circuit. For this reason the four transistors that were required to deliver the proper current pulse to the laser diode were connected in a parallel configuration. A parallel mode of operation was necessary since simple circuit analysis shows that for the sake of delivering current to a load using a multitude of identical sources, parallel connection is superior to cascode connection when the individual source resistances are higher than the load resistance and vice versa.

D1 is a germanium diode which provides a path for the charging current of the collector capacitors, while maintaining a small reverse voltage across the laser diode. D2 and D3 are spare silicon diodes used to take over the function of D1 in the case of an open circuit failure. This precaution is necessary in order to minimize the probability of damaging the laser diode by reverse voltages.

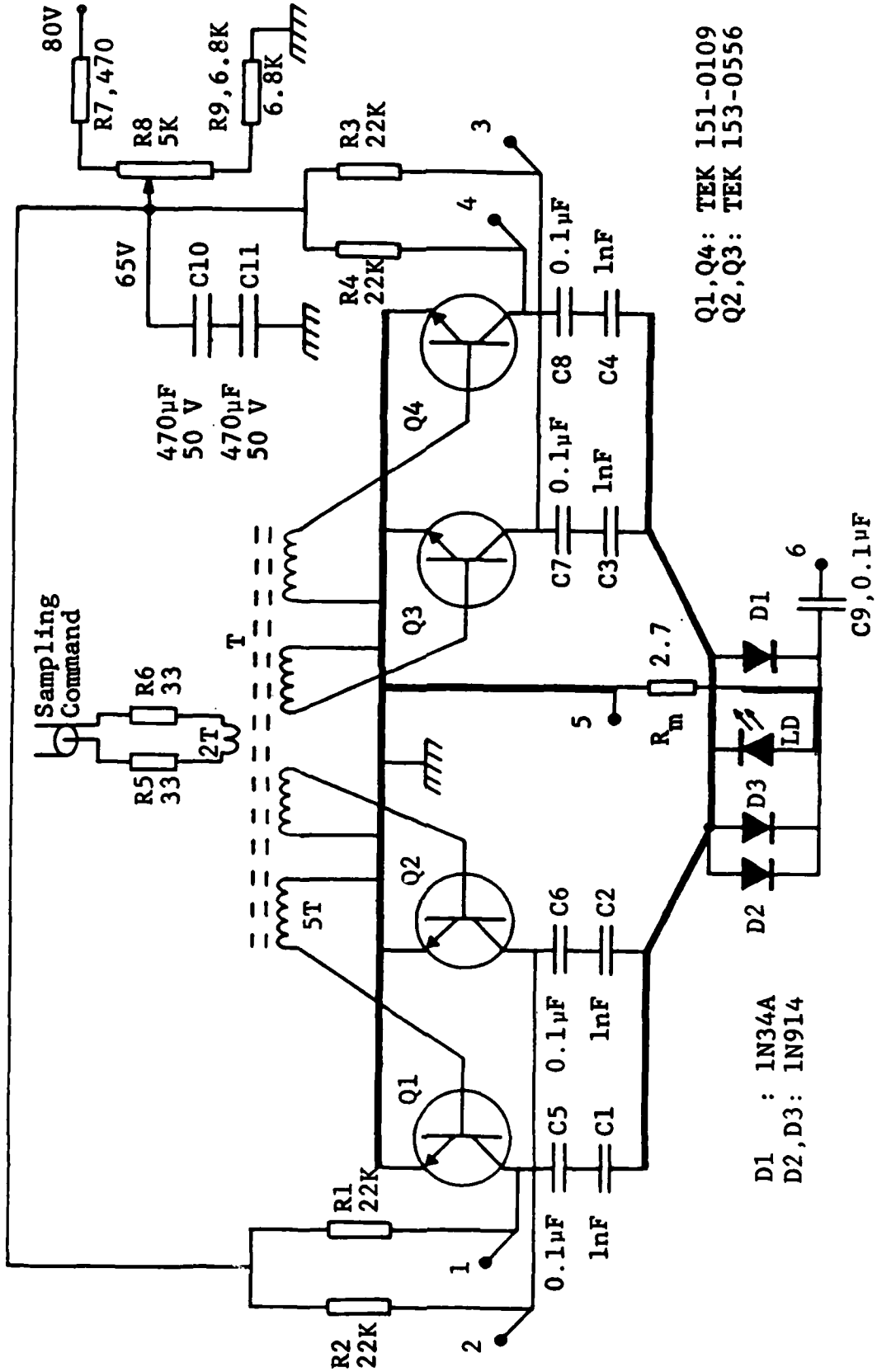

Figure 2.10. Circuit diagram of the practical pulsed laser diode driver.

R_m is a carbon resistor of small physical size which is used to monitor the diode current by observing the voltage drop across it. C9 permits connecting an oscilloscope for this purpose without risking the accidental creation of hazardous DC loops.

C1, C2, C3, and C4 are the charge storage capacitors which determine the current pulse width. C5, C6, C7, and C8 are much larger than the previous set of capacitors, and their only function is to protect the laser diode against a short circuit failure in any of C1, C2, C3, or C4, respectively.

The value of C1, C2, C3, and C4 was obtained from Figure 2.9 to give a current pulse width of nearly 15 ns, assuming that the breakdown voltage profile of the transistors used is very roughly that of equation 2.5, and that this circuit would behave like the single transistor circuit of Figure 2.7. For this purpose the curves of Figure 2.9 had to be scaled to an experimental estimate of 16 ohms for the total resistance in the transistor circuit.

In order to arrive at a conservative estimate of the maximum repetition frequency at which this circuit could be operated without exceeding the duty factor of the laser diode, the collector capacitors were assumed to be able to deliver to the laser diode its maximum current of 10 amperes, undiminished at high repetition rates. With these assumptions and using the diode's maximum allowable duty factor of 0.1%, the maximum repetition frequency $(f_{rep})_{max}$ was calculated from the following equation:

$$\frac{1}{(f_{rep})_{max}} = \frac{15\ ns}{0.001}$$

yielding an $(f_{rep})_{max} = 66.7$ KHz.

This repetition frequency was, in turn, used to calculate the value of R1 through R4. This was done by requiring the recharging RC time constant to be such that C1 through C4 would be able to charge only to the minimum voltage required for avalanche to occur in the transistors used. For this purpose equation 2.6 for the circuit of Figure 2.7 could be used since the recharging circuits of C1 through C4 are isolated from each other. Equation 2.6 is written as:

$$V_{Bmin} = V_{cc} - (V_{cc} - LV_{CES})\, e^{-\Delta T/R_c C} \qquad (2.7)$$

where V_{Bmin} is the minimum voltage required for avalanche to occur, and the small voltage drop across R_c due to I_{CO} has been neglected resulting in a maximum possible reverse bias of V_{cc} at the collector. Substituting $\Delta T = 1/(66.7 \times 10^{3})$ seconds, $C = 10^{-9}$ Farad, and the experimentally determined $V_{Bmin} = 40$ volts, $LV_{CES} = 15$ volts with $V_{cc} = 65$ volts in Equation 2.7, and solving for R_c, we obtain:

$$R_c = 21.6 \text{ kilohm} = R1, R2, R3, R4 \approx 22K$$

R5 and R6 are damping resistors that minimize ringing in the sampling command pulse which drives the primary of T. The polarity of the four separate secondaries of T with respect to the primary is such

that the falling edge of the sampling command pulse causes a positive current pulse to be injected into the base of each one of the avalanche transistors.

R7, R8, and R9 provide a means for adjusting V_{cc} in the circuit. C10 and C11 are power supply bypass capacitors. The minimum 60 Hz attenuation offered by this lowpass filtering circuit can be calculated from C10, C11 and R7. This attenuation is 32 dB. The extra power supply filtering ensures a constant reverse bias on the avalanche transistors, and consequently, a constant energy imparted to the laser diode every time it is pulsed, thus, eliminating one source of time jitter in the sampling command signal.

The thick lines in the circuit indicate increased conductor width which is necessary for minimizing the resistance and the inductance in the path of the laser diode fast current pulse.

It is worthwhile mentioning here that an effort was made when building the circuit to maintain symmetry for the sake of equal propagation times and, also, to maintain closeness of the components in order to minimize path impedance.

2.8.5. Laser Pulse Detection at the S-6

In keeping with the first and third of the objectives set for the design of the sampling command link, no special detector and/or buffer stages were used to detect the laser sampling command pulse. Instead the avalanche transistor Q70 in the S-6 strobe generator board was used

to detect the laser pulse directly. In this technique [8], the cap of the metal case of the transistor was removed and the transistor chip was exposed. Figure 2.11 depicts a photomicrograph of the transistor chip. The end of the glass fiber pigtail core was then brought into direct contact with the top of the chip, as shown in Figure 2.12, and was held there using a self hardening epoxy.

The infrared photons imparted into the silicon chip by the laser pulse cause the production of electron-hole pairs at the reverse biased junction. The electrons are accelerated by the high reverse bias electric field across the junction knocking off other electrons from the valance band and producing more electron-hole pairs. This multiplication leads to an avalanche and breakdown occurs. Once Q70 has avalanched a pair of strobe pulses which open the sampling gate are generated by the rest of the strobe generator circuit as explained in Appendix B.

2.9. Remote Power Source

The sampling head and its associated circuits, namely, the error transmitter and the feedback receiver were powered using a NICAD rechargeable battery pack arranged as shown in Figure 2.13. The voltages required by the sampling head are +50, -50, +15, -12.2 volts respectively. The voltages required by the fiber optic circuits are +5, +15, and -12.2 volts (used in place of -15 volts). The rechargeable batteries were used to supply the small voltages directly, while a DC-DC high

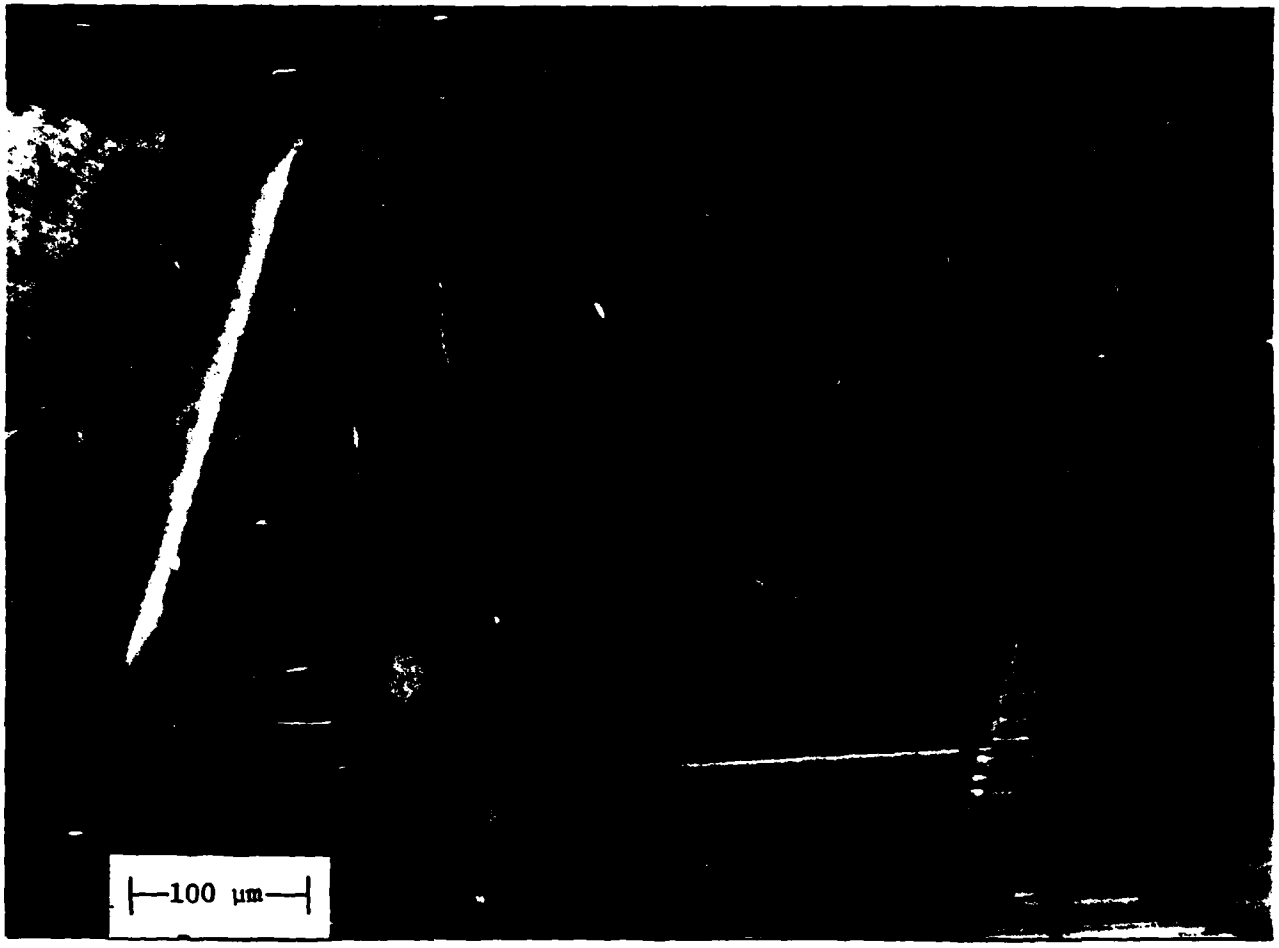

Figure 2.11. Photomicrograph of the chip of the optically triggered avalanche transistor used as Q70 in the strobe generator circuit of the S-6 sampling head.

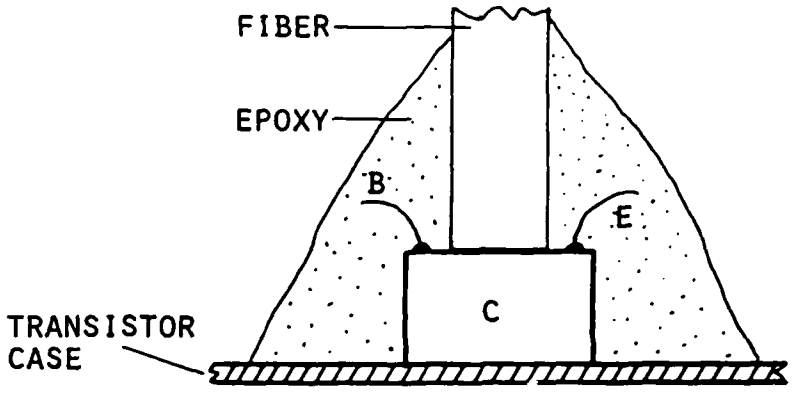

Figure 2.12. Mating the glass fiber end to the avalanche transistor chip.

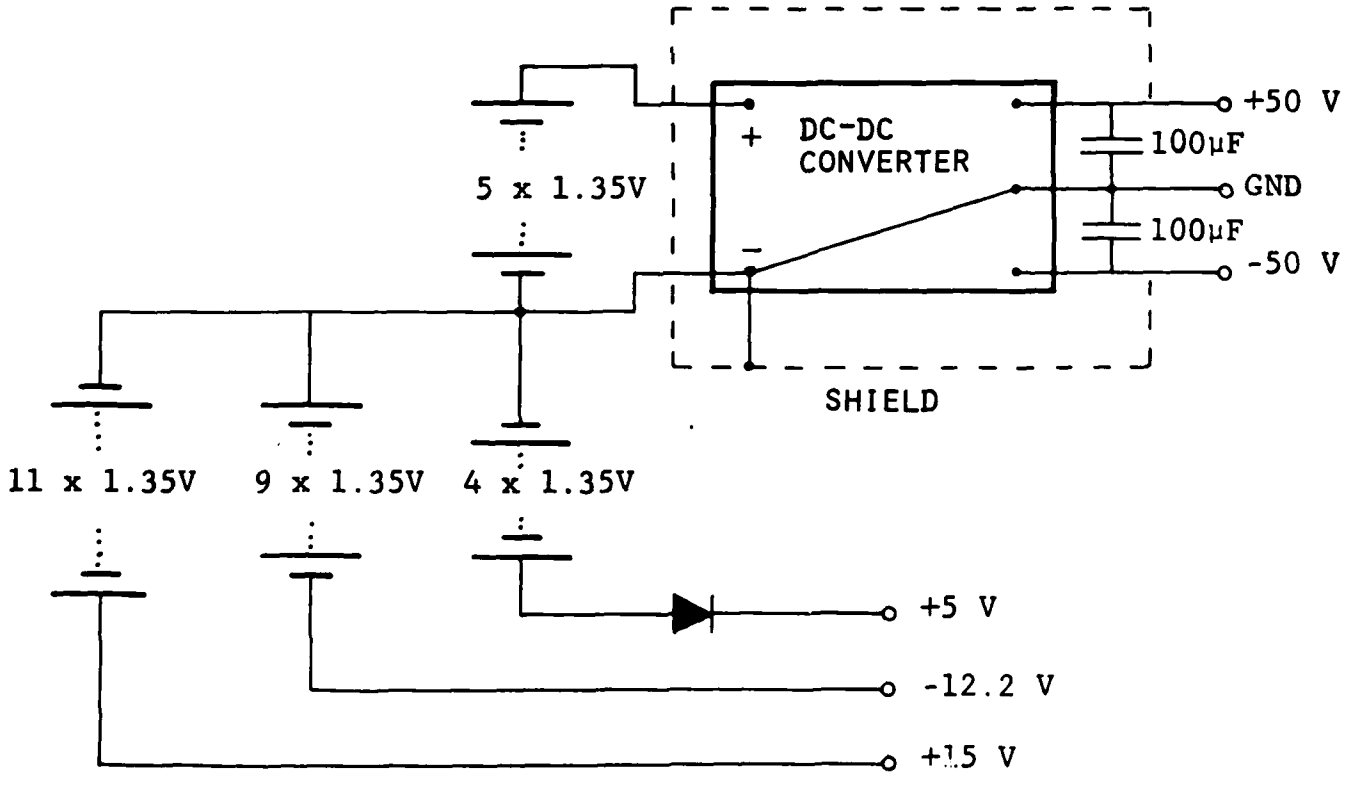

Figure 2.13. The rechargeable battery pack used to power the S-6 and its associated fiber optic interface circuits.

voltage converter was used to generate the high voltages. The power diode in the figure is used to lower the voltage of four batteries from 5.4 volts down to about 5 volts. The shield and the bypass capacitors prevent the internal high frequency oscillation produced by the DC-DC converter from reaching the sampling head and its associated circuits.

2.10. Performance of the Fiber Optic Links

In this section the results of the performance tests on each one of the three fiber optic links that were actually built, are reported. It should be noted that these tests help to evaluate each link as it stands alone and are not tests that evaluate the performance of the sampling system which uses these links. The latter tests and their results are presented in the next chapter.

2.10.1. Performance of the Fiber Optic Error Link

Figure 2.14a shows the input step that was used to test this link. The risetime of this step is 33 ns and its 1% settling time is about 75 ns. Figure 2.14b depicts the output response of the error link to this step. The sag in the top part of the response is due to the AC coupling of the link. The 10%-90% risetime of the output step is 429 ns. Neglecting the finite risetime of the input step by assuming it to be ideal and using equation 2.1, 820 KHz is obtained for the bandwidth of the error link.

The delay introduced into the error signal due to the limited bandwidth of the error link, plus the delay inherent in the S-6

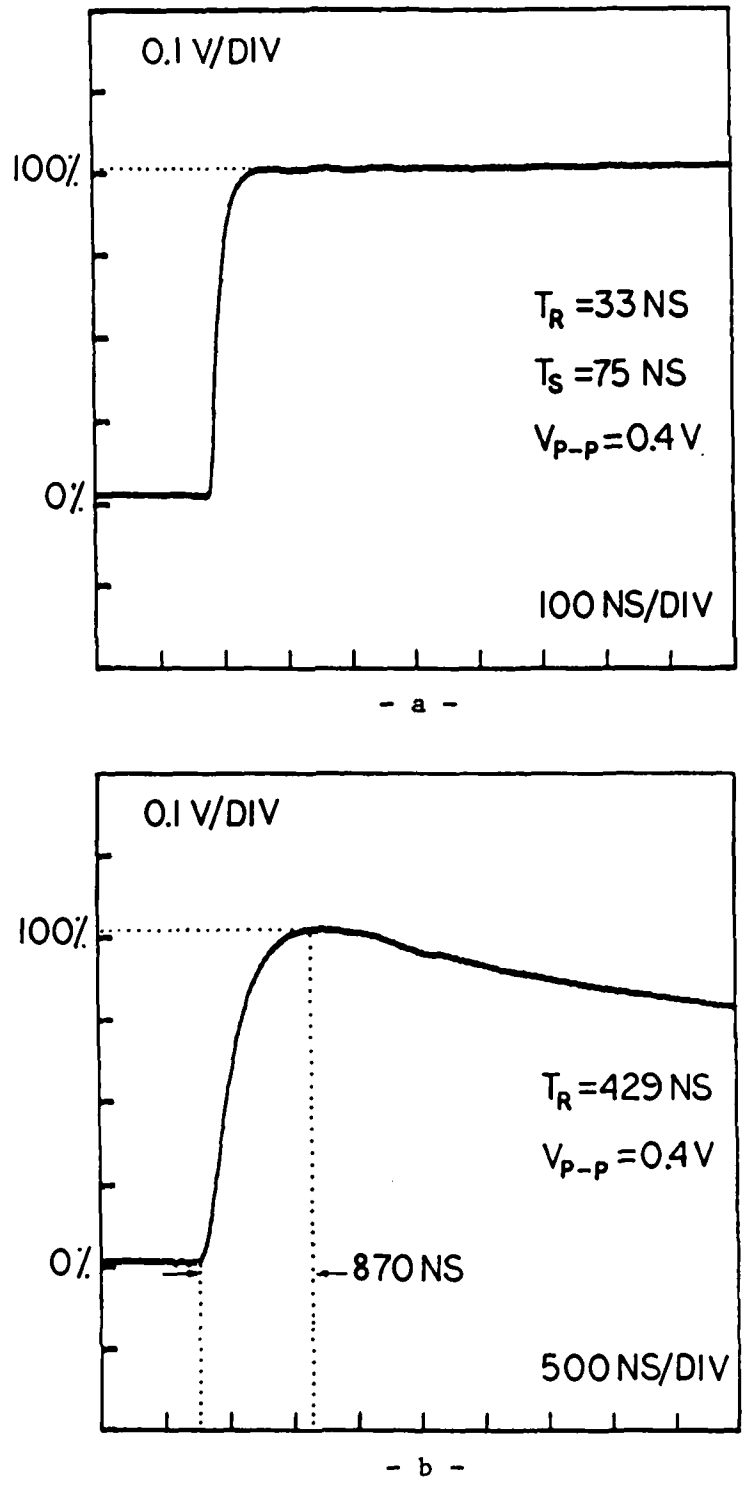

Figure 2.14. a) Test step at the input of the error link.
b) Output response of the error link.

preamplifier and the 7S12 post amplifiers, required that the memory gate width in the 7S12 (see section B.4) be increased to its maximum value to enable the memory circuit to capture the error signal. This necessary action has one shortcoming which is increasing the noise allowed into the memory circuit through the widely opened gate. The consequences of this are discussed in the next chapter.

The peak to peak amplitudes of the input and output signals are seen to be equal. This equality was achieved by adjusting R10 in the error receiver to give a peak to peak gain of unity. This choice of output amplitude is completely arbitrary. The memory gate may close before, at, or after the peak of the link's output is reached. For this reason an in-circuit adjustment of the gain while monitoring the sampling system display is necessary. This adjustment method is discussed in more detail in Appendix A.

2.10.2. Performance of the Fiber Optic Feedback Link

The test reported in this section was carried out for the case of a gain of 2 in the first stage of the feedback transmitter. Gains of 1 or 5 yield equivalent results.

Figure 2.15 shows the output response of the feedback link to a very fast rise input step. The risetime of the output is seen to be 4.37 μs, and its 1% settling time is about 9.2 μs. These values are well within the design objectives of this link, where a settling time of less than 16.3 μs is required.

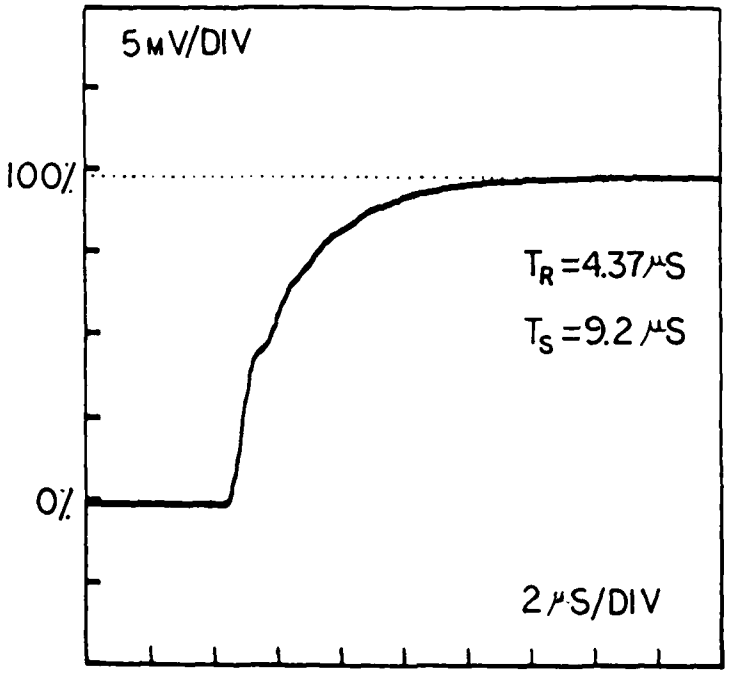

Figure 2.15. Output response of the feedback link to an input step.

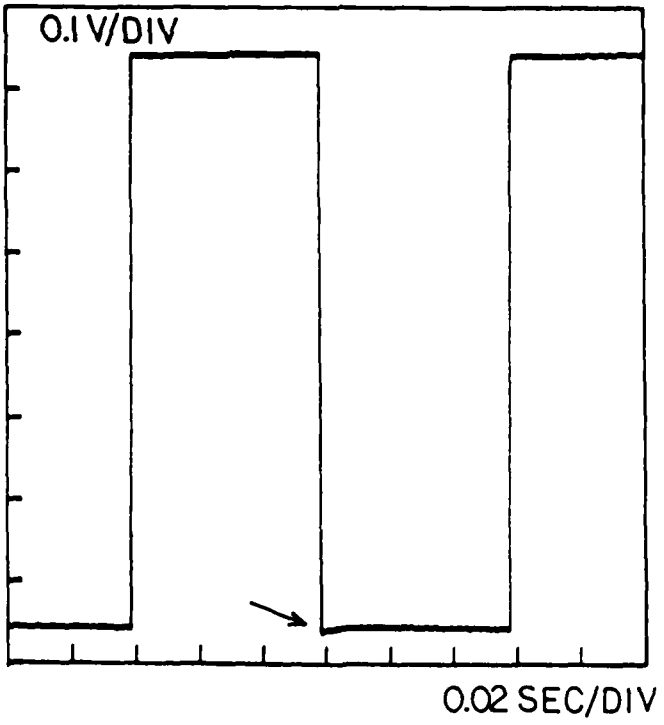

Figure 2.16. The output of the feedback link showing the distortion at the falling edge when responding to a large amplitude low frequency square wave input.

Figure 2.16 shows the output of the feedback receiver when responding to a large amplitude square wave at the link's input. The distortion at the edge which is believed to be due to the transmitter's LED warm-up (section 2.6) can be seen at the point indicated by an arrow. Due to the phase inverting nature of the fiber optic receiving device, this edge is actually associated with increasing LED current in the transmitter. Notice that this phenomenon does not occur at the end of rising edges where the LED current is dropping.

2.10.3. Performance of the Sampling Command Link

Figure 2.17a shows the voltage at the collector of avalanche transistor Q2 in the laser diode driver circuit (Figure 2.10), with V_{cc} set to 65 volts and a sampling command repetition rate of exactly 10 KHz. The charging cycle of capacitor C2 is obvious in the figure.

Figure 2.17b is an expanded view of the falling edge of the avalanche pulse of Q2. The ringing indicates the significance of the inductance in the discharge circuit, and is, otherwise, nondegrading to the link performance. The 10%-90% falltime of the avalanche step between the points marked 1 and 2, is seen to be 2.2 ns. Due to the finite bandwidth of the measurement system used to acquire this waveform, the falltime just cited is actually higher than the true falltime of the step. To obtain the true falltime, the following approximate formula [10] is used,

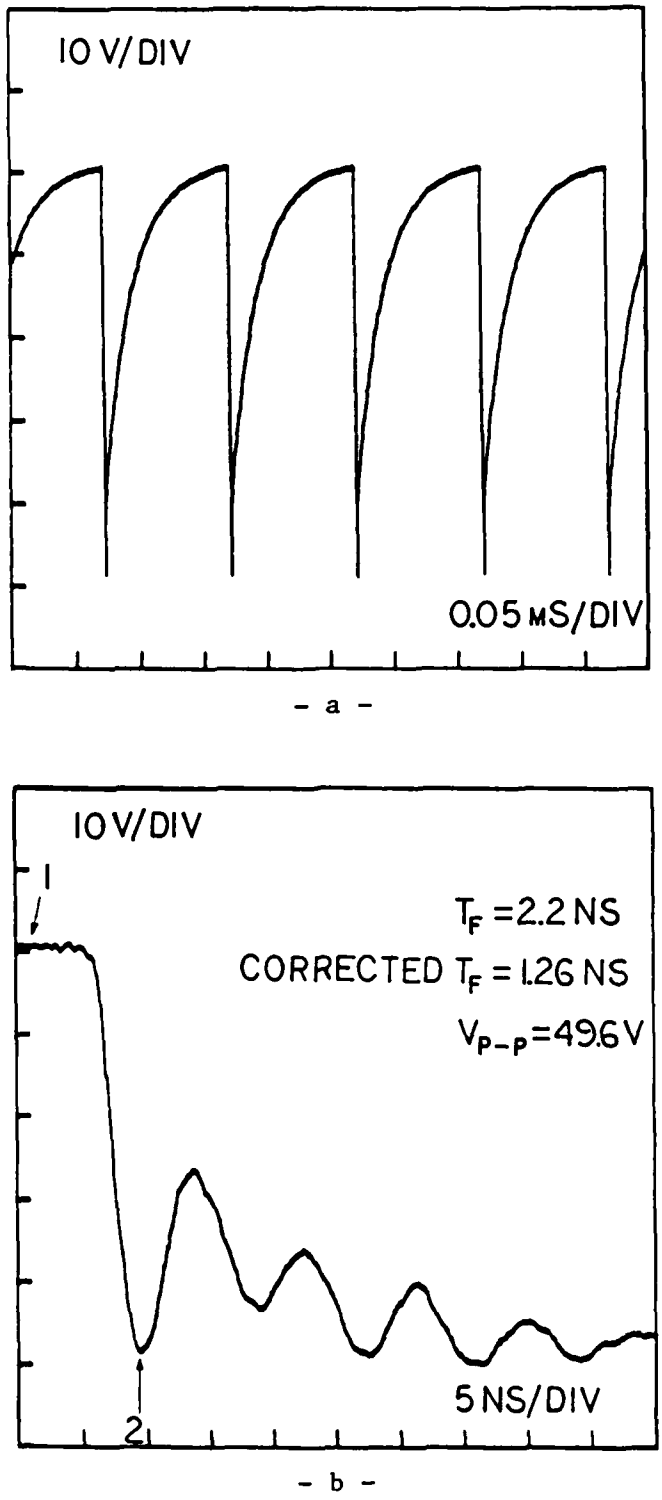

Figure 2.17. The voltage at the collector of avalanche transistor Q2.
a) Large time/div. showing the charging cycle of C2.
b) small time/div. showing the avalanche breakdown falling edge.

$$t_{ro} = (t_{ri}^2 + t_{rs}^2)^{0.5} \qquad (2.8)$$

where t_{ro} is the risetime (falltime) at the output of a linear system whose risetime is t_{rs}, and which is excited at its input by a step whose risetime (falltime) is t_{ri}. Substituting in this formula t_{ro} = 2.2 ns and t_{rs} = 1.8 ns for the measurement system used[2], 1.26 ns is obtained for the true falltime of the avalanche step.

Figure 2.18 shows the voltage developed across the current monitoring resistor R_m in the laser driver circuit. From this figure the peak forward current through the laser diode $(I_f)_{peak}$ can be computed by dividing the peak voltage by the value of R_m, thus

$$(I_f)_{peak} = \frac{22.7 \text{ volts}}{2.7 \text{ ohms}} = 8.4 \text{ A}$$

The true current is believed to be somewhat less than 3.4 Amps due to the fact that the inductive reactance intrinsic to R_m and its connections has been neglected in the above calculation. If this reactance is accounted for by adding roughly 1 ohm to the value of R_m, the peak current is seen to become 6.13 Amps. Using this value of current and knowing that the radiated power of the laser diode is proportional to its forward current, a peak radiated laser power of 735 mW is obtained.

---

[2]Tektronix: 7854 mainframe oscilloscope, 7A16A vertical amplifier, and 6063B, 10x, probe

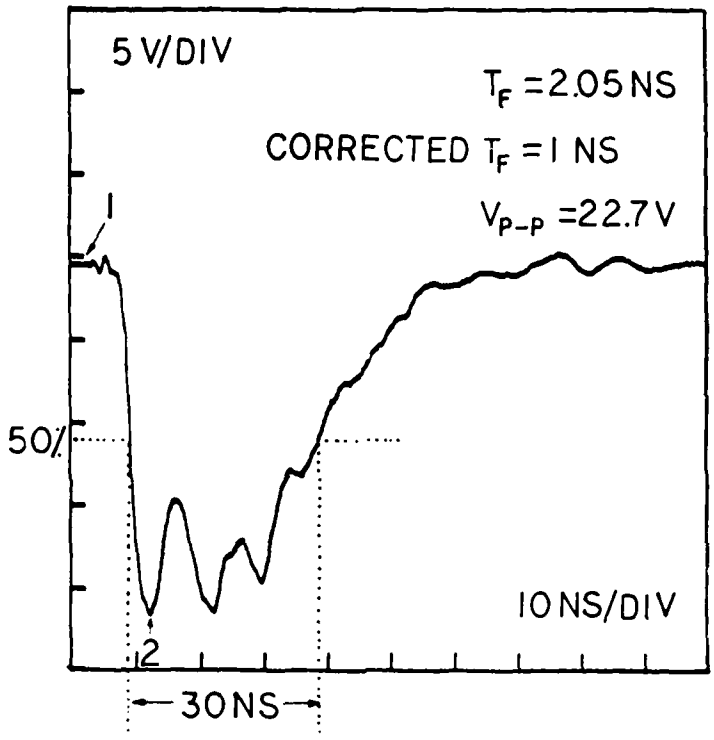

Figure 2.18. The voltage developed across the laser diode current monitoring resistance R_m .

The width of the laser diode current pulse at the 50% points is 30 ns. This is twice the design value of 15 ns. This increase in pulse width can be attributed to the different shape of the avalanche breakdown from that of equation 2.5, to the inductance in the circuit, and, also, to the approximation made in obtaining the design pulse width by assuming the four transistor circuit to act like the single transistor circuit of Figure 2.7.

The 10%-90% risetime of the laser current pulse is seen to be 2.05 ns between the pionts marked 1 and 2 in Figure 2.18. When equation 2.8 is used to remove the measurement system's risetime from the above value, 1 ns is obtained for the true risetime of the laser current (assuming R_m to be purely resistive). The fact that this risetime is smaller than the falltime of the avalanche step is due both to the differentiating effect of the discharge capacitors and, also, the presence of the other (possibly faster) avalanche transistors in the circuit.

Despite the current pulse width being twice the design value, the laser driver was driven with trigger pulses that had a repetition rate of up to 60 KHz without any damage to the laser diode. This was possible since the peak current in the diode was smaller than the maximum allowable value, and, also, because the collector capacitors acted to reduce this current progressively with increased repetition rate as discussed in subsection 2.8.3. The optical radiated power also dropped as a result of current reduction. Figures 2.19a and 2.19b show the

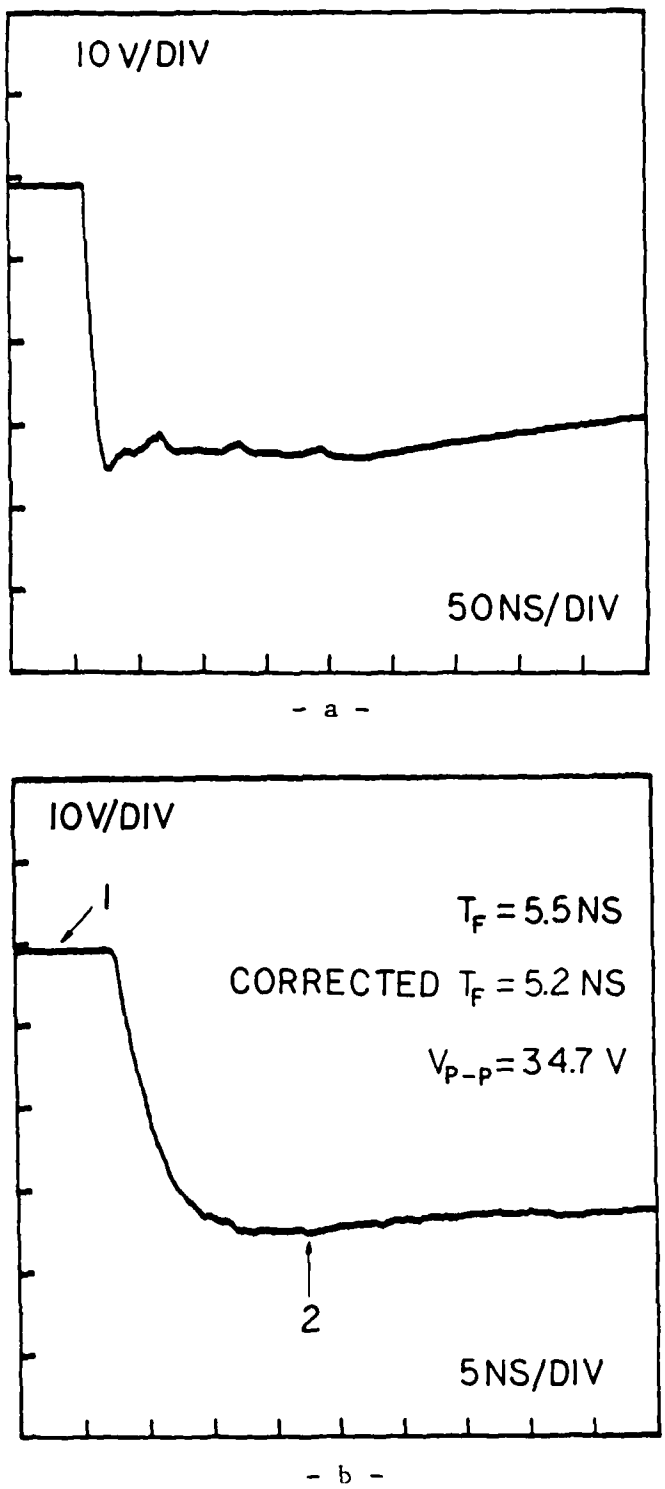

Figure 2.19. The voltage at the collector of avalanche transistor Q70 in the S-6, when the sampling command is hardwired.
a) Large time/div. showing breakdown and recovery period.
b) small time/div. showing the avalanche breakdown falling edge.

collector voltage of the S-6 avalanche transistor Q70 when triggered by the hardwired sampling command signal. The corrected falltime of the avalanche step is 5.2 ns.

Figures 2.20a and 2.20b depict the collector voltage of Q70 when the avalanche is triggered by applying the infrared laser pulse directly to its silicon chip. The corrected falltime is seen to be 7.35 ns.

The jitter introduced into the sampling command by this link was too small to be measured with conventional means. However, it could be characterized by considering the overall sampling system performance, as will be shown in the next chapter.

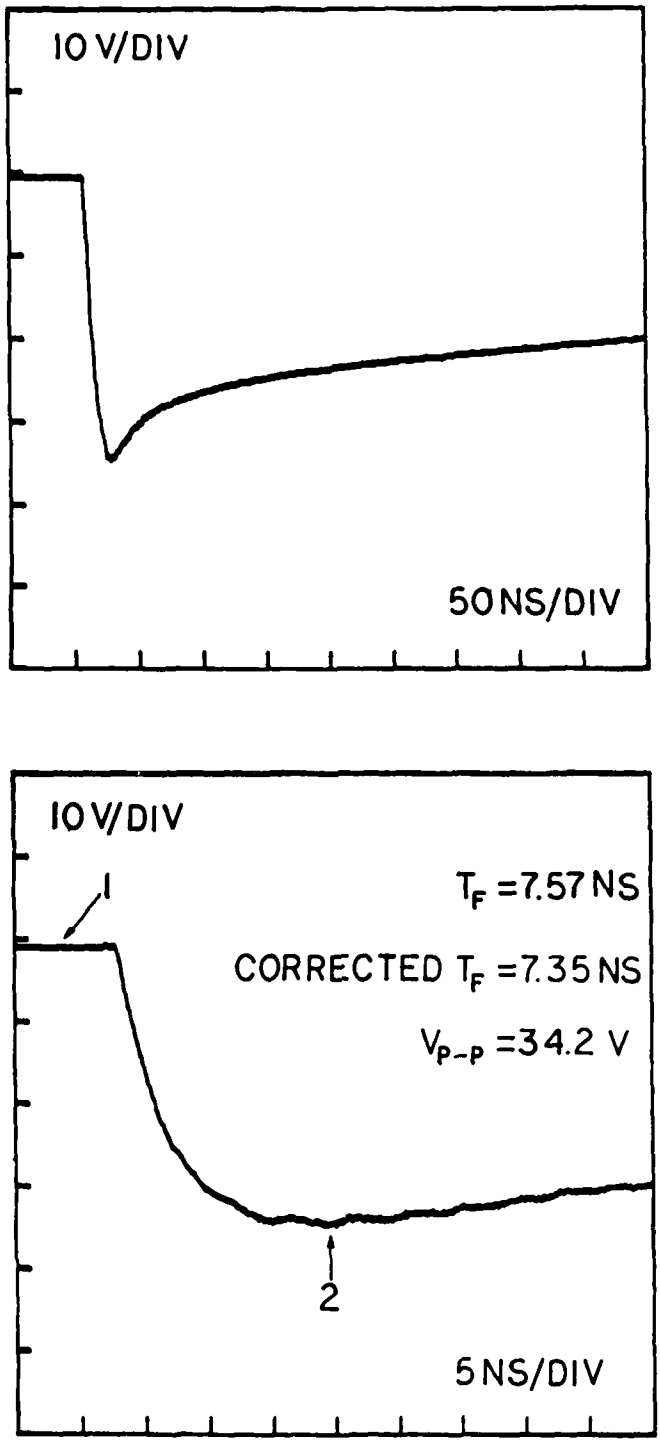

Figure 2.20. The voltage at the collector of avalanche transistor Q70 in the S-6, when triggered by the laser pulse.
a) Large time/div. showing breakdown and recovery period.
b) Small time/div. showing the avalanche breakdown falling edge.

CHAPTER 3

SYSTEM TESTING

3.1. Introduction

This chapter presents the results of the tests conducted on the fiber optically coupled sampling system constructed by the author. These tests fall into two categories; in the first, a visual or qualitative evaluation of system performance was sought, while in the second a quantitative evaluation was carried out.

3.2. Test Strategy

The fiber optically coupled sampling system was tested by acquiring a pulse with a risetime on the order of 100 ps. Both large and small pulse amplitudes were used, and for both cases, large and small sampling windows were utilized.

By comparing the waveforms acquired using the optically coupled system with the corresponding "reference" waveforms acquired using the normal (hardwired) system, it was possible to determine the effect of introducing the fiber optic links on the overall sampling system performance.

Large amplitude test pulses were used (approximately 270 mV p-p) to characterize strobe jitter, along with any nonlinearities introduced by

the fiber optic error and feedback links. The large amplitude of these pulses was necessary in order to minimize the effect of noise in the acquired waveforms. Small amplitude test signals (approximately 15 mV p-p) were used to characterize the noise behavior of the optically coupled system. This order of signal amplitudes is of special interest, since it covers the amplitudes of signals obtained from surface current probes and antennas.

Small time windows (500 ps) were employed to observe the fast-rise (leading) edge of the test pulse in order to determine the effect of the optically coupled system on signal risetime. Large time windows (5 ns) were necessary for signal processing purposes, where a quantitative evaluation of system performance was carried out. One large time window (50 ns) measurement was done in order to show the test pulse in its totality for visual evaluation.

The waveforms obtained in these tests were either, the result of a single acquisition, or the result of additive signal averaging (see Appendix C). For uniformity purposes throughout the measurements, the number of averaged signals was always chosen to be the same (100). Signal averaging is preferable to the smoothed "high resolution" mode of the 7S12 because it avoids the noise sequence correlation introduced by the integrating smoothing process.

In addition to testing the fully optically coupled sampling system, other tests were carried out with certain links being optically coupled while others are hardwired. This was necessary in order to identify separately the factors affecting system performance.

The system configurations which were tested in order to achieve the goal stated in the last paragraph are:

1. Fully Optically Coupled Sampling System (F.O.C.S.S.). The error, feedback, and sampling command links all being fiber optically coupled.
2. Laser Strobed Sampling System (L.S.S.S.). The sampling command is delivered by the laser link while the error and feedback are hardwired.
3. Error and Feedback Optically Coupled Sampling System (E.F.O.C.S.S.). Error and feedback being fiber optically coupled, while sampling command is hardwired.

In addition to the above 3 configurations, waveforms were also acquired for the normal (hardwired) sampling system in order to serve as reference waveforms.

It should be noted that for the system configurations 1, 2, and 3 above, the memory gate was opened to its maximum width. Although this was not necessary for 2, it was done for the sake of uniformity throughout the measurements.

The transmitter gain/receiver attenuation ratio of the fiber optic feedback link was set to 1/1 for large signal tests. For small test signals, this ratio was set to 5/5 in order to enhance the signal to noise ratio of the link.

3.3. Test Set-Up and Equipment Used

Figure 3.1 shows the test set-up used to acquire waveforms using the F.O.C.S.S. After minor reconnections, the same set-up was used to test the other system configurations mentioned in the previous section.

The test signal was supplied by a commercially available pulse generator[1] which produces a pulse with a risetime on the order of 100 ps. A low frequency pulse generator was used to trigger the system with a repetition rate of exactly 10 KHz. The trigger pulse was split into two pulses; one was used to trigger the 7S12 electronics via the S-53 trigger recognizer plug-in, while the second pulse was delayed by about 60 ns and then used to trigger the test pulse generator. Some delay was necessary in order to compensate for the delay in the sampling command pulse introduced by the laser link.

The 7S12 was plugged into a commercially available oscilloscope mainframe.[2] The oscilloscope features both a single acquisition facility and a waveform averaging facility with the final waveform stored internally as an array of numbers in screen grid units. A desktop computer[3] in conjunction with a GPIB was used to transfer the 512 element

---

[1] Model 4000, option-01 Picosecond Pulse Labs, generator.

[2] Tektronix 7854 signal processing oscilloscope.

[3] Tektronix 4051 computer.

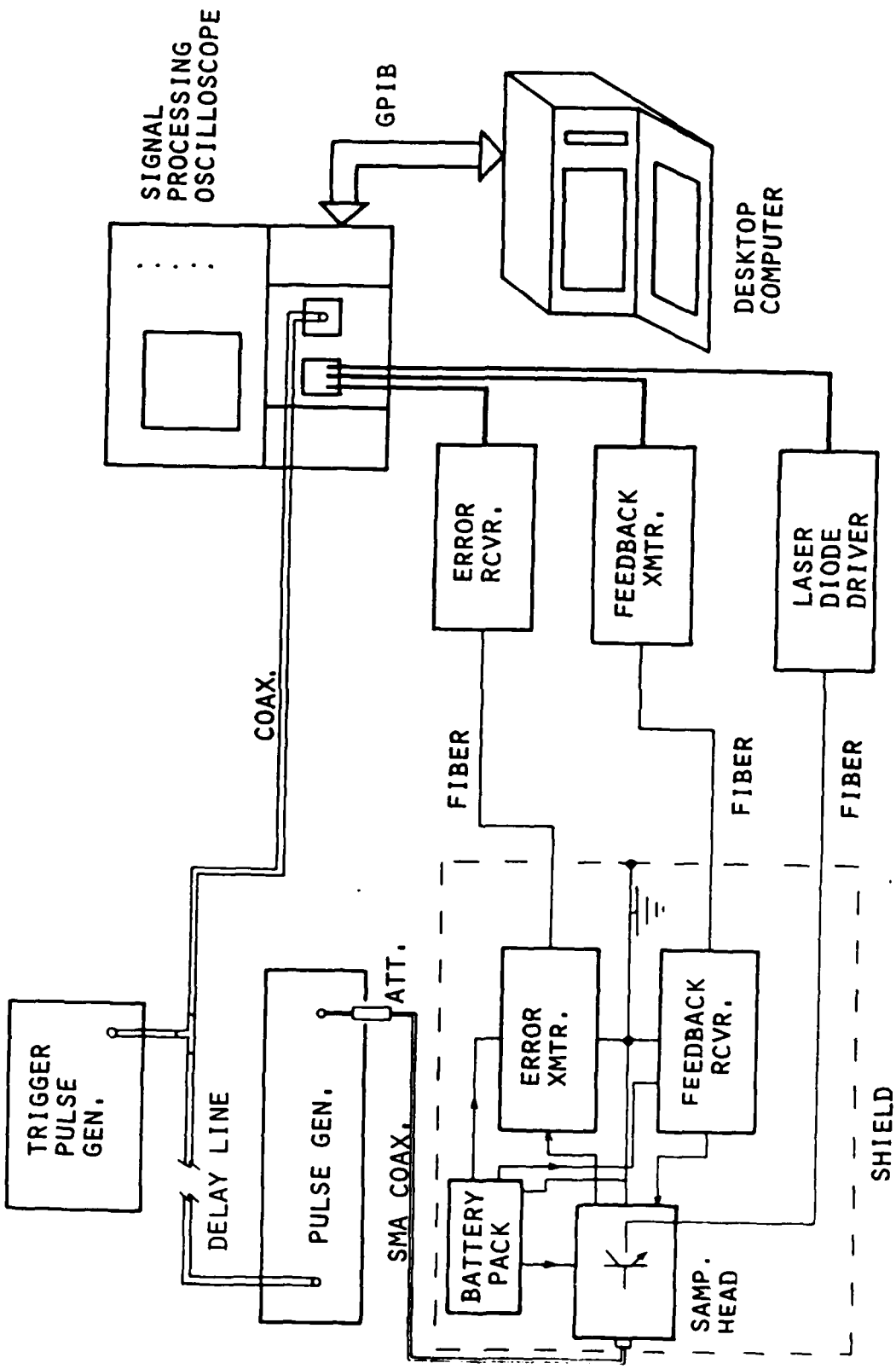

Figure 3.1. Set-up for testing the fiber optically coupled sampling system.

waveform arrays from the oscilloscope's internal memory to binary tape files.[4]

When the reference signals were acquired, the S-6 sampling head was connected to the 7S12 by an S-6 extender cable. Also, the memory gate was set to its calibration width.

Before each measurement session was started, the S-6 (connected by an extender cable) and the 7S12 were warmed-up for about 2 hours prior to the introduction of the fiber optic links. The S-6 extender cable was then removed and the fiber optic links introduced. The F.O.C.S.S. was then left to warm-up for an additional half hour allowing time for a freshly charged battery pack to reach a voltage level that was slowly decaying with time. This procedure minimized drifts and allowed about 30 minutes of waveform acquisition before the battery pack discharged to an unacceptably low level. The vertical sensitivity that was used with large test signals is 50 mV/div, and the one used with small test signals is 5 mV/div.

3.4. Qualitative Tests

3.4.1. Introduction

The aim of the tests presented here is giving the reader a visual or qualitative perception of the fiber optically coupled sampling system

---

[4]The author wishes to acknowledge the kind assistance of Mr. Ronald E. Correll of Tektronix, Inc. in providing the the Basic program used for waveform transfer.

performance. In addition, these tests provide the information necessary for judging the performance of the different links. This qualitative information was necessary for designing the quantitative tests which were run on the system. Both large and small test signals were used with the F.O.C.S.S., the L.S.S.S., and the E.F.O.C.S.S. configurations.

3.4.2. Large Signal Test Results

Figure 3.2.a shows a single acquisition of the leading edge of the reference signal acquired with the hardwired (standard) sampling system. Figures 3.2.b, c, and d show the same waveform acquired by the three sampling system test configurations, namely, the F.O.C.S.S., the L.S.S.S., and the E.F.O.C.S.S. The strobe jitter introduced by the laser link is apparent on the rising edge of waveform c. The jitter is nonexistent in the case of waveform d, but the noise level is seen to be higher than that of the reference waveform. The higher noise is due to, both, the widely opened memory gate and the noise introduced by the fiber optic error and feedback links. Waveform b acquired with the F.O.C.S.S. shows the effects of both the superimposed noise and the strobe jitter. The spikes associated with the strobe jitter are less pronounced here than those of waveform c. This smoothing-out of strobe spikes does not imply that jitter is smaller in the case of the F.O.C.S.S. than it is for the L.S.S.S.; instead, it is the lowpass nature of the error link which causes the spikes to be smoothed out.

Figure 3.3 depicts the waveforms obtained as a result of signal

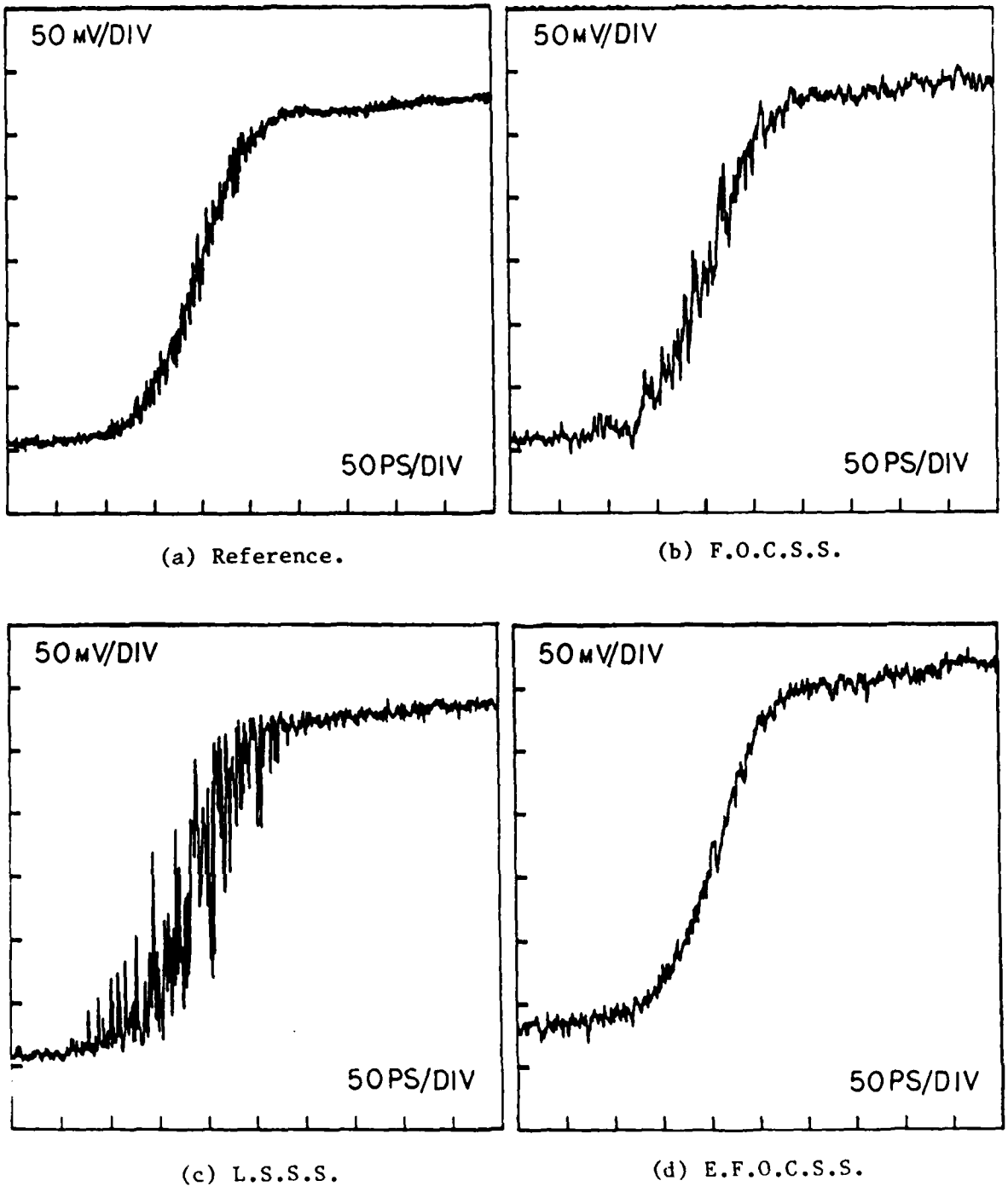

(a) Reference.

(b) F.O.C.S.S.

(c) L.S.S.S.

(d) E.F.O.C.S.S.

Figure 3.2. Single acquisition of the leading edge of the large signal test pulse.

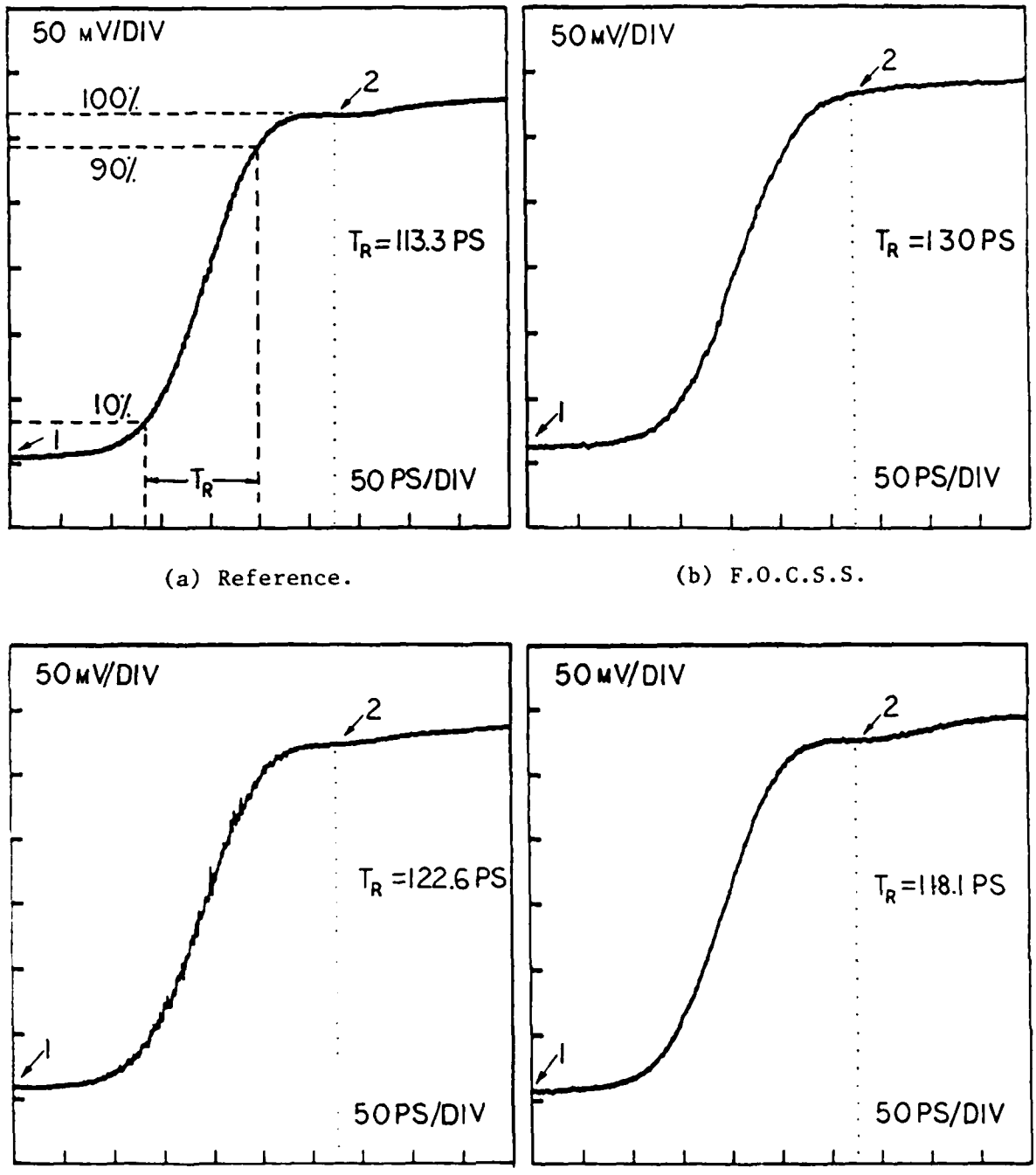

(a) Reference.

(b) F.O.C.S.S.

(c) L.S.S.S.

(d) E.F.O.C.S.S.

Figure 3.3. The waveforms resulting from averaging 100 acquisitions of the leading edge of the large signal test pulse.

averaging 100 of the waveforms of Figure 3.2 for the respective system configurations. The risetime indicated on the waveforms of Figure 3.3 is largely a subjective parameter and is defined as: the time it takes the pulse to rise from 10% to 90% of its peak value, with the reference level being the beginning of the waveform at the left end of the window (point marked 1). The peak of the pulse being the highest value it attains prior the point marked 2.

The risetime of the waveform acquired when only the error and feedback links are optically coupled is seen to be only slightly longer than that of the reference waveform. This indicates the slight lowpass effect introduced by these links. The risetime of the waveform c is longer than that of the reference waveform. This is the first indication of the lowpass nature of the optically coupled sampling system due to the jitter introduced to the sampling command signal by the laser link. The risetime of waveform b acquired with the F.O.C.S.S. is seen to be the longest, reflecting the lowpass nature of the system which is caused mainly by the laser link and, to some extent, by the fiber otpic error and feedback links.

Figure 3.4 shows a single acquisition of the test pulse in its entirety using a large time window of 50 ns. Figure 3.5 depicts the waveforms resulting from the additive signal averaging of the waveforms in the previous figure. The waveforms of Figure 3.5 indicate the degree of fidelity with which the three fiber optic links preserve the shape of the test pulse.

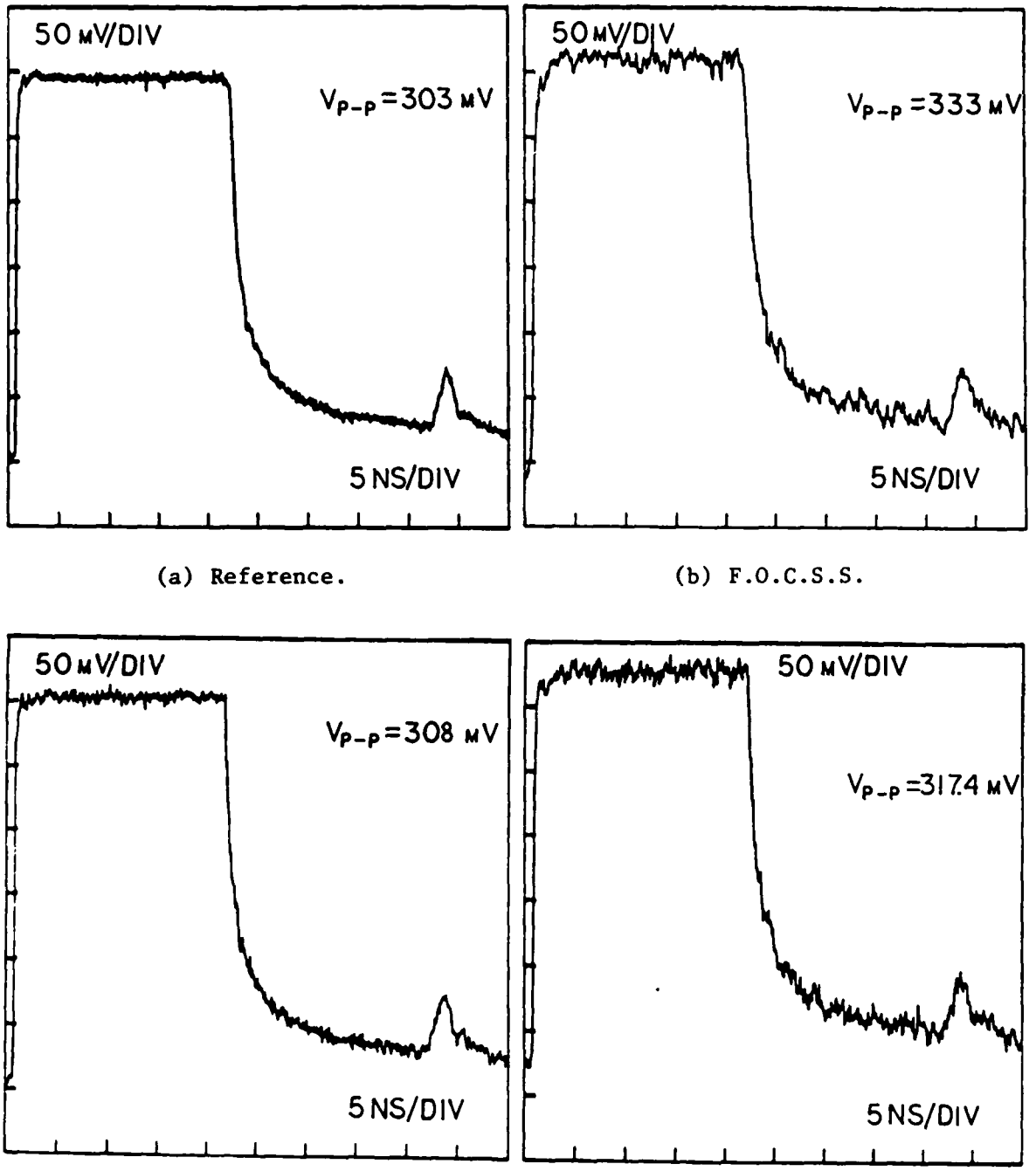

(a) Reference. (b) F.O.C.S.S.

(c) L.S.S.S. (d) E.F.O.C.S.S.

Figure 3.4. Single acquisition of the large signal test pulse.

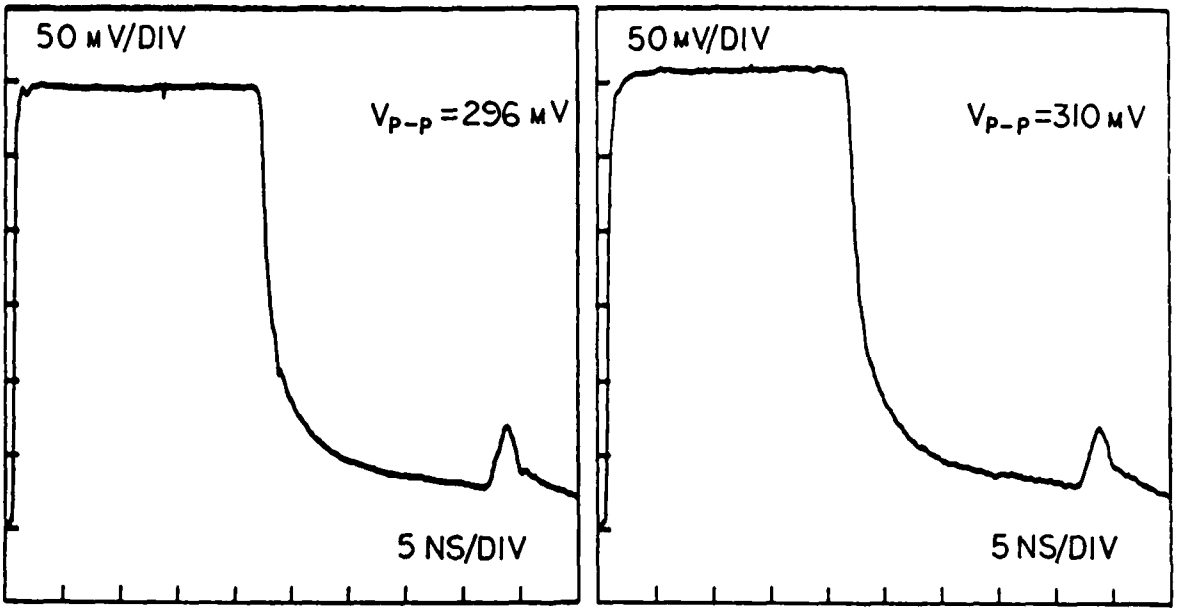

(a) Reference. (b) F.O.C.S.S.

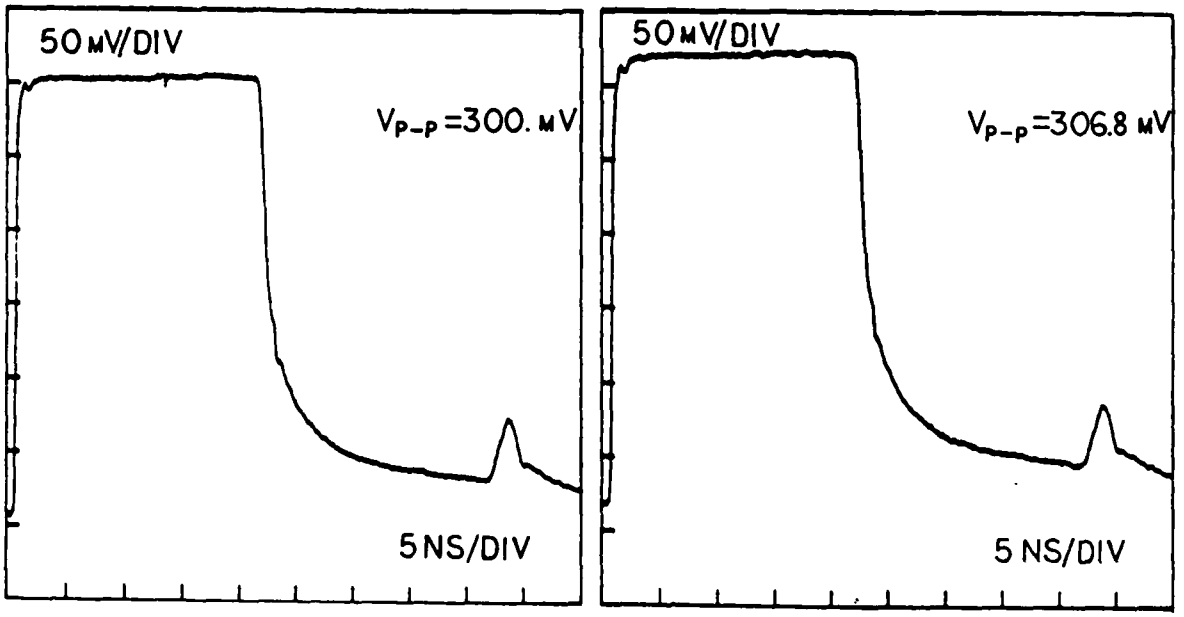

(c) L.S.S.S. (d) E.F.O.C.S.S.

Figure 3.5. The waveforms resulting from averaging 100 acquisitions of the large signal test pulse.

Figure 3.6 shows a single acquisition of the baseline noise level for the hardwired (reference) system and the three optically coupled test configurations. These waveforms were acquired with zero signal (a short) at the sampling head input. The peak to peak noise voltage of the noise within the sampling window is indicated on each waveform. In the case of waveform c of the L.S.S.S., the noise level is higher than that of the refernce system due to the opened memory gate. For waveforms b and d, the noise is due, both, to the opened memory gate and the noise introduced to the error and feedback signals by their respective fiber optic links.

Figure 3.7 depicts the baseline noise levels of Figure 3.6 after signal averaging was employed on 100 acquisitions. The drop in the peak to peak noise level is seen to be in acceptable agreement with the $1/\sqrt{N}$ improvement in noise expected of additive signal averaging (appendix C).

3.4.3. Small Signal Test Results

Figure 3.8 depicts single acquisitions of the small signal reference waveform and the waveforms acquired using the three sampling system test configurations. Strobe jitter is present in the waveform of b and c but is masked by the relatively large noise level. The noise on the waveforms of Figure 3.8 is more obvious than for the waveforms of Figure 3.2 due to the small amplitude of the test signals used here.

Figure 3.9 shows the waveforms resulting from averaging 100 acquisitions of the waveforms in Figure 3.8. The lowpass nature of the

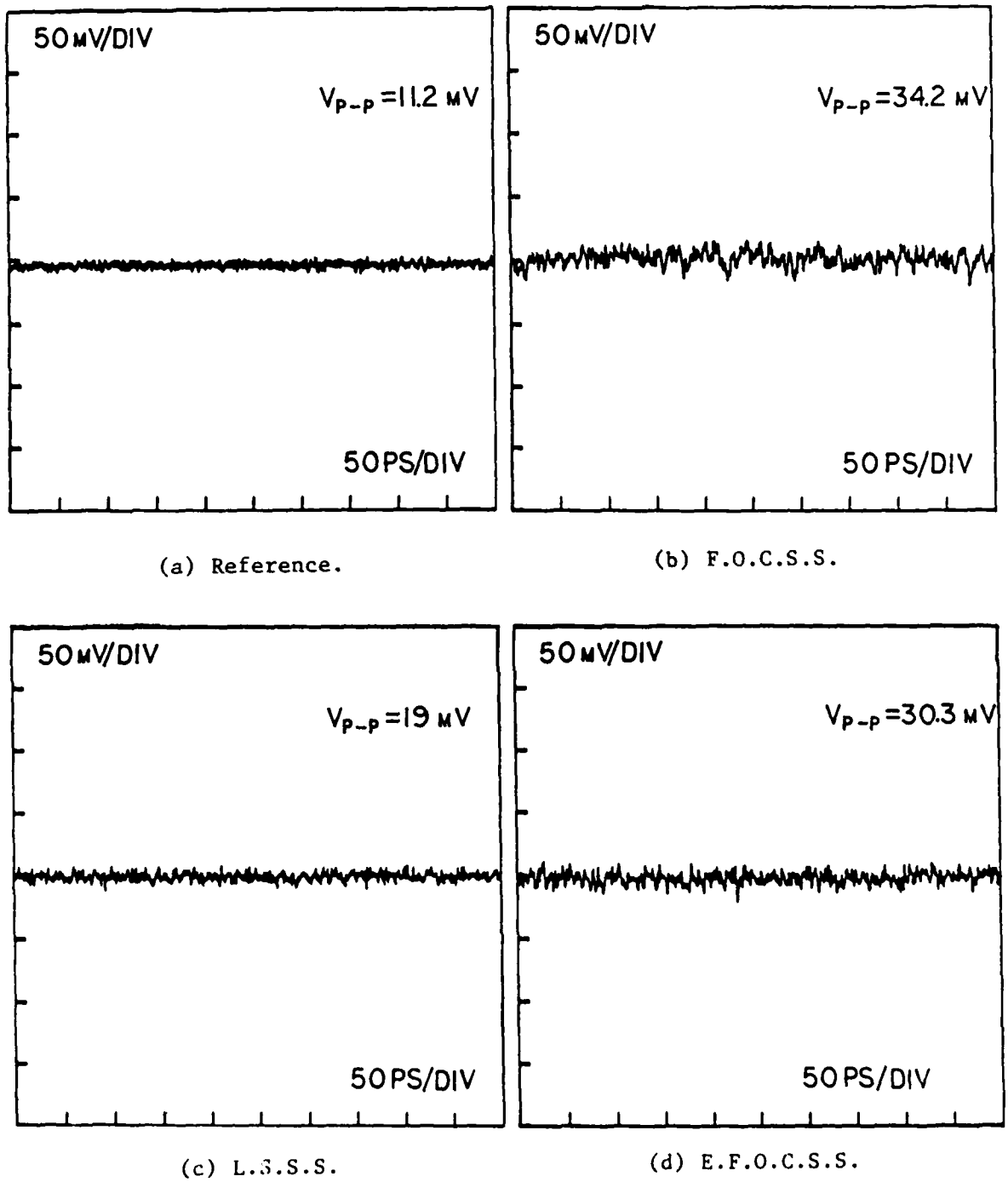

(a) Reference.

(b) F.O.C.S.S.

(c) L.S.S.S.

(d) E.F.O.C.S.S.

Figure 3.6. Single acquisition of the baseline noise level for large vertical scale factor (50 mV/div.) .

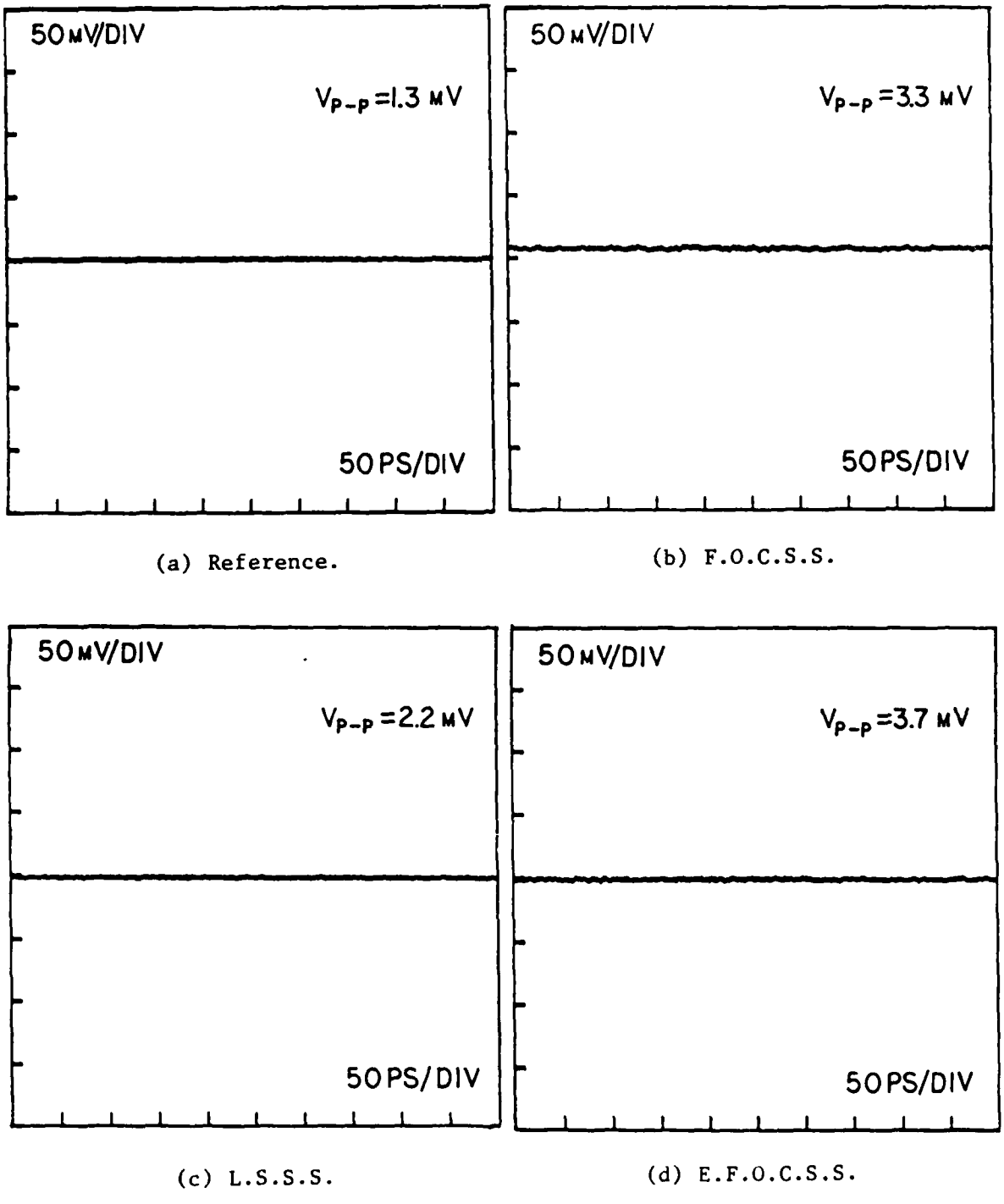

(a) Reference.

(b) F.O.C.S.S.

(c) L.S.S.S.

(d) E.F.O.C.S.S.

Figure 3.7. The average of 100 acquisitions of the baseline noise level for large vertical scale factor (50 mV/div.) .

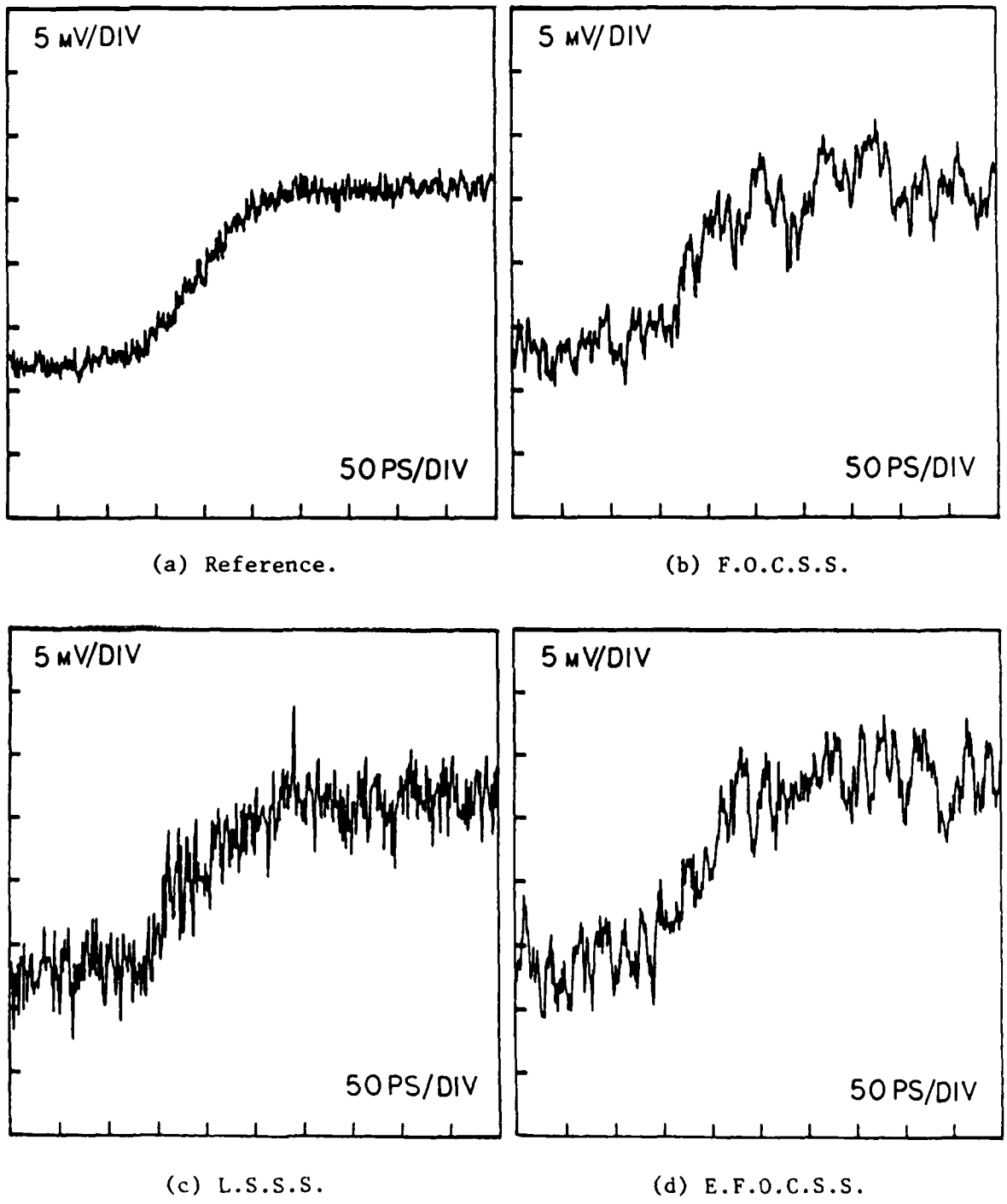

(a) Reference.

(b) F.O.C.S.S.

(c) L.S.S.S.

(d) E.F.O.C.S.S.

Figure 3.8. Single acquisition of the leading edge of the small signal test pulse.

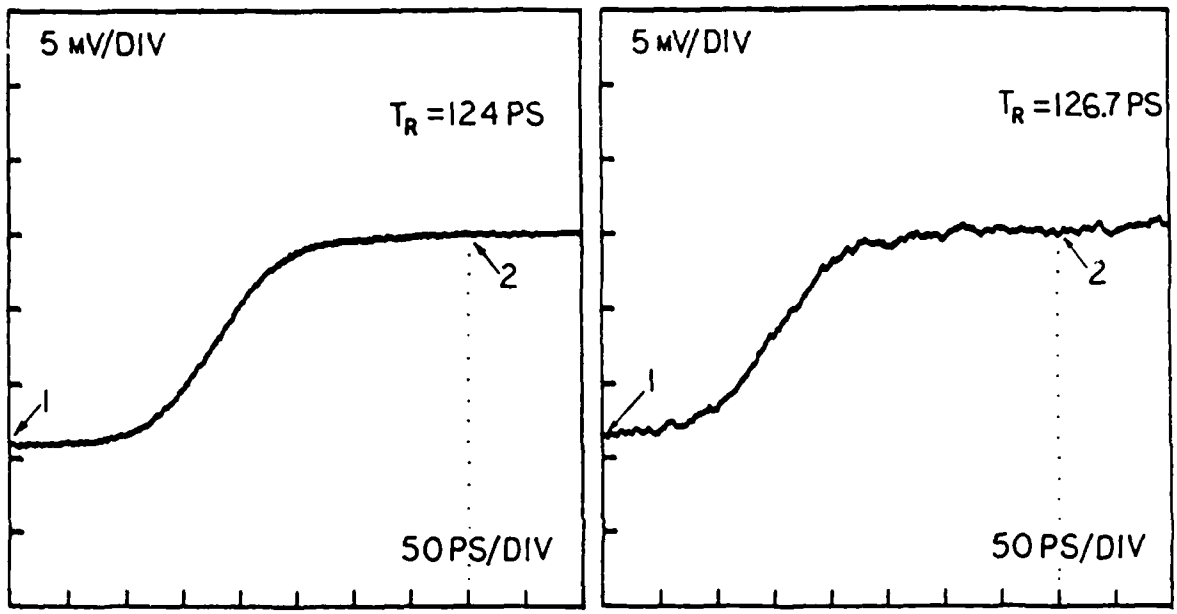

(a) Reference.

(b) F.O.C.S.S.

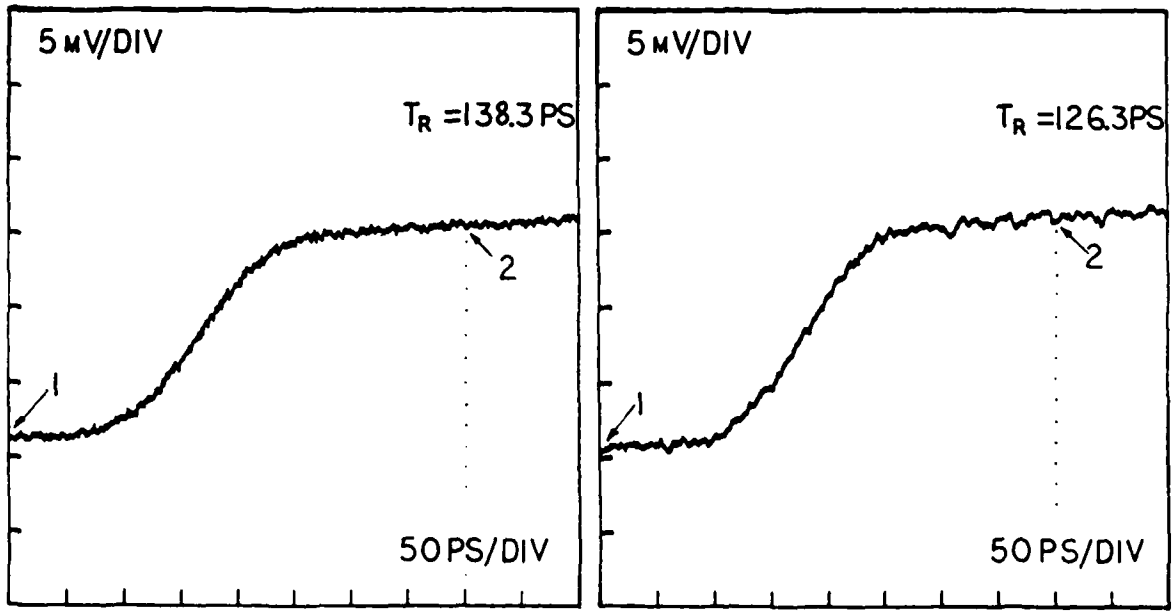

(c) L.S.S.S.

(d) E.F.O.C.S.S.

Figure 3.9. The waveforms resulting from averaging 100 acquisitions of the leading edge of the small signal test pulse.

sampling system caused by the laser link is, again, obvious in waveform c. The risetime of waveform b acquired using the F.O.C.S.S. is smaller than expected. This is due to the noise which causes an error in the voltage levels used to compute the risetime.

Figure 3.10 depicts a single acquisition of the test pulse in its entirety. Figure 3.11 shows the waveforms resulting from applying additive signal averaging to 100 acquisitions of the waveforms in Figure 3.10.

Figure 3.12 shows a single acquisition of the baseline noise level obtained with zero signal (a short) at the input of the S-6. The noise in Figure c is caused by the widely opened memory gate, while that in Figures b and d is caused by the wide memory gate and the noise contributed by the fiber optic error and feedback links.

Figure 3.13 depicts the result of applying additive signal averaging to the baseline noise of the refernce (hardwired) system and the three smapling system test configurations. The noise level is seen to be acceptably consistent with the $1/\sqrt{N}$ improvement associated with additive signal averaging.

3.5. Quantitative Tests

3.5.1. Introduction

Waveforms acquired by sampling systems are slightly distorted due to the effect of the sampling system's transfer function on the measurement. The waveforms obtained using the optically coupled sampling

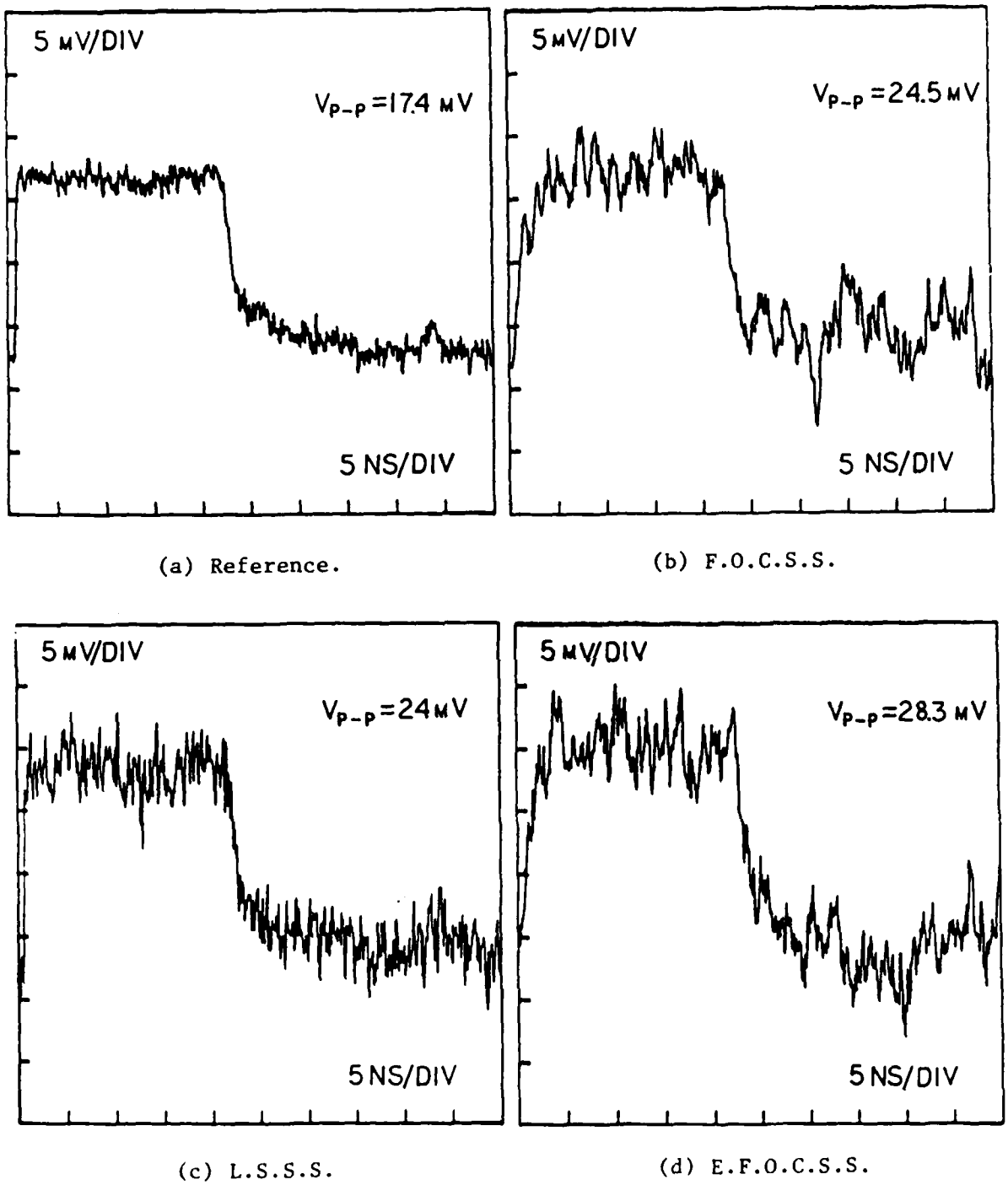

(a) Reference.

(b) F.O.C.S.S.

(c) L.S.S.S.

(d) E.F.O.C.S.S.

Figure 3.10. Single acquisition of the small signal test pulse.

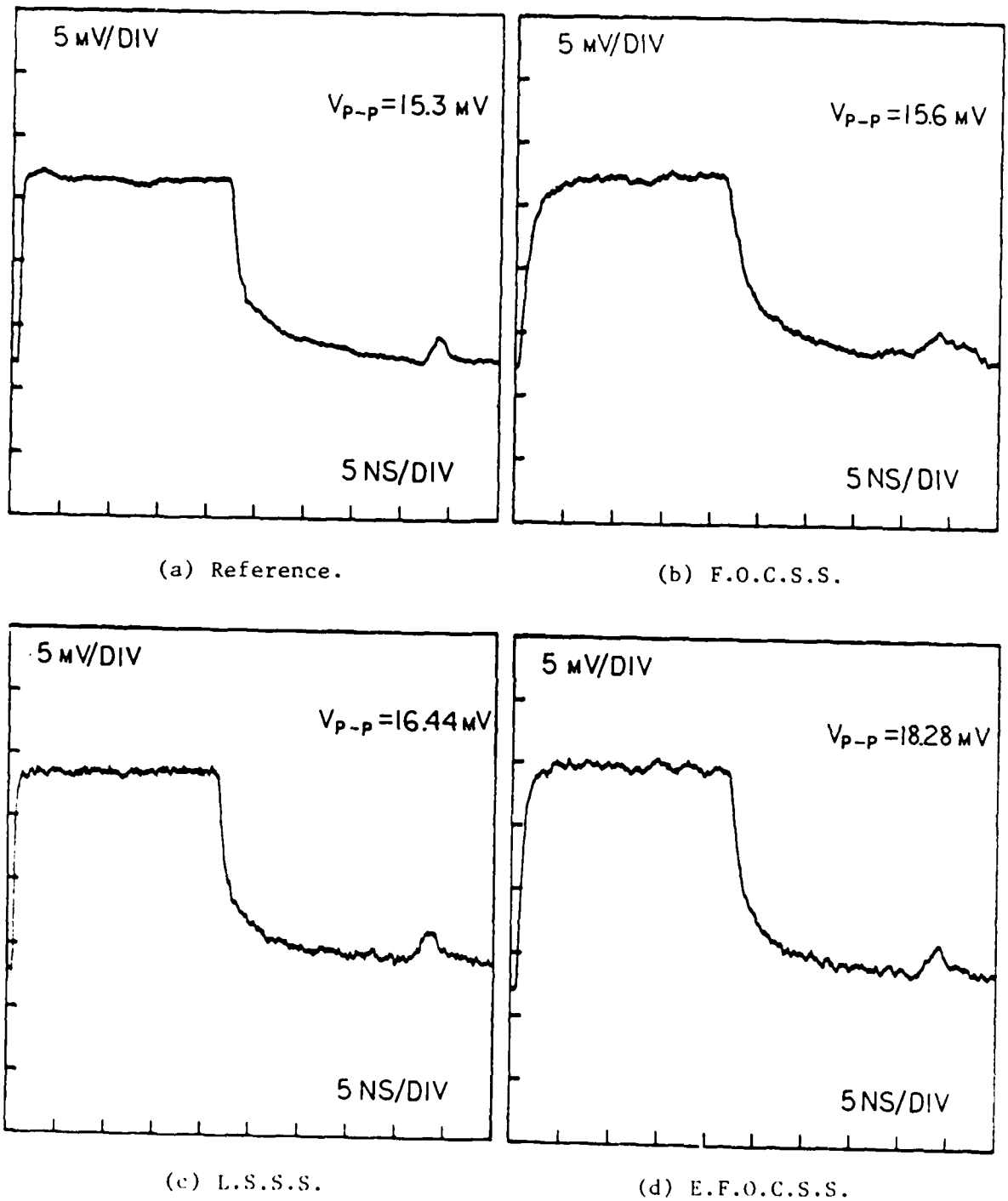

(a) Reference.

(b) F.O.C.S.S.

(c) L.S.S.S.

(d) E.F.O.C.S.S.

Figure 3.11. The waveforms resulting from averaging 100 acquisitions of the small signal test pulse.

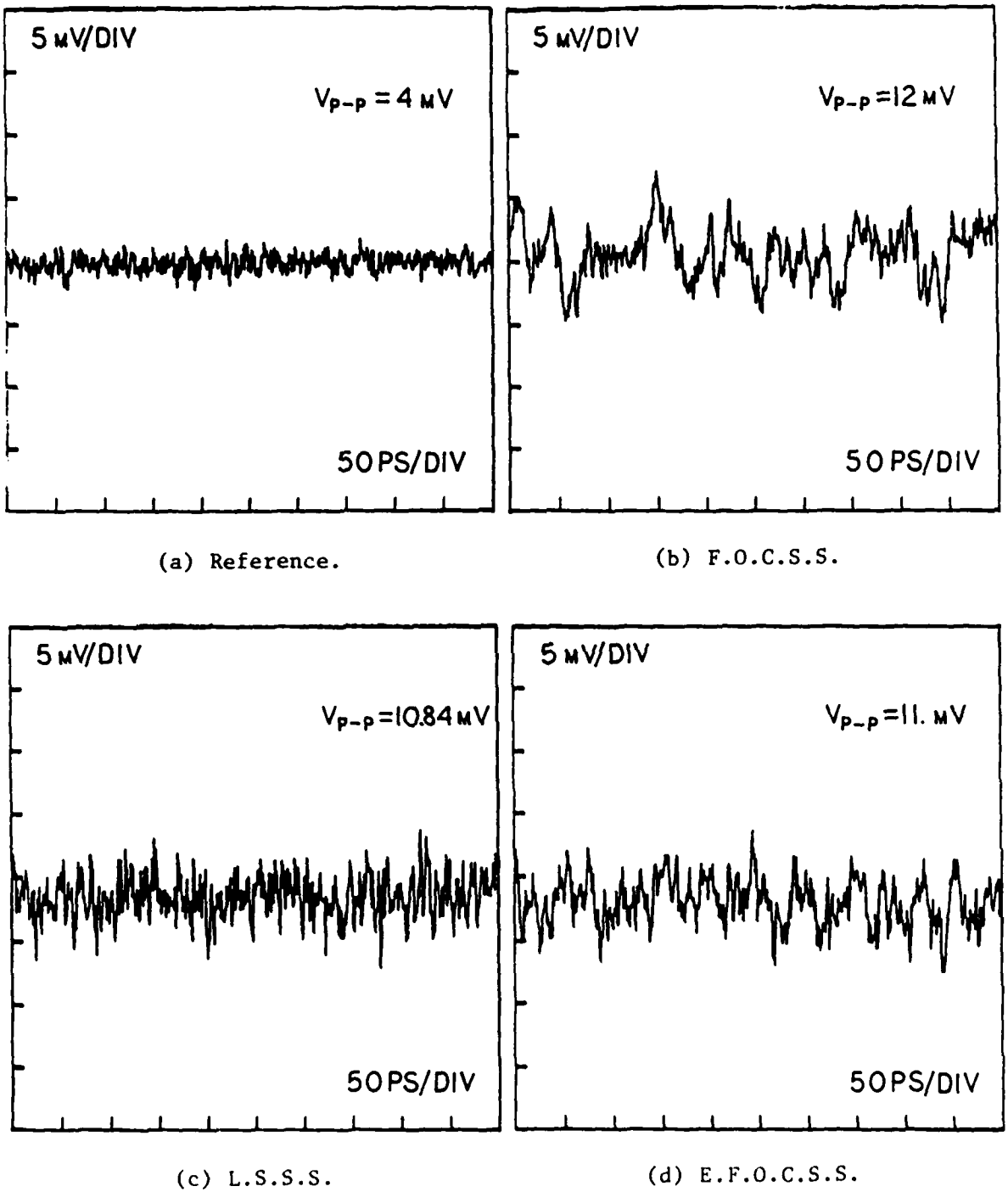

(a) Reference.

(b) F.O.C.S.S.

(c) L.S.S.S.

(d) E.F.O.C.S.S.

Figure 3.12. Single acquisition of the baseline noise level for small vertical scale factor (5 mV/div.) .

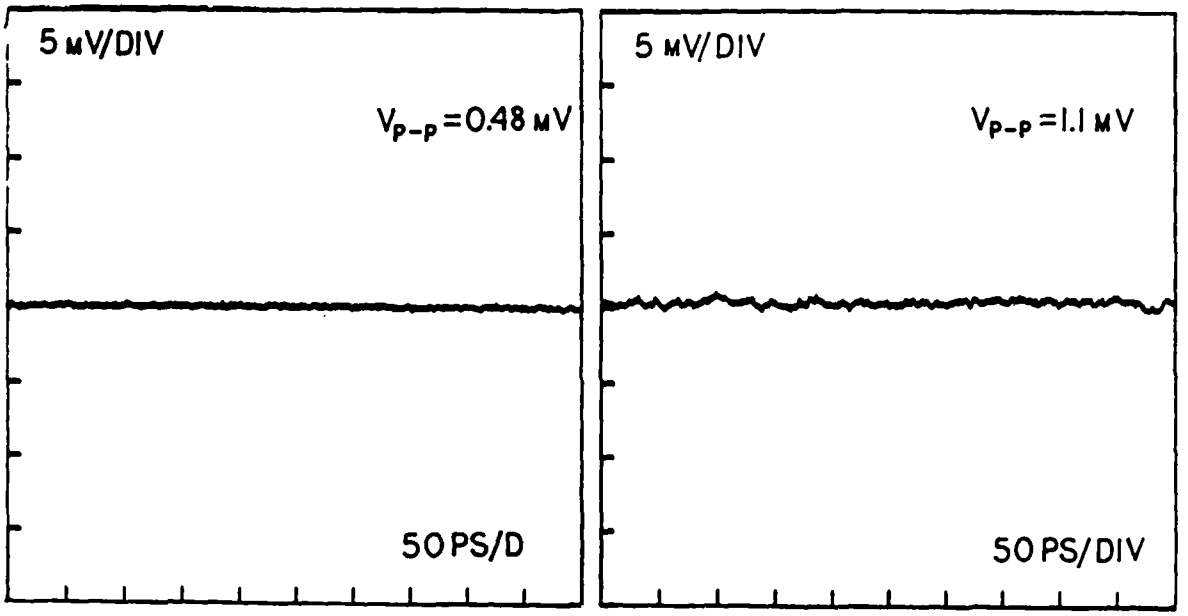

(a) Reference. (b) F.O.C.S.S.

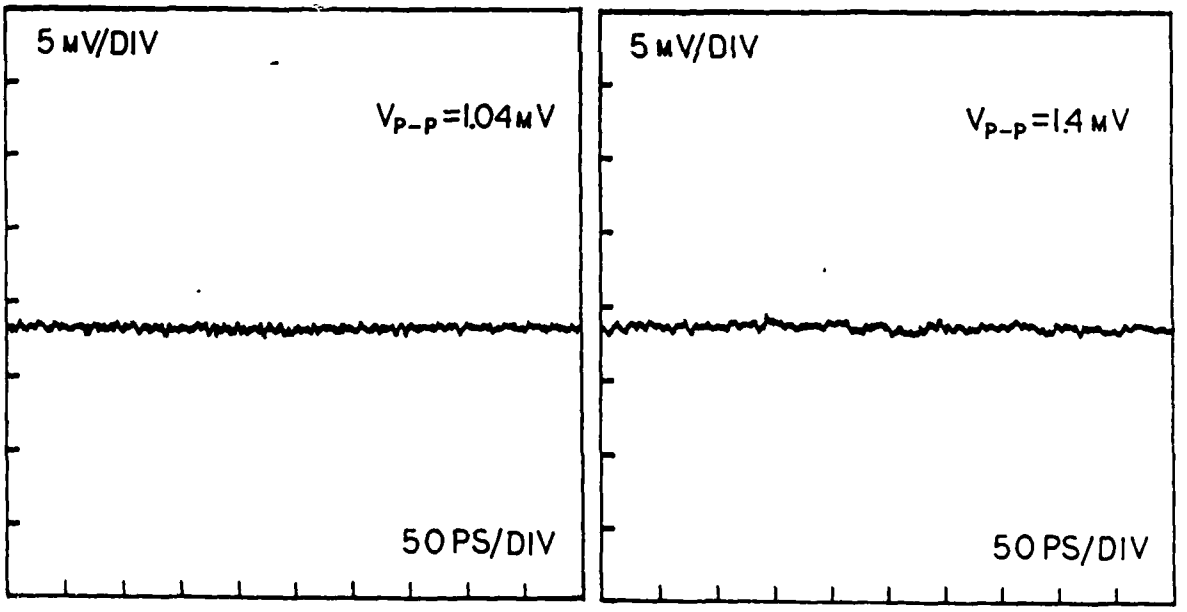

(c) L.S.S.S. (d) E.F.O.C.S.S.

Figure 3.13. The average of 100 acquisitions of the baseline noise level for small vertical scale factor (5 mV/div.) .

system are distorted further, due to the modification of the sampling system's transfer function caused by the introduction of the error, feedback, and sampling command links.

The aim of the tests reported in this section is finding frequency domain transfer functions (S(f)) which characterize the performance of the fully (or partially) optically coupled system configurations (section 3.2) with respect to that of the standard (hardwired) system. In other words, the transfer functions obtained, here, represent the following relationship:

$$S(f) = \frac{\text{Trans. func. of an optically coupled system configuration (if known)}}{\text{Trans. func. of hardwired system (if known)}}$$

Neither one of the transfer functions in the above equation is known due to the fact that the shape of an input stimulus, which would be used to empirically obtain either transfer function, is known only to the extent by which it is displayed by the standard hardwired system which is the only means of observing it.

The above difficulty was circumvented by simply acquiring a signal using both the system configuration under study and the hardwired system, and then dividing the transforms of the waveforms obtained in the two cases. Because waveforms acquired by sampling systems are only available in discrete form, the discrete Fourier transferm (DFT) of both waveforms had to be used, thus, the generic transfer funcrtions S(f) were obtained using the following formula:

$$S(f) = \frac{\text{DFT (wvfrm. acq. with an optically coupled system configuration)}}{\text{DFT (wvfrm. acquired using the hardwired system)}} \quad \ldots(3.1)$$

Such transfer functions were obtained for the three tests configurations, namely, the F.O.C.S.S., L.S.S.S., and the E.F.O.C.S.S. Both large signal and small signal tests were carried out. In the case of large signals, the three transfer functions are denoted by $S_F(f)$, $S_L(f)$ and $S_{EF}(f)$, respectively, while for small signals, they are denoted by $s_F(f)$, $s_L(f)$ and $s_{EF}(f)$. By studying the magnitude parts of these transfer functions, the limitations on the optically coupled sampling system performance were determined and their causes identified. Although the above transfer functions are defined only at a discrete number of equally spaced frequencies, their magnitude and phase parts will be shown as continuous functions of frequency for convenience.

The test strategy of section 3.2 and the test set-up shown in Figure 3.1 were employed for the tests under hand. The signal processing technique used to obtain the transfer functions is described in the following subsections.

3.5.2. Signal Processing Prior to Transformation

The signals which were used to characterize the frequency domain behavior of the optically coupled sampling system, relative to that of the standard (hardwired) system, were step-like in nature considering the sampling time window required by these tests. Figure 3.14a depicts a step-like waveform which will be used in this discussion. The direct

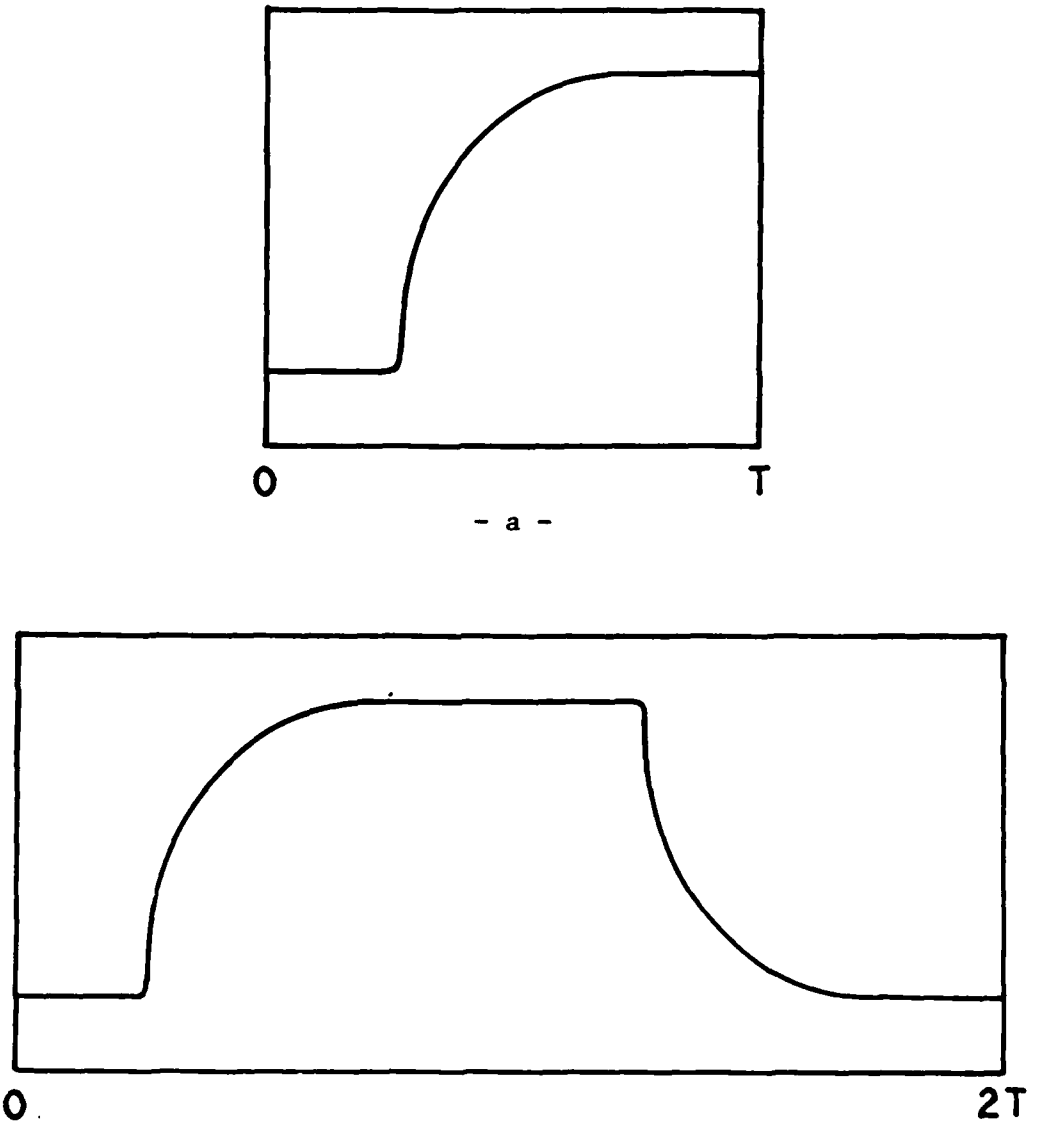

Figure 3.14. Pulse synthesis out of a step using the Gans-Nahman method.

a) Step-like waveform.
b) Pulse-like synthetic waveform.

transformation of the test signals for use in Equation 3.1 would yield erroneous transfer functions due to the leakage error in the discrete Fourier transforms caused by the abrupt time domain discontinuity at the right end of the sampling window [11], [12]. The criteria that a waveform should meet in order to guarantee that its DFT is free of leakage are that it should begin and end at the same level in the time window used and, also, that its leading and its trailing ends should have the same slope [11], [12].

The method which was used in order to make the test waveforms conform to the criteria of leakage free transformation is due to Gans and Nahman [13]. In this method, which can be applied to waveforms which begin with zero slope and have reached a constant final level, a pulse-like waveform (of 2N sample points) is synthesized using the original step-like waveform of (of N sample points), as shown in Figure 3.14b. This is done by inverting (multiplying by -1) the step-like waveform, then shifting it vertically and horizontally in order to make the leading end of the inverted waveform meet with the trailing end of the original waveform. The resulting waveform begins and ends at the same voltage level and with the same slope, namely, zero.

Gans and Nahman have shown that the DFT of the pulse-like waveform, obtained using their synthesis method described above, yields a number of nonzero discrete frequency coefficients which is equal to the number of DFT coefficients of the original waveform. The N even harmonics in the synthetic waveform transform are all zero, leaving N odd nonzero

harmonics. It was also shown in [13] that the effect of the synthesis method is to cause the discrete Fourier spectrum of the origianl waveform to be weighed by a factor of 2 with its phase left intact.

An interpretation of the shape of the synthetic waveforms which indicates the validity of the Gans-Nahman method is the fact that this is how a linear time-invariant lowpass system would respond to a pulse of proper length. The shape of the trailing edge of the response of such a system is usually an inverted replica of the response's leading edge.

Some of the drawbacks of using this method of pulse-synthesis-out-of-a- step is the possible error caused by a test waveform which has not reached a constant final value. Also, some error might be caused by any horizontal misplacement of the acquired steps in their time windows causing the synthetic pulses to be either narrower or wider than what they should be. This error was empirically kept to a minimum during waveform acquisition. The merits of using the method of pulse synthesis to eliminate frequency domain leakage more than outweigh its possible shortcomings.

3.5.3. Signal Processing, Practical Considerations

The step-like waveforms obtained in the test are the result of averaging 100 acquisitions. Each waveform is an array of 512 sample points with magnitudes in the range of -4 to 4 screen grid units. A Basic language program was written in order to generate the pulse-like

AD-A148 057 AN OPTICALLY COUPLED SAMPLING SYSTEM WITH 4 GHZ BANDWIDTH(U) MISSISSIPPI UNIV UNIVERSITY DEPT OF ELECTRICAL ENGINEERING S B SAMAAN ET AL. 30 OCT 84 2/2

UNCLASSIFIED N00014-81-K-0256 F/G 20/6 NL

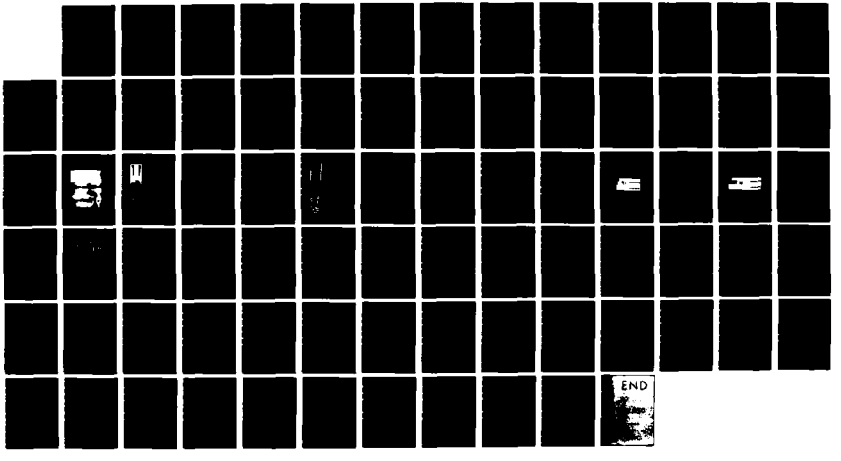

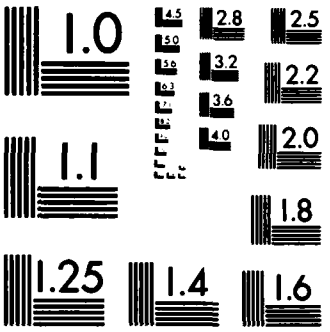

waveforms, find the discrete Fourier transformations, and obtain the required transfer functions.

Each 512 point waveform was decimated in time and a new 128 point waveform was obtained by taking one out of every four cosecutive samples of the 512 point sequence, starting at sample number 2. The 128 point step was then used to synthesize a pulse-like waveform of 256 points using the Gans-Nahman method described in the previous subsection. For the class of waveforms used in the test, the resulting 256 point waveform had a series of points on both its leading and its traiting ends which are all at the same level (corrupted only by the superimposed noise). In the following step, an estimate of this level (the average of the 2nd., 3rd., and 4th. sample levels) was subtracted from the 256 samples resulting in a lowered waveform with a baseline level of essentially zero, and hence, a standardized DC content. The resulting waveform was then transformed and its DFT used in an equation like 3.1 to find the required transfer functions.

The discrete Fourier transform of an array of N data points is defined [11], [12] by

$$X(k) = \sum_{n=0}^{N-1} x(n)\, e^{-j2\pi nk/N} \qquad k = 0,1,\ldots,N-1$$

where X(k) is the kth complex discrete Fourier coefficient, x(n) is the nth element of the transformed array which can be either real or complex, and j is $\sqrt{-1}$. In the present application x(n) is real and represents the nth sample of the time domain waveform.

The discrete Fourier transforms in this work were computed using a Fast Fourier Transform (FFT) algorithm available as a single command on the computing system used [14]. The FFT algorithm implemented is the Sande-Tukey decimation-in-frequency algorithm [12]. Only the DC component and the positive half of the frequency spectrum are returned by this FFT command.

The step signal used in these tests had a rise time on the order of 100 ps (Section 3.3). The useful harmonic content of this pulse extends up to about 7 GHz only. Above this frequency, the amplitude of the harmonics becomes too small to be distinguishable from the baseline noise level of the sampling system.

The horizontal scale setting used to acquire the 512 point waveforms in this series of tests was 500 ps/div. The sampling period resulting from this scale setting, waveform decimation, and pulse-like waveform synthesis can be computed as follows:

$$\Delta T = \frac{500 \text{ ps/div} \times 10 \text{ div}}{512/4} = 39.0625 \text{ ps.}$$

where ΔT is the sampling period. This corresponds to a sampling frequency pf 25.6 GHz, and a Nyquist frequency of 12.8 GHz. This bandwidth is optimum for showing the frequency range of interest while minimizing alias errors. For the 256 point synthetic waveforms the resulting spectral resolution in the frequency domain (Δf) is

$$\Delta f = \frac{12.8 \text{ GHz}}{128} = 100 \text{ MHz}$$

It should be noted that the decimation-in-time of the 512 point waveform could have been avoided, while maintaining the same measurement bandwidth and an increased resoltuion, simply by choosing a horizontal scale setting of 4 x 500 ps/div = 2 ns/div. This setting was found to be detrimental to the computed transfer functions, however, due to the effect of drift and noise on the small number of sample points remaining on the rising edge of the waveform.

To substantiate the claim made earlier that the noise level of the measurement is such that it makes the useful freuqency content of the reference test signal extend up to about 7 GHz only, two test waveforms were acquired using the standard sampling system, and the quotient of their DFT's was found. The magnitude and phase parts of the quotient are shown in Figure 3.15. Random noise is seen to be prevalent above 7 GHz.

3.5.4. Large Signal Test Results

Figure 3.16a depicts the reference step-like waveform acquired using the hardwired (standard) sampling system. Figure 3.16b shows the pulse-like reference waveform resulting from the application of the Gans-Nahman synthesis method and the DC level shifting described in the previous subsections. In Figure 3.17a, the magnitude spectrum of the reference pulse-like waveform is shown in units of dBV[5], while its phase spectrum is depicted in Figure 3.17b.

---

[5] V in dBV = 20 $\log_{10}$(V in volts/1 volt).

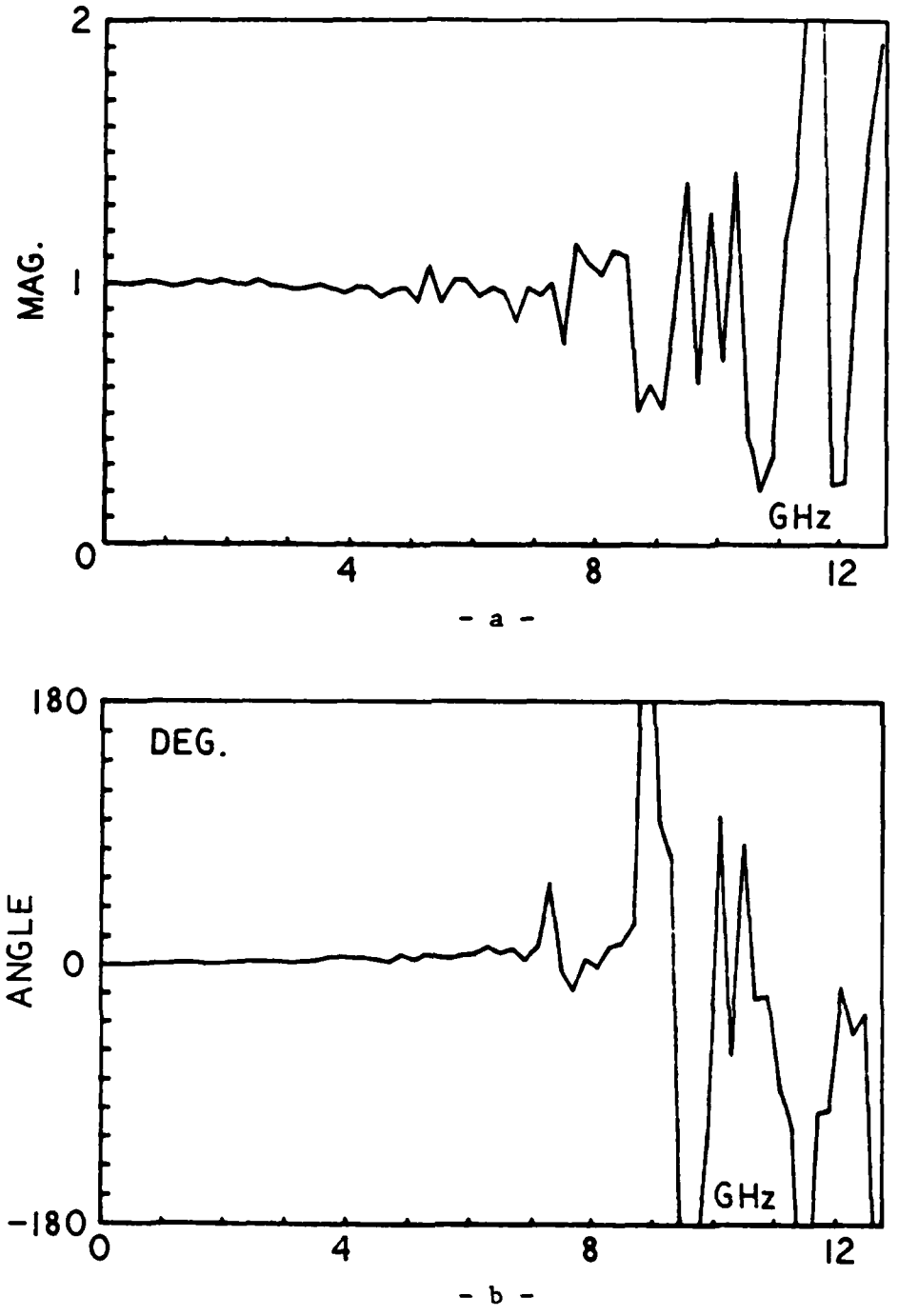

Figure 3.15. The quotient of the DFT's of two reference waveforms.
a) The magnitude part.
b) The phase part.

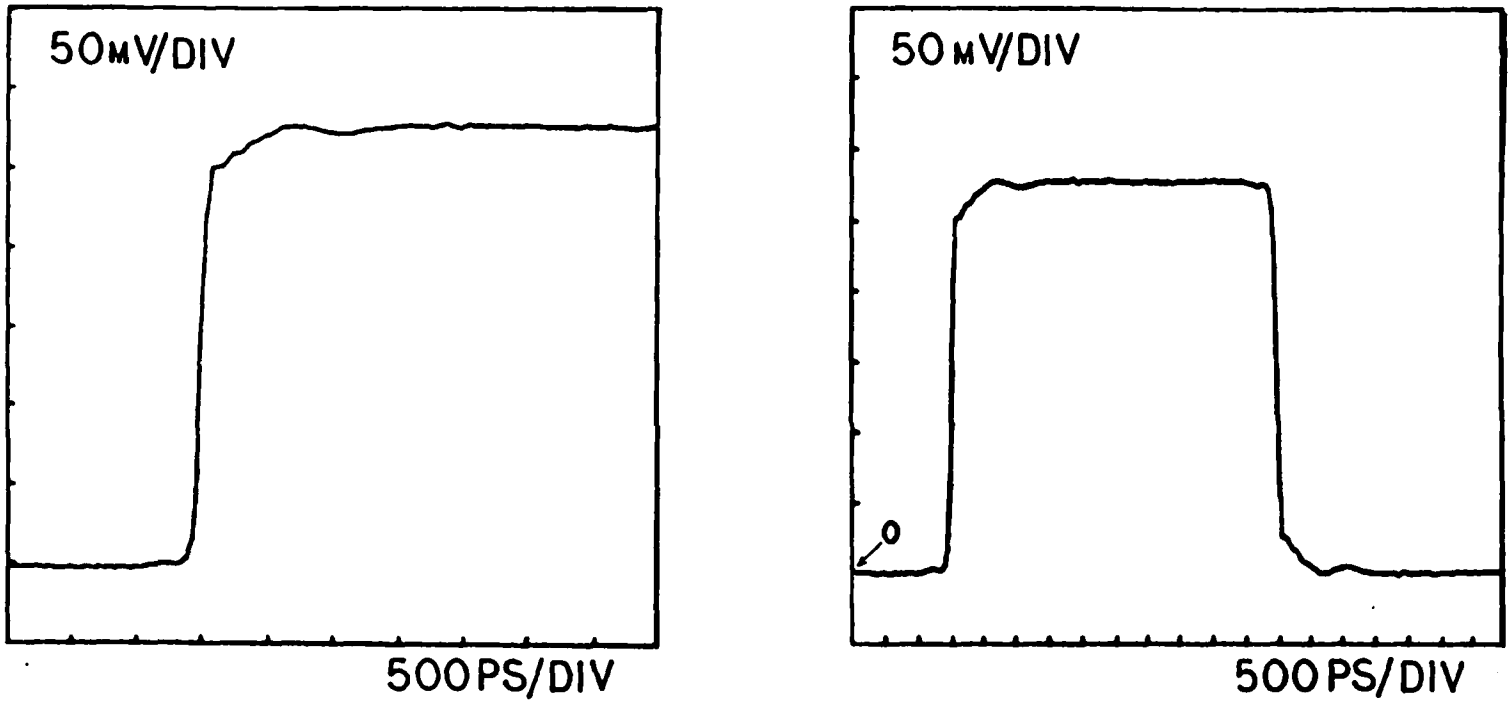

Figure 3.16. a) The large signal reference step-like waveform.
b) The large signal reference synthetic pulse-like waveform.

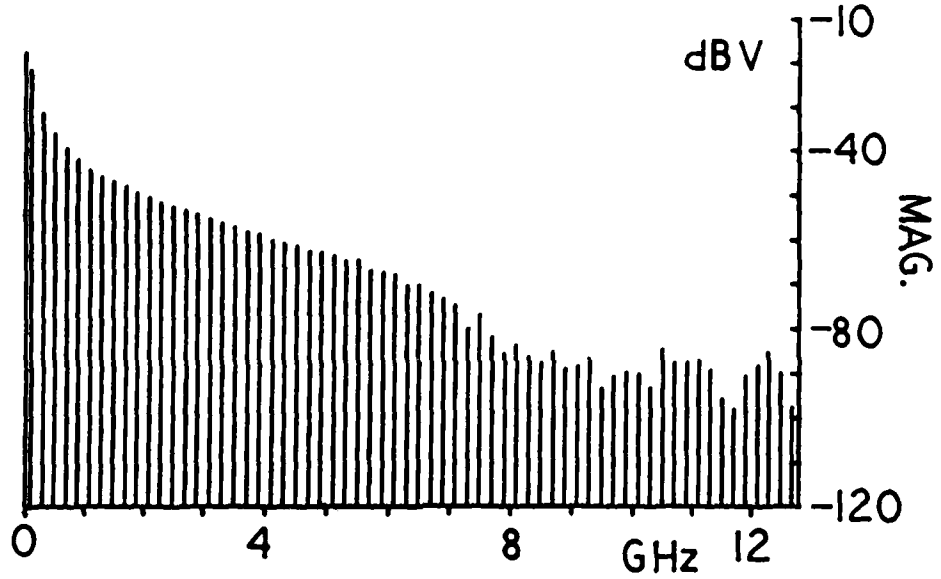

- a -

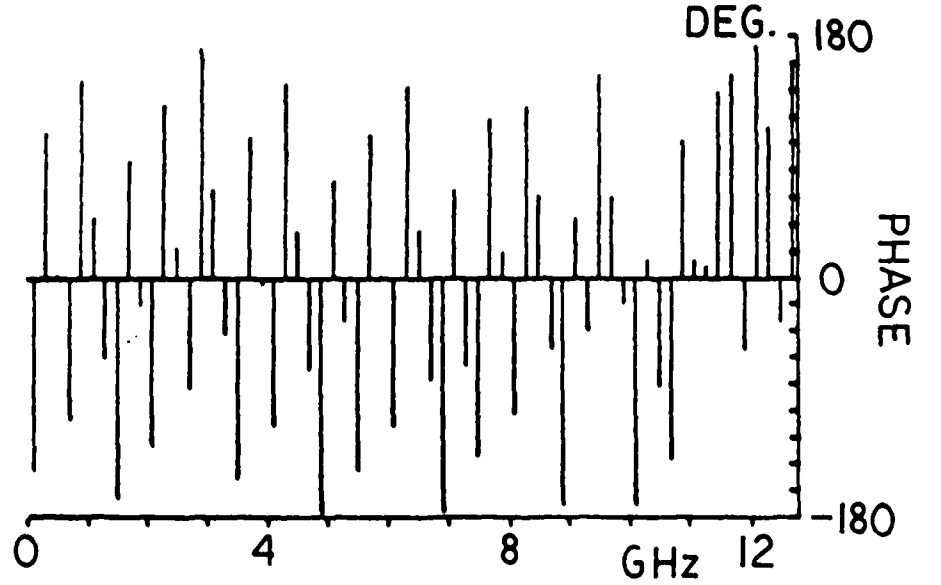

- b -

Figure 3.17. The DFT of the large signal reference pulse-like waveform.
a) The magnitude part.
b) The phase part.

Figure 3.18 depicts the step-like test waveforms acquired using the three test configurations, namely, the F.O.C.S.S., the L.S.S.S., and the E.F.O.C.S.S. The reference waveform is repeated in the same figure for convenience. In Figure 3.19, the pulse-like synthetic waveforms obtained from those of Figure 3.18 are shown.

Figure 3.20 depicts the magnitude part of the transfer functions $S_F(f)$, $S_L(f)$, and $S_{EF}(f)$ defined in Subsection 3.5.1. The range of frequencies of interest in these figures extends only from 0 to about 6 GHz; above this frequency, the spectra are random due to the prevailing noise level.

The lowpass character of the F.O.C.S.S. relative to the standard system is evident in the magnitude part of $S_F(f)$. Since the bandwidth of the hardwired (7S12)-(S-6) system extends up to 11.5 GHz, it can be safely assumed that the bandwidth of the F.O.C.S.S. is the 3 dB cutoff frequency indicated on Figure 3.20a, namely, 4 GHz.

Figure 3.20c shows the slight lowpass behavior caused by the error and feedback links alone, while Figure 3.20b shows the lowpass effect of the sampling command laser link. The reason behind the lowpass character caused by the laser link will be discussed further in the conclusions presented in Chapter 4.

Figure 3.21 shows the phase part of the transfer functions $S_F(f)$, $S_L(f)$, and $S_{EF}(f)$. The phase of the three functions is essentially zero,except for a linear component which extends from 0 to about 20 degrees in the range 0-6 GHz. The linear phase increase indicates a

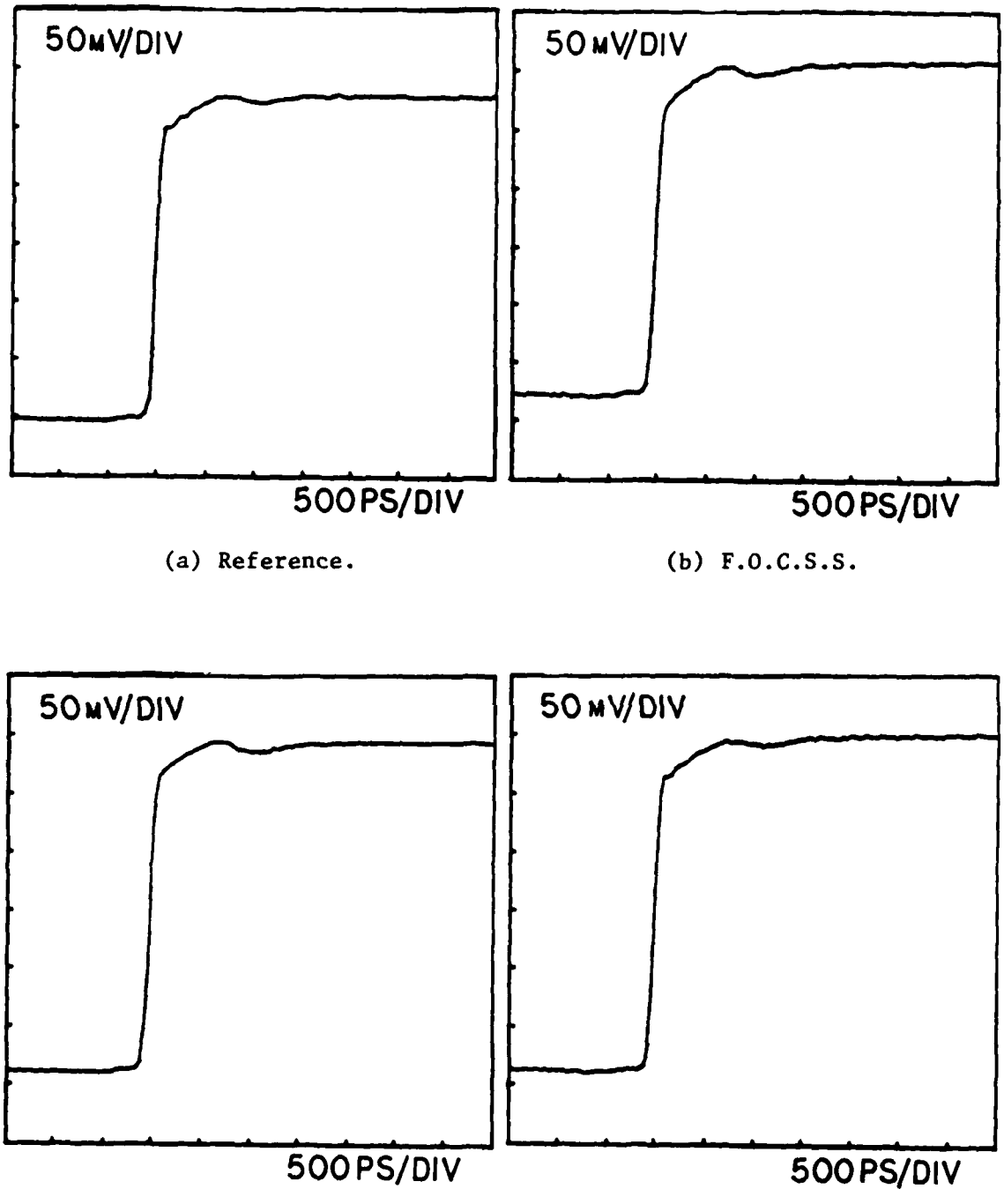

(a) Reference. (b) F.O.C.S.S.

(c) L.S.S.S. (d) E.F.O.C.S.S.

Figure 3.18. The large signal step-like waveforms used for quantitative analysis (average of 100 acquisitions).

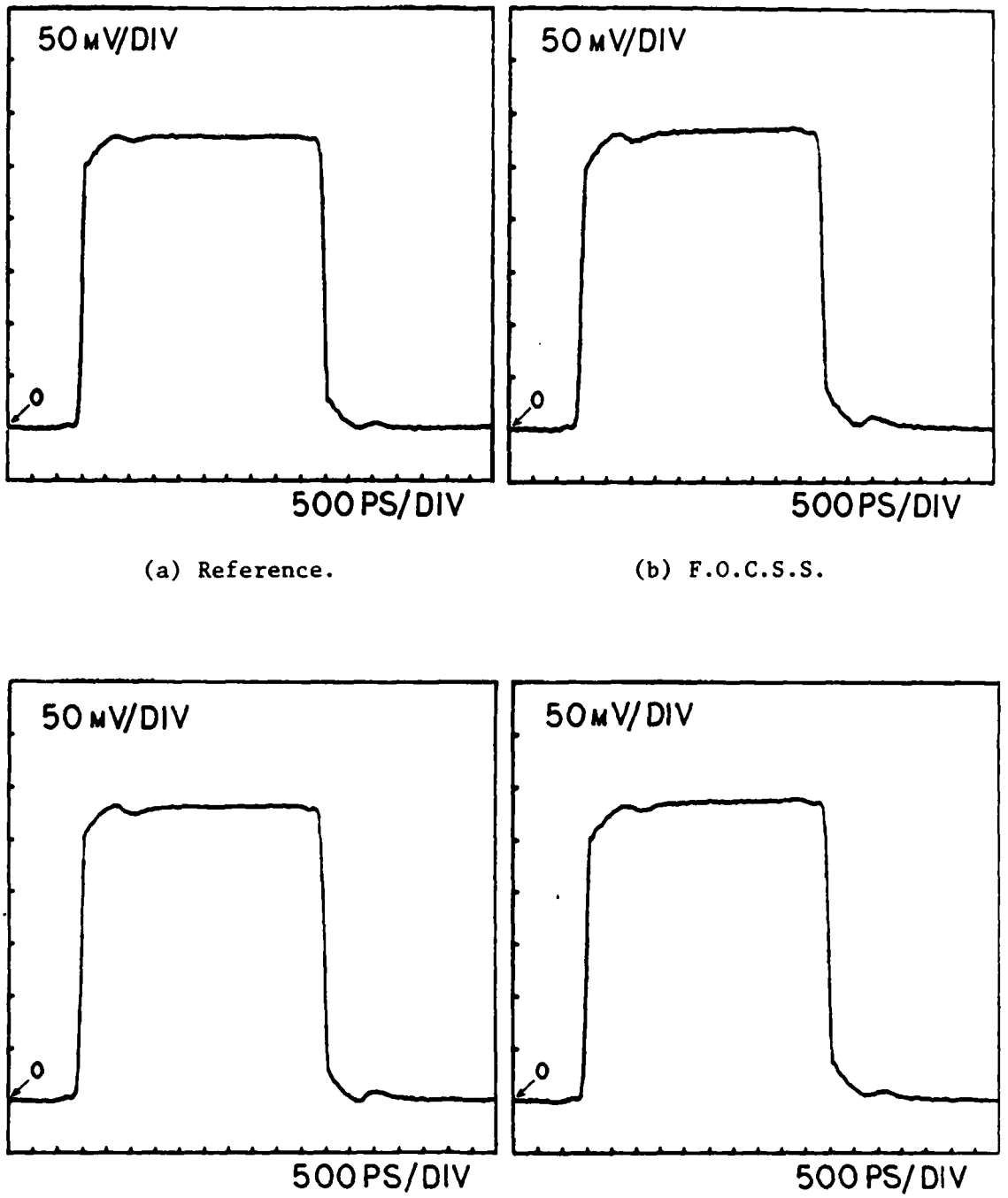

(a) Reference.

(b) F.O.C.S.S.

(c) L.S.S.S.

(d) E.F.O.C.S.S.

Figure 3.19. The large signal synthetic pulse-like waveforms obtained by applying the Gans-Nahman method with DC level shifting to the waveforms of figure 3.18.

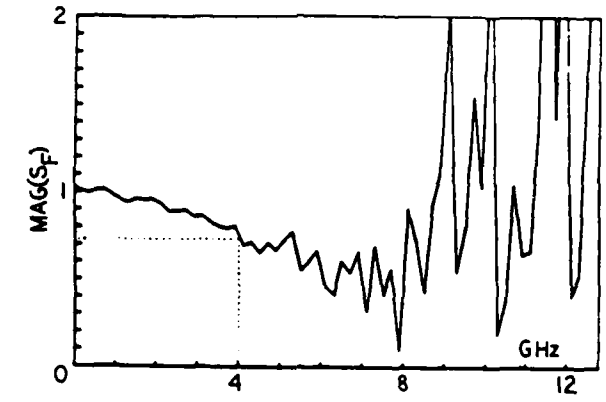

(a) F.O.C.S.S.

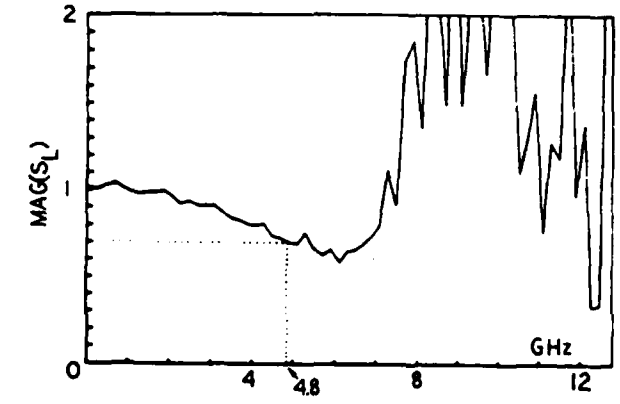

(b) L.S.S.S.

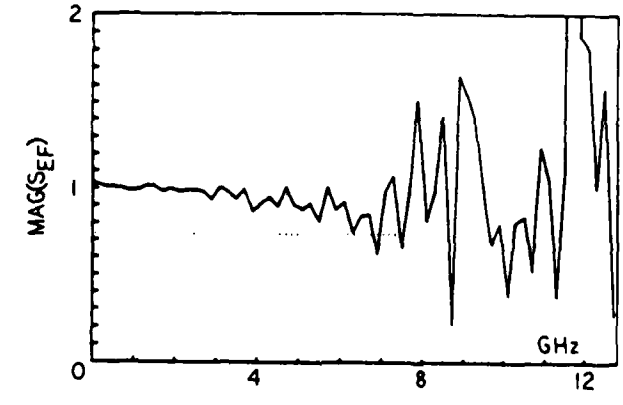

(c) E.F.O.C.S.S.

Figure 3.20. The magnitude part of the transfer functions: $S_F(f)$, $S_L(f)$, and $S_{EF}(f)$.

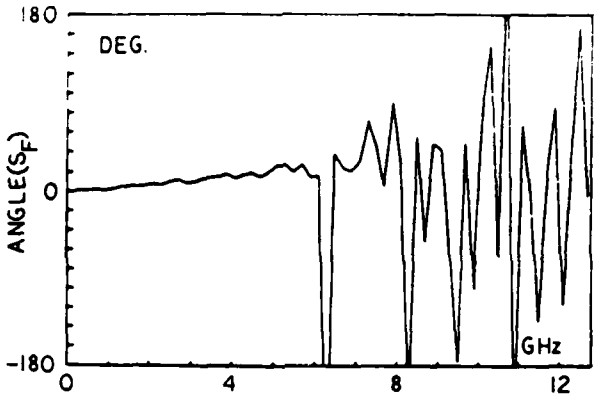

(a) F.O.C.S.S.

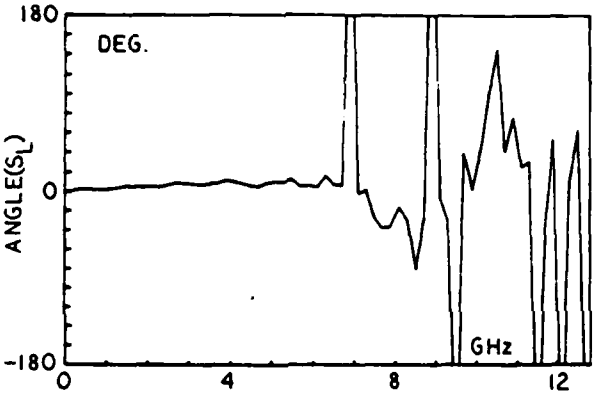

(b) L.S.S.S.

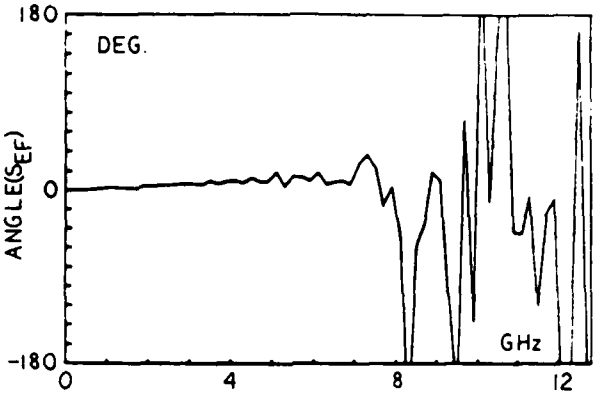

(c) E.F.O.C.S.S.

Figure 3.21. The phase part of the transfer functions: $S_F(f)$, $S_L(f)$, and $S_{EF}(f)$.

temporal shift in waveforms b, c, and d of Figure 3.19 relative to the reference waveform a and is, otherwise, nonharmful.

3.5.5. Small Signal Test Results

Figure 3.22 depicts the pulse-like small amplitude reference signal and the pulse-like synthetic reference signal obtained from it. Figure 3.23 depicts the magnitude and phase spectra of the reference waveform. The early appearance of noise in the spectrum of this signal is due to its small amplitude.

Figure 3.24 depicts the step-like test waveforms acquired using the three test configurations, namely, the F.O.C.S.S., the L.S.S.S., and the E.F.O.C.S.S. The reference waveform is repeated in the same figure for convenience. In Figure 3.25, the pulse-like synthetic waveforms obtained from those of Figure 3.24 are shown.

Figure 3.26 shows the magnitude part of the small signal transfer functions $s_F(f)$, $s_L(f)$, and $s_{EF}(f)$. Figure 3.26c shows the slight lowpass effect of the error and feedback links. Figure 3.26b shows the lowpass effect of the sampling command link. The F.O.C.S.S. is lowpass in nature relative to the standard (hardwired) system, as can be seen in Figure 3.26a. Due to the noise distorting $s_F(f)$, only an estimate of the 3 dB cutoff frequency of the F.O.C.S.S. can be sought, and this is seen to be about 3.7 GHz.

Figure 3.27 depicts the phase part of the small signal transfer functions. The phase is essentially zero except for a small linear

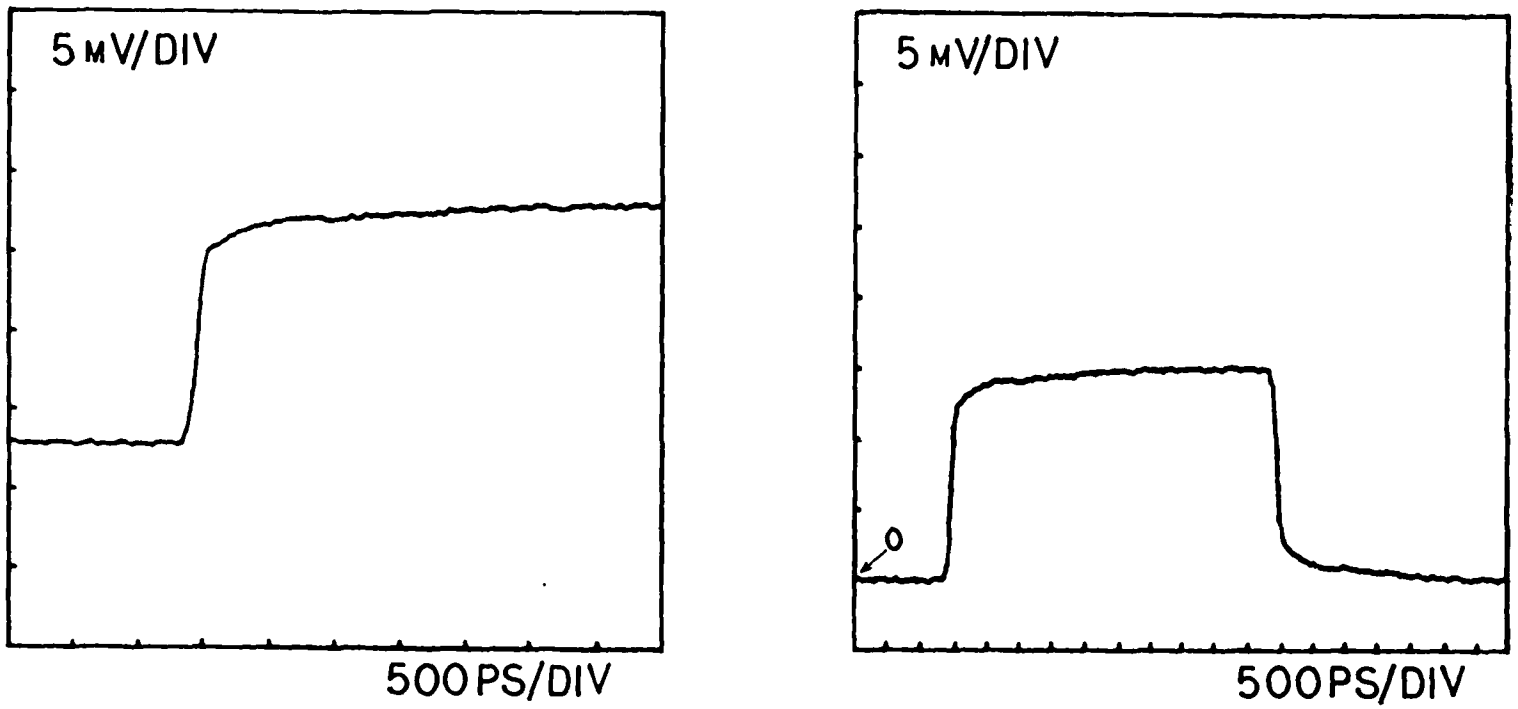

- a -

Figure 3.22. a) The small signal reference step-like waveform.
b) The small signal reference synthetic pulse-like waveform.

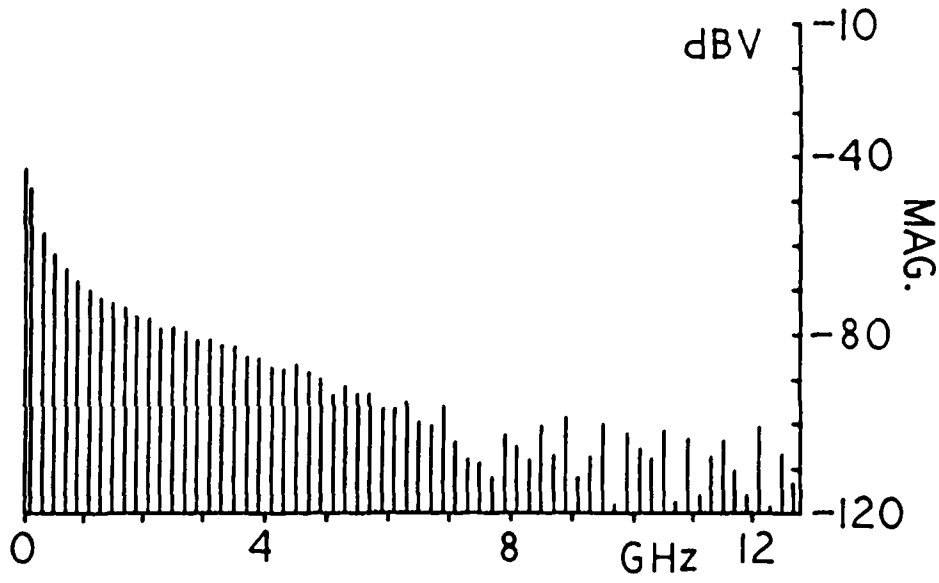

- a -

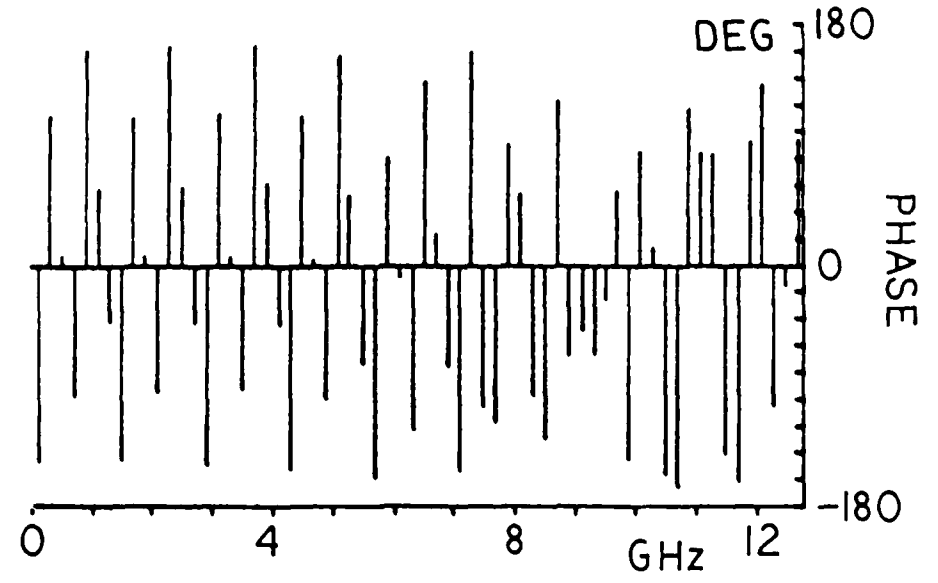

- b -

Figure 3.23. The DFT of the small signal reference pulse-like waveform.
a) The magnitude part.
b) The phase part.

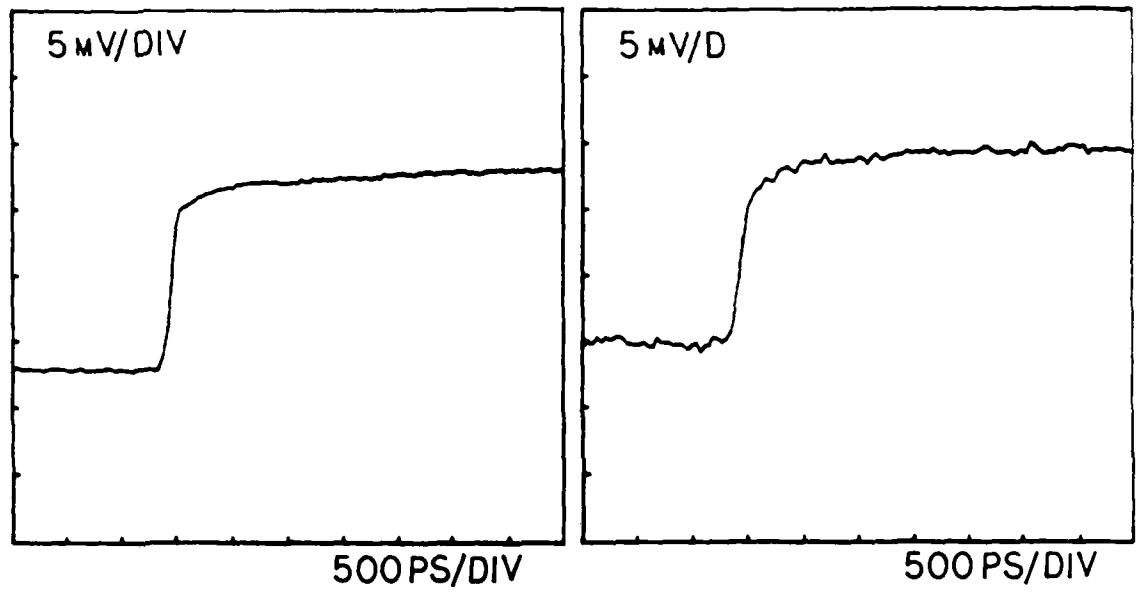

(a) Reference.

(b) F.O.C.S.S.

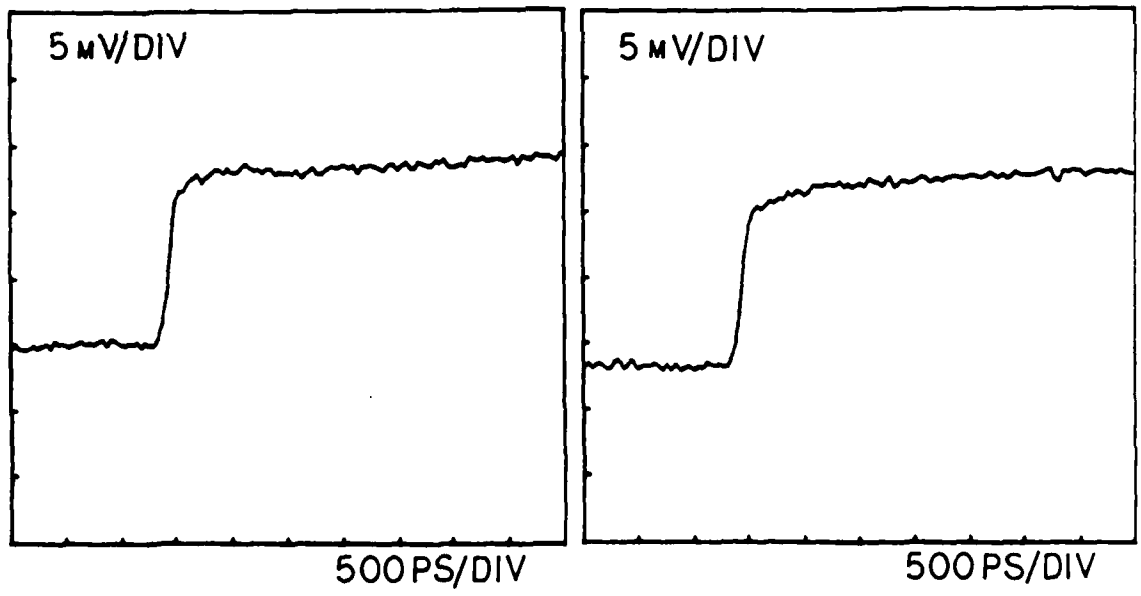

(c) L.S.S.S.

(d) E.F.O.C.S.S.

Figure 3.24. The small signal step-like waveforms used for quantitative analysis (average of 100 acquisitions).

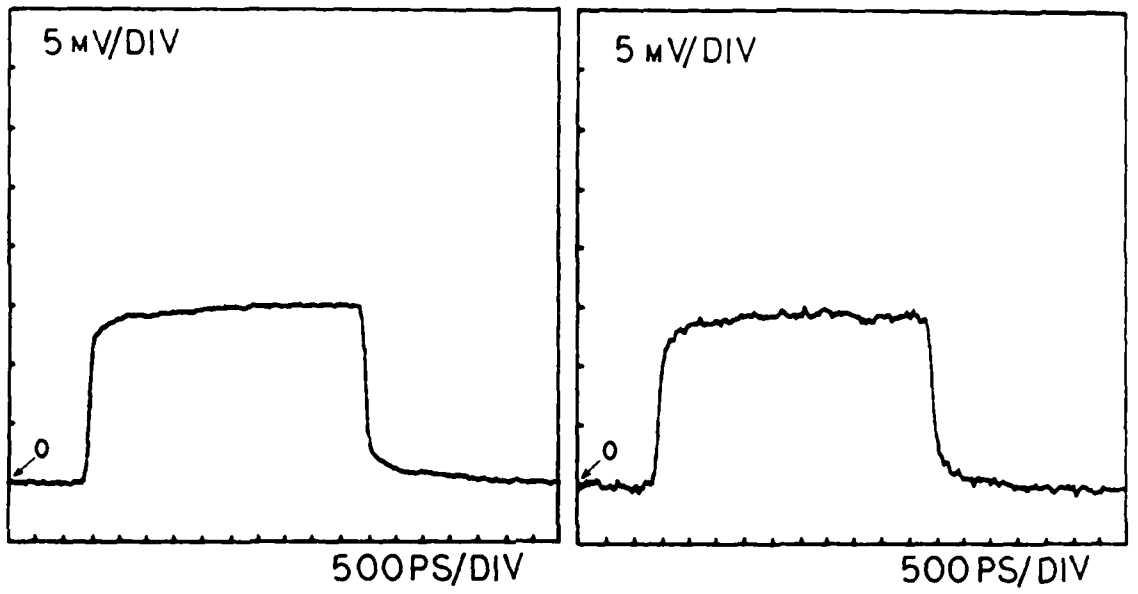

(a) Reference. (b) F.O.C.S.S.

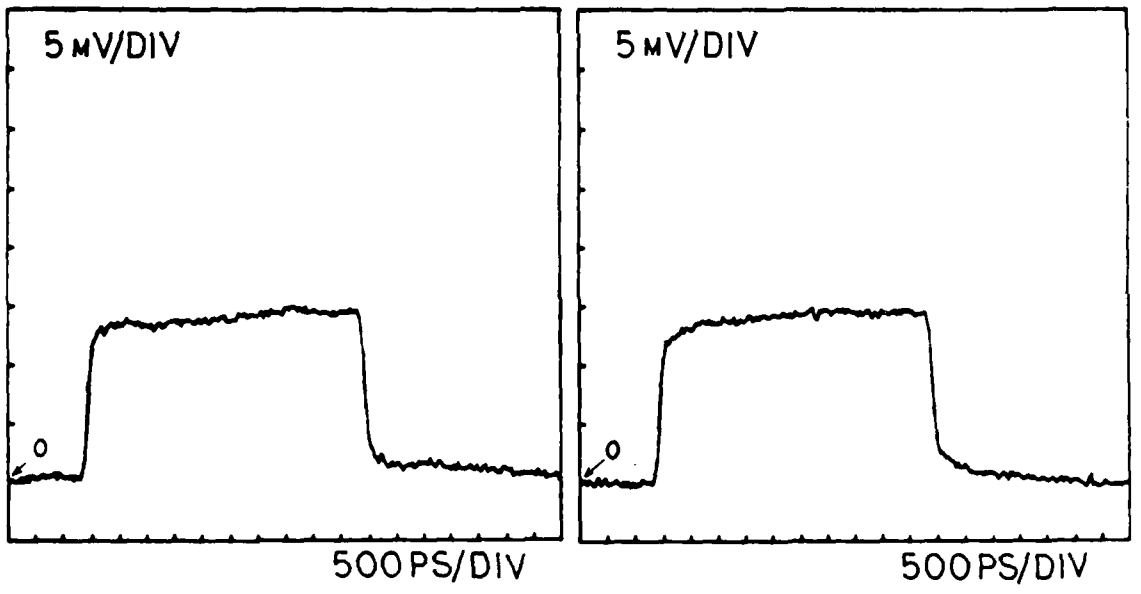

(c) L.S.S.S. (d) E.F.O.C.S.S.

Figure 3.25. The small signal synthetic pulse-like waveforms obtained by applying the Gans-Nahman method with DC level shifting to the waveforms of figure 3.24.

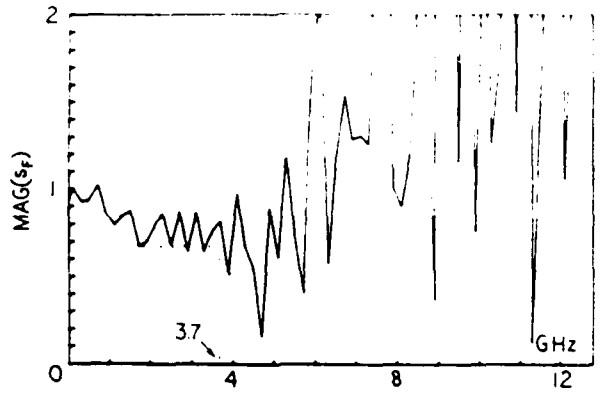

(a) F.O.C.S.S.

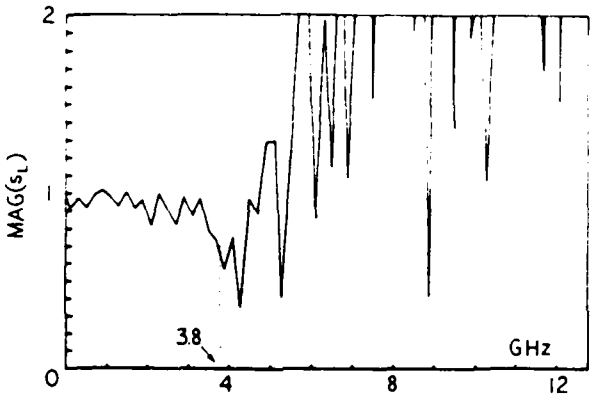

(b) L.S.S.S.

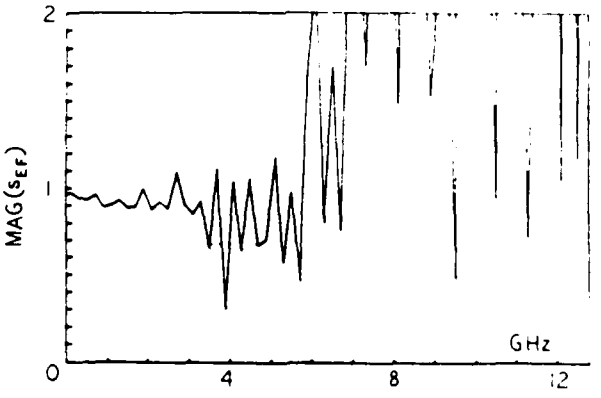

(c) E.F.O.C.S.S.

Figure 3.26. The magnitude part of the transfer functions: $s_F(f)$, $s_L(f)$, and $s_{EF}(f)$.

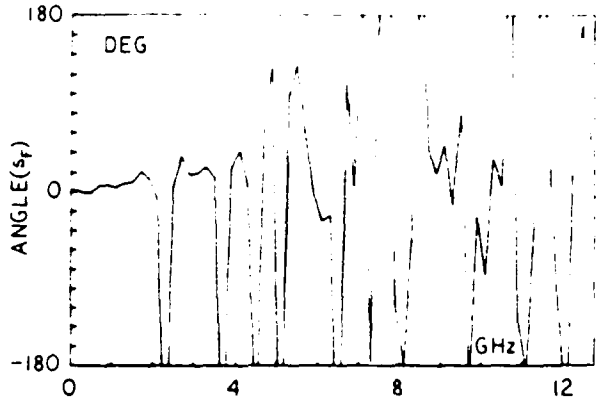

(a) F.O.C.S.S.

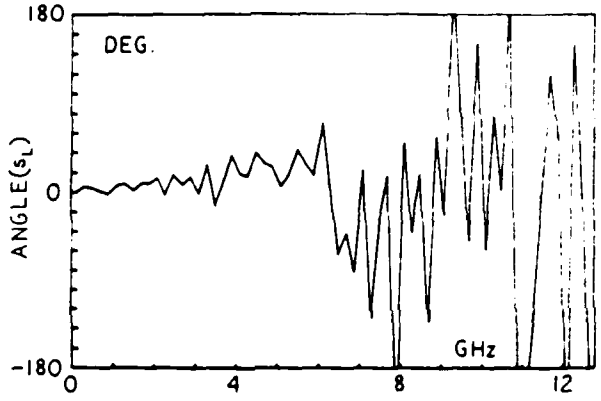

(b) L.S.S.S.

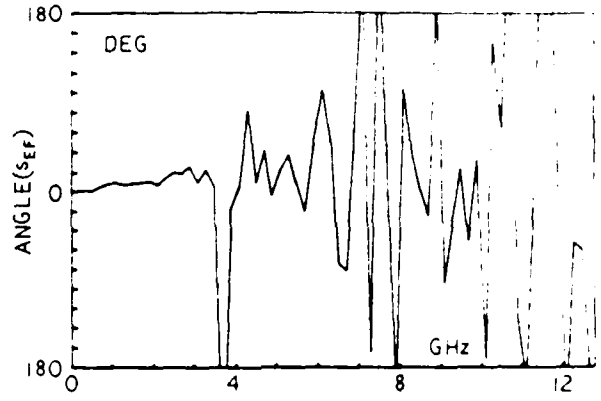

(c) E.F.O.C.S.S.

Figure 3.27. The phase part of the transfer functions: $s_F(f)$, $s_L(f)$, and $s_{EF}(f)$.

component in the range 0-2 GHz. The linear component of the phase can be attributed to a slight displacement of the test waveforms in their time windows.

The small signal transfer functions presented, here, were expected to be identical to the large signal transfer functions presented earlier. This is not the case due to the small S/N ratio of the acquired waveforms. The noise in the small amplitude time domain waveforms distorts their DFT spectra, mainly by introducing alias errors due to the high frequency nature of the noise. Horizontal drift and vertical drift (which is somewhat more significant for small vertical voltage settings of the sampling oscilloscope) cause a distortion in the acquired waveforms, consequently, affecting the shape of the small signal transfer functions.

CHAPTER 4

CONCLUSION

4.1. Conclusions on System Performance

From the results of the qualitative and quantitative tests performed on the fiber optically coupled sampling system reported in this work, the following conclusions regarding its performance and the performance of its different parts can be made.

1. The lowpass behavior of the optically coupled sampling system when additive signal averaging is employed is mainly due to the time jitter introduced by the laser link into the sampling strobe pulses. This can be seen from the lowpass nature of $S_F(f)$ and $S_L(f)$ while $S_{EF}(f)$ is only slightly lowpass (Figure 3.20). The above conclusion is further supported by the fact that the phase (Figure 3.21) of $S_F(f)$, $S_L(f)$ (and also $S_{EF}(f)$) is essentially zero, except for a linear component which can be attributed to a slight relative displacement of the time domain waveforms in their respective time windows. This zero phase shift, along with the Gaussian-like shape of the magnitude parts of $S_F(f)$ and $S_L(f)$ (in the frequency range of interest), is exactly what Gans [15] has predicted for a system where additive signal averaging is employed in the presence of strobe jitter (Appendix C).

The lowpass nature of the system can, also, be inferred from the increased risetime of the waveforms of Figures 3.3b and 3.3c with respect to the reference waveform. The error and feedback links contribute only slightly to the lowpass behavior of the system, as can be seen from the slightly lowpass character of $S_{EF}(f)$ and the slightly higher risetime of the waveform in Figure 3.3d. The lowpass effect of the error and feedback links can be attributed to a maladjustment of their transient gains rendering the sampling loop gain somewhat smaller than unity (Subsection B.4.6).

2. The distortion in the waveforms acquired by the optically coupled sampling system, aside from being caused by the lowpass nature of the system, as described above, is, also, produced by nonlinear distortion in the error and feedback links. In the case of the feedback link, a contributing factor to its nonlinearity is what appears to be a thermally induced distortion. Here, the optical output power of the transmitter's LED drops after a sudden increase in the LED's forward current. This phenomenon was discussed in Subsection 2.10.2.

3. The widely opened memory gate allows more noise into the memory circuit of the 7S12 resulting in noisy sampled waveforms. This effect is obvious in waveform c of Figure 3.2 where the flat parts of the waveform are noisier than those of the reference waveform. The baseline noise level is, also, seen to be higher as shown in Figures 3.6c and 3.12c.

The error and feedback links introduce additional noise into the system as can be inferred from the qualitative test results for the E.F.O.C.S.S. and F.O.C.S.S. configurations (especially obvious in the case of small test signals), as well as from the transfer functions $S_F(f)$, $S_{EF}(f)$, $s_F(f)$, and $s_{EF}(f)$. The noise introduced by the error and feedback links is due to photodetector noise, thermal noise, and electromagnetic pickup. The noise is more significant in the case of small test signals due to the lower signal to noise ratio associated with small signal amplitudes. Additive signal averaging of 400 to 1000 waveforms, instead of only 100, would improve the signal to noise ratio for small test signals. The number of averaged waveforms was limited to 100, however, in order to shorten the acquisition time and avoid the horizontal and vertical drift which cause a distortion in the acquired waveforms. Vertical drift is somewhat significant for small voltage settings of the oscilloscope due to the discharging of the battery pack used to power the sampling head and its associated fiber optic circuits.

4. Due to the independence of the sampling command link from the vertical voltage setting, strobe jitter must be the same for small acquired waveforms as it is for large ones. Also, if the fiber optic error and feedback links are assumed to perform at least as well as they do for large waveforms, then the transfer functions $s_F(f)$, $s_L(f)$, and $s_{EF}(f)$ must be identical to $S_F(f)$,

$S_L(f)$, and $S_{EE}(f)$, respectively. This is not exactly the case due to the fact that the signal to noise ratio associated with the small test waveforms is smaller than for large waveforms, which matter, affects the results of the deconvolution process used to obtain $s_F(f)$, $s_L(f)$, and $s_{EF}(f)$.

5. An estimate of the standard deviation of the strobe jitter in the optically coupled system can be obtained by assuming the magnitude part of $S_L(f)$ in Figure 3.20b to be essentially Gaussian in the range 0-6 GHz and applying Gan's formulas (Eq. C.3 and Eq. C.4). Thus for the L.S.S.S. which has a 3 dB bandwidth of 4.8 GHz, Equation C.3 gives for the frequency standard deviation σ_f the value

$$\sigma_f = 5.76 \text{ GHz}$$

and from Equation C.4 the standard deviation of the strobe pulse jitter is seen to be

$$\sigma_t = 28 \text{ ps}$$

4.2 Recommendations for Future Work

Improvement in the noise and bandwidth performance of the optically coupled sampling system can be achieved in a future version of the system which takes into consideration the following points:

1. If a fiber optic error link of limited bandwidth is used then the memory gate generator in the 7S12 sampling unit must be modified by introducing a circuit which delays the memory gate pulse by about 0.5 μs. With this arrangement, increasing the gate width to compensate for the delay introduced into the error signal by the fiber optic link can be avoided. This is expected to reduce substantially the noise superimposed on the waveforms acquired by the system.

2. Analog fiber optic links with a maximum noise level of less than 0.1 mV rms must be used in order to reduce the noise introduced into the feedback and error signals. These links could be built using discrete components in order to reduce space requirements and provide the designer a choice of low noise LED's and photodetectors. Expert shielding and grounding of the analog links should further reduce the noise by minimizing the EM interference within the system.

3. On board voltage regulation must be added to the remote part of the system in order to avoid the drift which is caused by the drop in the voltage supplied by the rechargeable battery pack. By eliminating the drift, a larger number of acquired waveforms may be averaged in order to enhance the S/N ratio of the measurements carried out using the F.O.C.S.S. system.

4. A higher bandwidth than the 4 GHz reported in this work may be obtainable. If the present sampling command link is to be

used, a reduction in the strobe jitter responsible for limiting the bandwidth may be achieved by increasing the current through the laser diode to its maximum value and/or experimenting with different avalanche transistors to be used as Q70 in the S-6. In addition to avalanche noise, the jitter in the sampling command is believed, also, to be due to the scintillation of the optical intensity of the laser diode between consecutive pulses. This scintillation, which is on the order of a few percent, contributes to the jitter by varying the time that Q70 needs to integrate enough optical energy in order to avalanche.

Pulsed laser diodes whose optical power output is more than 10 Watts are commercially available. Such a diode may be employed in order to reduce sampling command jitter. However, building a driver to deliver the current pulses of 50 to 100 amperes with a risetime on the order of one nanosecond required for these diodes may be a tough design challenge. Medium power switching transistors which can sustain non-destructive avalanche may be investigated for this purpose.

APPENDIX A

SYSTEM CONSTRUCTION AND CALIBRATION

A.1. Introduction

In this appendix the construction and calibration of the optically coupled sampling system is outlined. The material will be presented in a condensed form which assumes that the reader is familiar with the (7S12)-(S-6) sampling sytem operation, and has thoroughly reviewed the design of the three fiber optic links in Chapter 2.

In the construction part information will be given regarding parts lists, printed circuit board patterns, component placement diagrams and construction hints. This will be done for all three links.

In the latter part of this appendix, first time operation/calibration of the separate parts of the system will be reviewed. This is followed by a description of first time overall system operation/calibration. the author's recommendations and hints are given when proper.

A photograph of the complete system is shown in Figure A.1 to aid the reader in visualizing the construction details which follow. Notice that on the sampling head side of the system the S-6 plugs into a 6-pin connector which attaches it to the error transmitter and feedback receiver boards. The laser pigtail is seen to enter the S-6 where it is connected to its avalanche transistor (Q70, Figure B.2) as will be explained later in this appendix.

A.2. Construction of the Fiber Optic Error Transmitter

Figure A.2a shows the land pattern associated with the soldering side of the transmitter board as seen from the component side. In

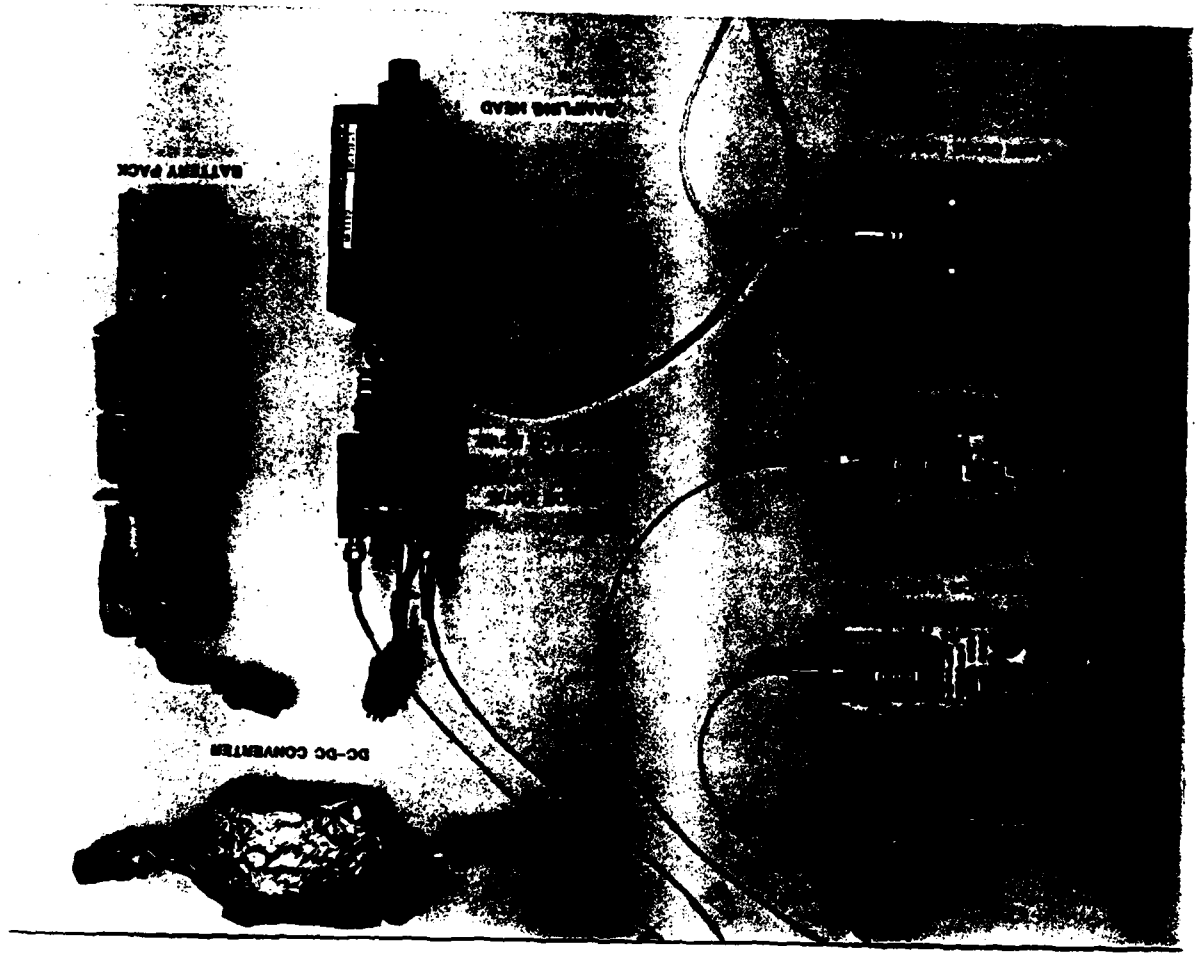

Figure A.1. Photograph of the fiber optically coupled sampling system constructed in this work.

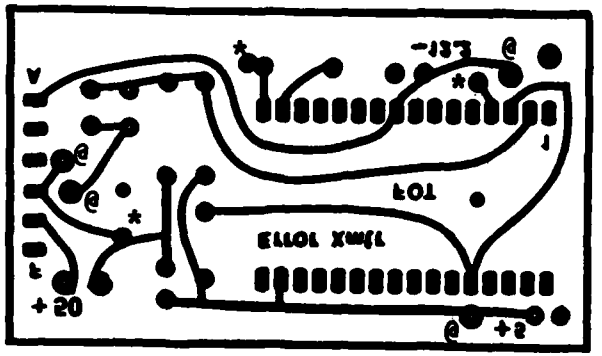

Figure A.2a. Soldering side layout of the error transmitter board.

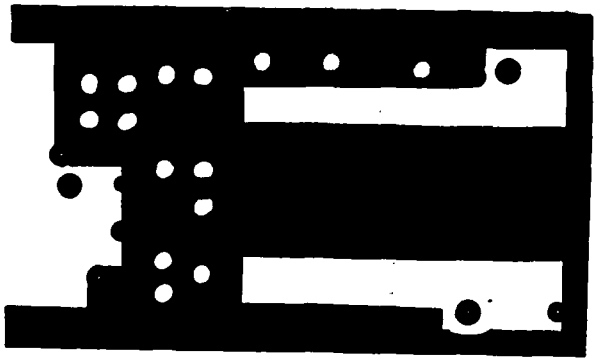

Figure A.2b. Ground Plane layout of the error transmitter board.

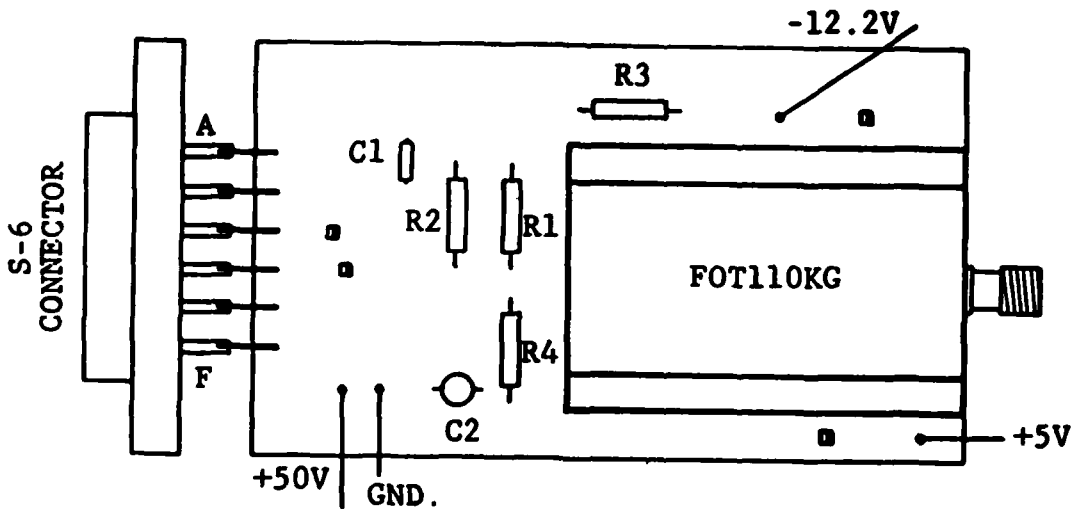

Figure A.3. Component placement diagram of the error transmitter board.

Figure A.2b the ground plane layout on the component side is shown. The holes marked with an asterisk on the soldering side of the layout signify that a through connection to the ground plane side of the board is to be made there. At the points where an ampersand is indicated, a pin socket is soldered in order to hold wire wrap pins that serve to connect these points to corresponding points on the opposing feedback receiver board. (see photograph of Figure A.1). Figure A.3 shows the component placement of the error transmitter.

Parts List:

Resistors		
R1	470 Ohms, 1/4W, 5%	Carbon Film
R2	2.2K, 1/4W, 5%	Carbon Film
R3	47 Ohm, 1/4W, 5%	Carbon Film
R4	1K, 1/4W, 5%	Carbon Film
Capacitors		
C1	0.1 μF	Ceramic
C2	22 μF, 16V	Tantalum
Devices		
FOT110KG	Fiber Optic Transmitter	Burr-Brown
Hardware		
Double sided PCB		2" × 1 11/16"
Socket, pin term.	× 4	Tek. 136-0263-03
Wire wrap pins	× 2	0.8" - 1" long
32 pin DIP socket for FOT110KG		0.1", 0.9" wide

A.3. Construction of the Fiber Optic Feedback Receiver

Figure A.4a depicts the soldering layout of the receiver board as seen from the component side. Figure A.4b shows the ground plane layout on the component side of the board. The soldering side of the board faces the soldering side of the error transmitter. The two boards are held together by the connections to the 6-pin connector into which the S-6 plugs in and also by four interconnecting wirewrap pins at the points marked with ampersands. Figure A.5 shows the component placement of the feedback receiver.

Parts List:

Resistors

R14	100 Ohm, 1/4W, 5%	Carbon Film
R15	47K, 1/4W, 5%	Carbon Film
R16	1K, 1/4W, 5%	Carbon Film
R17	10K, 1/4W, 5%	Carbon Film
R18	22K, 1/4W, 5%	Carbon Film
R19	47K, 1/4W, 5%	Carbon Film
R20	500 Ohm, 10T, Pot.	
R21	10K, 1/4W, 5%	Carbon Film
R22	100K, 1/4W, 5%	Carbon Film
R23	100K Pot.	
R24	33K, 1/4W, 5%	Carbon Film
R25	10K, 1/4W, 5%	Carbon Film

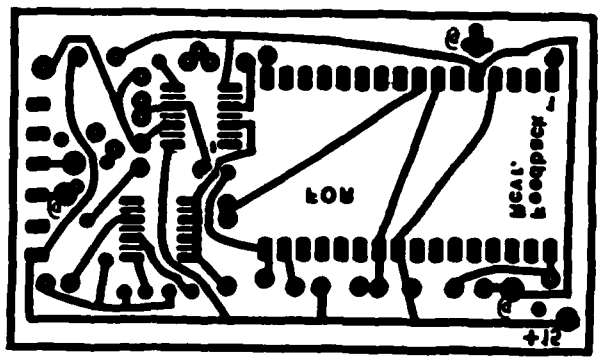

Figure A.4a. Soldering side layout of the feedback receiver board.

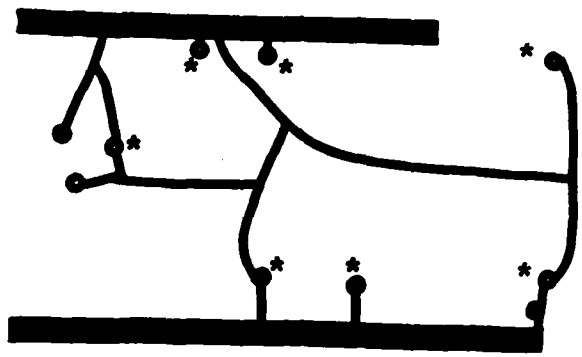

Figure A.4b. Component side layout of the feedback receiver board.

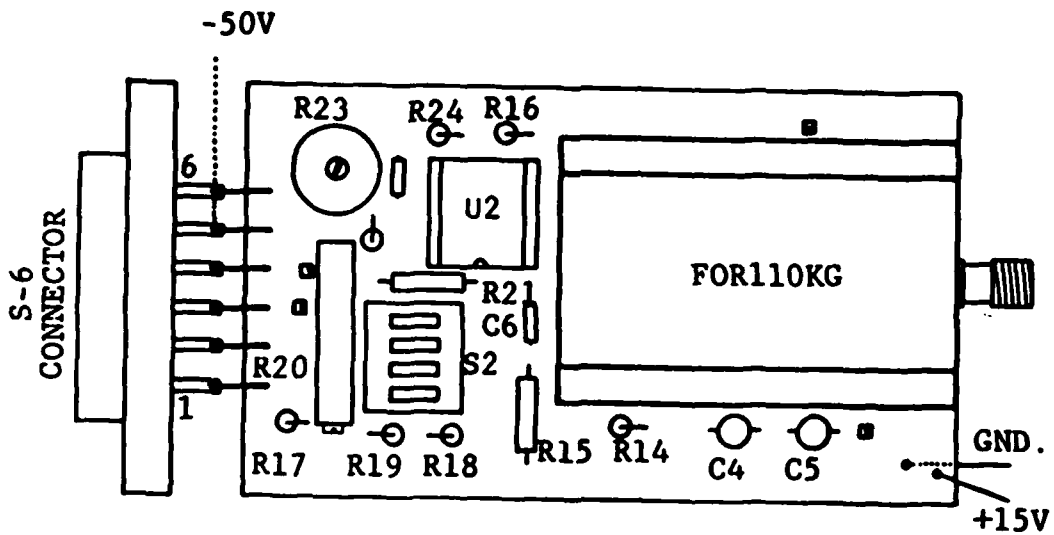

Figure A.5. Component placement diagram of the feedback receiver board.

Capacitors		
C4,C5	22 μF, 16V	Tantalum
C6	120 pF	Disc
C7	220 pF	Disc
Devices		
FOR110KG	Fiber Optic Receiver	Burr-Brown
U2	Op-Amp, LF353	National Semiconductor
Hardware		
Double sided PCB		3" × 1 11/16"
Socket, pin term.	× 4	Tek. 136-0263-03
Wire wrap pins	× 2	0.8" - 1" long
32 pin DIP socket for FOR110KG		0.1", 0.9" wide
4-position DIP switch		
Bent wire wrap pin for scope tap	× 1	

A.4. Implementation of the Sampling Command Laser Detection Technique

In order to mate the laser pigtail to the avalanche transistor chip of the S-6, the top of the transistor's metal case must be shaved-off using a machine shop belt sander. The author recommends that this technique be apprehended using a couple of cheap metal case transistors before attempting its application to the avalanche transistor. Practice and patience will enable the interested reader to remove the top of the metal case while leaving the rest of it intact. Care should be taken to

avoid excessive heating of the transistor due to friction. After the cap is removed the transistor must be rinsed in a dry environment using a high purity volatile solvant such as acetone. The solvent must be dried out using a warm and dry air stream, and the chip must be examined under a microscope to ensure that no metal dust particles are shorting the metallization islands on the chip.

The exposed transistor must then be installed in an avalanche circuit like the one in Figure 2.5 with R_c set to about 40K, V_{cc} set to 50V, and C set to 150 pF.

At this point the laser fiber pigtail is ready to be attached to the transistor chip as will be described shortly. Before attempting this procedure, the reader is cautioned against the possible hazards of laser radiation.

CAUTION

```
* * * * * * * * * * * * * * * * * * * * *
*                                         *
* The Laser diode employed is not visi-  *
* ble to the human eye. It may cause      *
* permanent damage to the eye if viewed   *
* directly. The Laser driver board        *
* must be disconnected from its supply    *
* or the fiber pigtail end must be        *
* covered to avoid eye exposure to the    *
* laser beam.                             *
*                                         *
* * * * * * * * * * * * * * * * * * * * *
```

With the laser driver board disconnected from its DC supply and using a micromanipulator and a microscope the fiber pigtail must be

brought perpendicularly in direct contact with the top surface of the transistor chip as depicted in Figure 2.12. Before operating the laser diode driver the operator must remove the microscope and screen the transistor and pigtail setup with a dark and thick barrier to avoid exposing his/her eyes to the scattered laser beam. The laser driver board must be enabled next and driven with a variable repetion rate of 5-10 KHz. With the aid of an oscilloscope connected to the avalanche transistor collector the operator must verify that the transistor is avalanching with a repetition rate that follows that of the driver trigger source. The micromanipulator may now be used (without a microscope) to move the fiber end around the top of the chip until a reliable and satisfactory avalanche is obtained. In all cases the final position of the pigtail must be such that it makes a gentle but firm contact with the chip surface.

The fiber can now be bonded to the transistor by gently filling the open transistor case with a quick, self hardening epoxy. The supply voltage must be disconnected from the avalanche transistor circuit in order to avoid electrolytic reaction between the chip and the epoxy. The supply must be connected intermittently however to ensure that the optically triggered avalanche is still possible until the hardening of the epoxy is complete.

The outside surface of the epoxy must then be painted with a thick black ink in order to eliminate the hazard of scattered laser rays.

The avalanche transistor of the S-6 (Q70) can be removed using a pair of tweezers without having to dismantle the sampling head. Next the avalanche transistor to which the fiber pigtail was bonded is inserted into Q70's socket. The back cover of the S-6 case may have to be permanently removed in order to allow the laser pigtail to pass into the sampling head.

A.5. Construction of the Fiber Optic Error Receiver

Figure A.6 depicts the ground plane pattern and the soldering side conductor pattern of the error receiver. Figure A.7 shows the component placement on the error receiver board.

The output of the error receiver is connected to the 7S12 sampling head bay with a flexible shielded cable. The S-6 bay socket inside the 7S12 is accessed using a modified Tektronix sampling head extender plug-in. To this extender are attached the shielded cables which connect the error receiver, feedback transmitter and the laser diode driver boards. See [16] for pin assignment.

Parts List:

Resistors

R5	1K, 1/4W, 5%	Carbon Film
R6	100 ohm, 1/4W, 5%	Carbon Film
R7	3.3K, 1/4W, 5%	Carbon Film
R8	15K, 1/4W, 5%	Carbon Film
R9	10K, 1/4W, 5%	Carbon Film
R10	10K, 10T, Pot.	

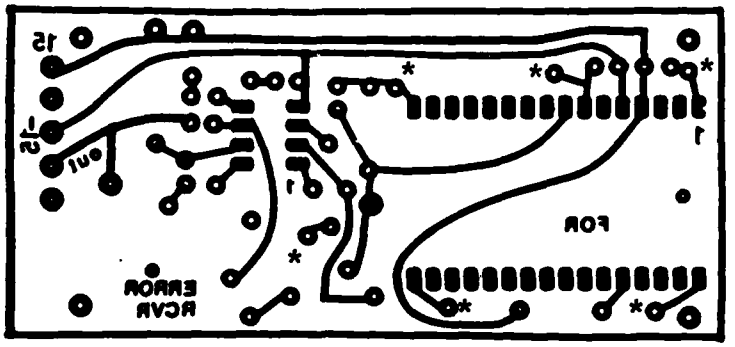

Figure A.6a. Soldering side layout of the error receiver board.

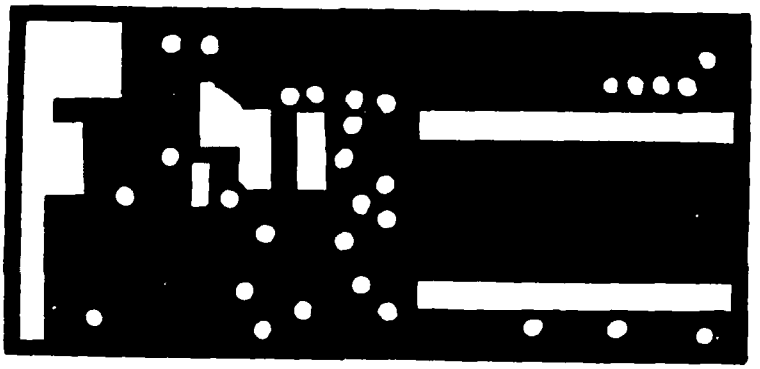

Figure A.6b. Ground Plane layout of the error receiver board.

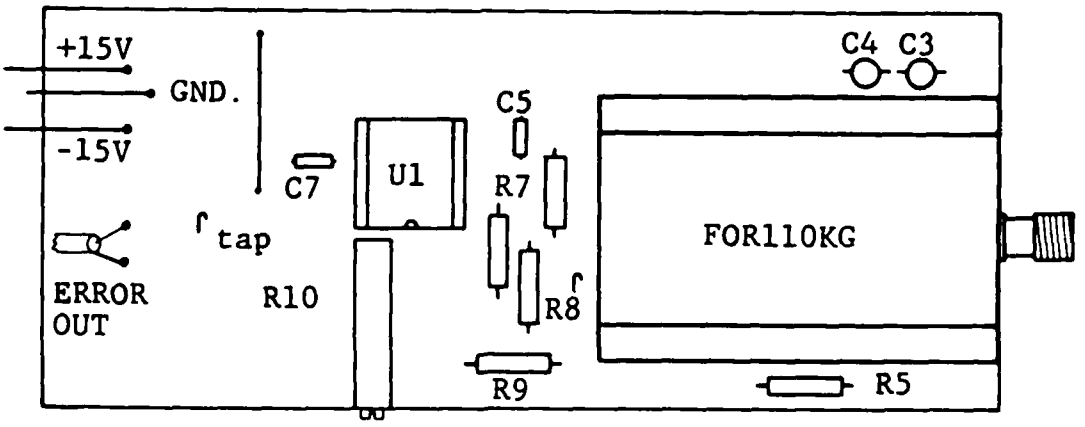

Figure A.7. Component placement diagram of the error receiver board.

Capacitors		
C3,C4	22 µF, 16V	Tantalum
C5	47 pF	Disc
C6	5 pF	Disc
C7	0.1 µF	Ceramic
Devices		
FOR110KG	Fiber Optic Receiver	Burr-Brown
U1	Op-Amp, LM318	Harris
Hardware		
Double sided PCB		1 11/16" × 3 7/8"
32 pin DIP socket for FOR110KG		0.1", 0.9" wide
8 pin DIP socket for LM318		0.1"

A.6. Construction of the Fiber Optic Feedback Transmitter

Figures A.8a and A.8b depict the soldering side layout and the ground plane layout of this board, as seen from the component side. Figure A.9 shows the component placement of the feedback transmitter.

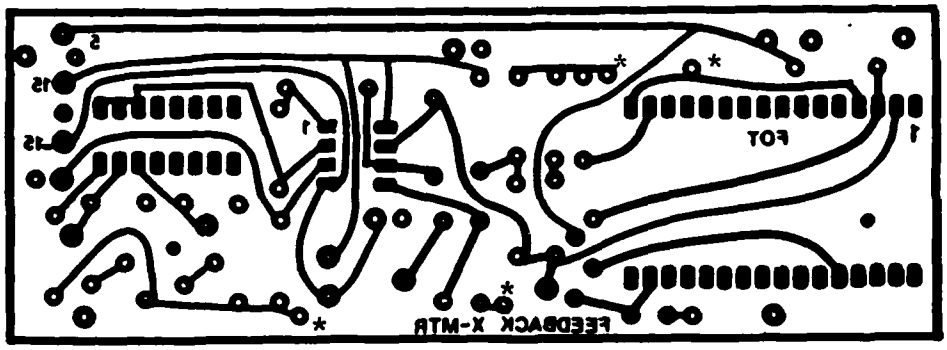

Figure A.8a. Soldering side layout of the feedback transmitter board.

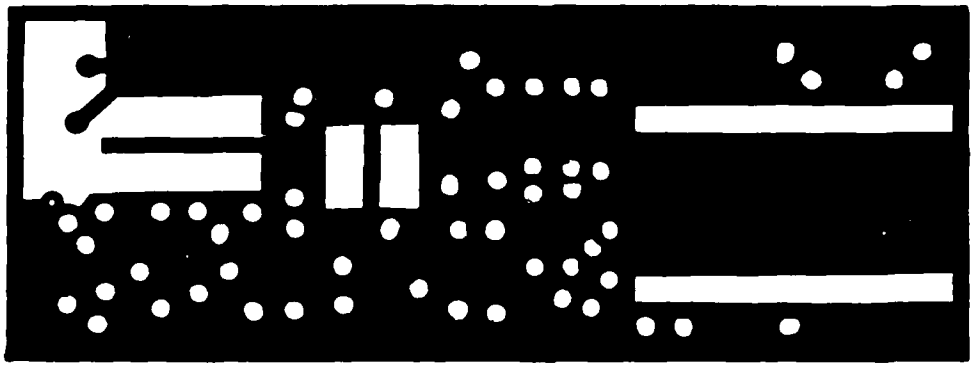

Figure A.8b. Ground Plane layout of the feedback transmitter board.

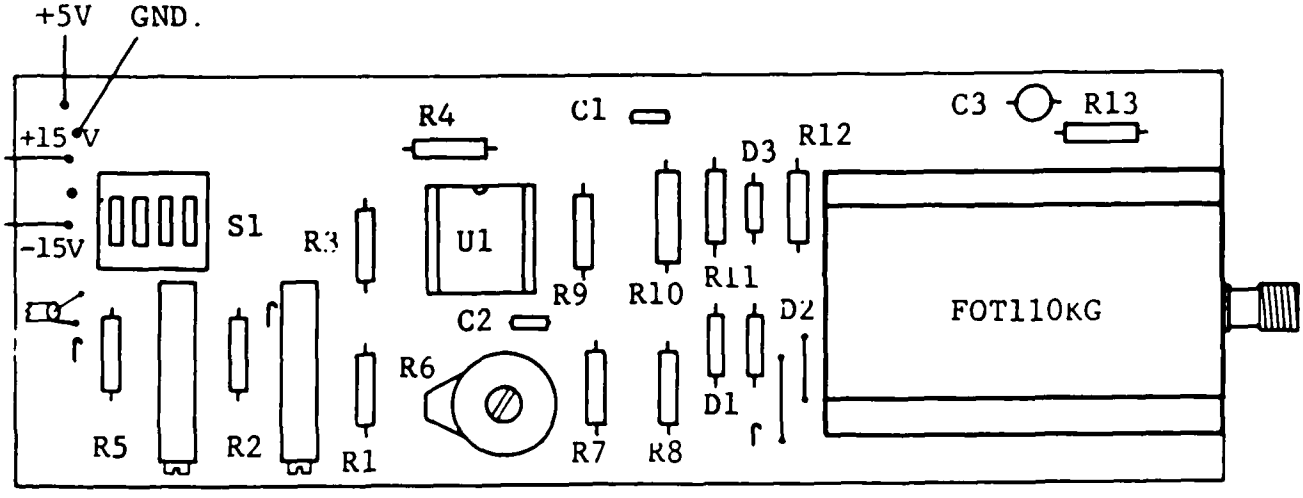

Figure A.9. Component placement diagram of the feedback transmitter board.

Parts List:

Resistors		
R1	47K, 1/4W, 5%	Carbon Film
R2	20K, 1/4W, 5% + 100K, 10T, Pot	
R3	47K, 1/4W, 5%	Carbon Film
R4	10K, 1/4W, 5%	Carbon Film
R5	4.7K, 1/4W, 5% + 10K, 10T, Pot	
R6	100K Pot	
R7	100K, 1/4W, 5%	Carbon Film
R8	33K, 1/4W, 5%	Carbon Film
R9	10K, 1/4W, 5%	Carbon Film
R10	470 ohm, 1/2W, 5%	Carbon Film
R11	150 ohm, 1/4W, 5%	Carbon Film
R12	47 ohm, 1/4W, 5%	Carbon Film
R13	1K, 1/4W, 5%	Carbon Film
Capacitors		
C1,C2	0.1 μF	Ceramic
C3	22 μF, 16V	Tantalum
Devices		
FOT110KG	Fiber optic transmitter	Burr-Brown
U1	Op-Amp, LF353	National Semicond.
D1,D2	Diode, 1N914	Silicon
D3	2.5V zener	

Hardware

Double sided PCB	1 11/16" × 4 13/16"
32-pin DIP socket for FOT110KG	0.1", 0.9" wide
8-pin DIP socket for LF353	
4-position DIP switch	

A.7. Construction of the Laser Diode Driver

Figure A.10 shows the conductor layout on the soldering side of this board as seen from the component side. Figure A.11 shows the component placement on the driver board.

The laser diode must not be soldered to the board in order to facilitate its removal when necessary. The anode screw stud of the laser diode can be used to physically hold the diode with a rigid wire loop soldered to the board, while a socket can be used to hold its cathode lead.

The toroid T is a modified Tektronix transformer to which 3 additional secondary windings with five turns each are added.

The current monitoring resistance must be soldered to the lower side of the board. This is due to space limitations near the laser diode and also the desire to keep the path length of the laser diode current as short as possible.

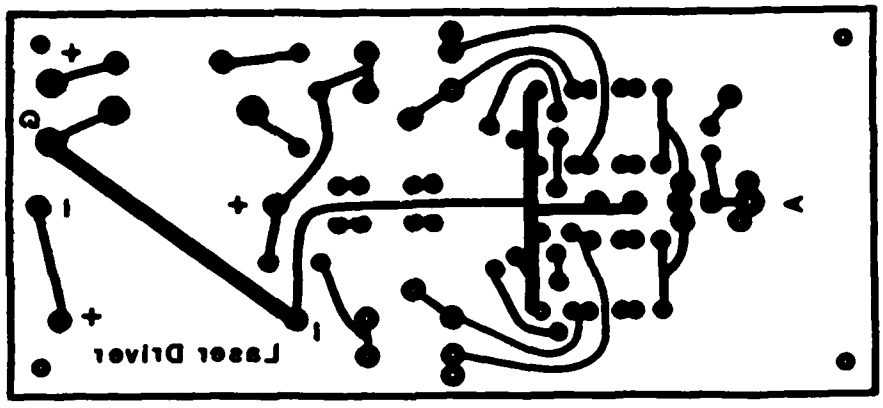

Figure A.10. Soldering side layout of the pulsed laser diode driver board.

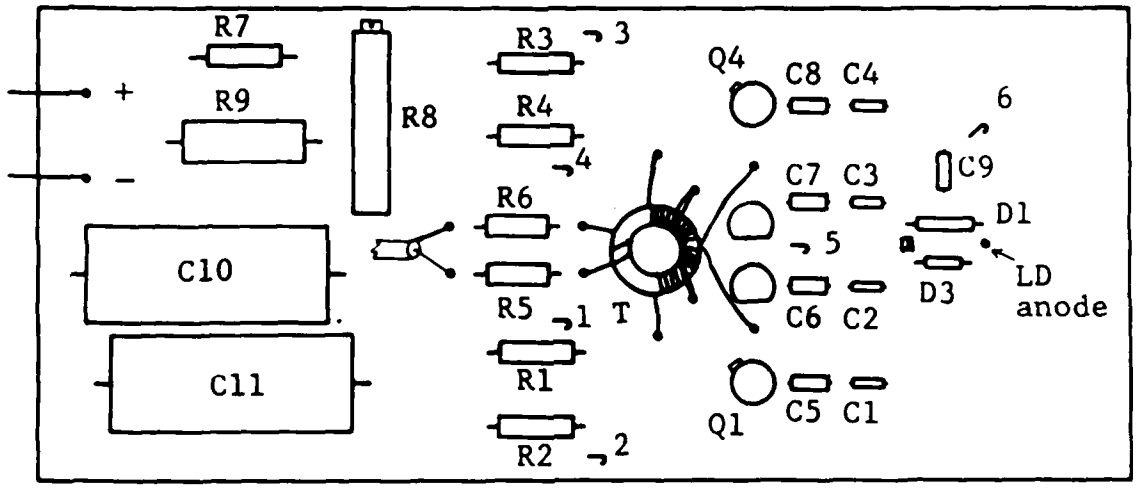

Figure A.11. Component placement diagram of the pulsed laser diode driver board.

Parts List:

Resistors

R1,R2,R3,R4	22K, 1/4W, 5%	Carbon Film
R5,R6	33 ohm, 1/8W, 5%	Carbon
R7	470 ohm, 1/4W, 5%	Carbon Film
R8	5K, 10T, Pot	
R9	6.8K, 1W, 10%	Carbon
R_m	2.7 ohm, 1/4 or 1/8W, 5%	Carbon

Capacitors

C1,C2,C3,C4	1000 pF. 100V	Miniature disc
C5,C6,C7,C8	0.1 μF	Small size ceramic
C9	0.1 μF	Small size ceramic
C10,C11	470 μF, 50V	Electrolytic

Transformer

Modified Toroid, Tektronix Part No. 120-0544-00

Devices

Q1,Q4	transistor, Tektronix Part No. 151-0109
Q2,Q3	transistor, Tektronix Part No. 151-0556
LD	LD-60 FR, Laser Diode Labs
D1	1N34A, Germanium
D2,D3	1N914, Silicon

Hardware

Single sided PCB		2" × 4.5"
Wirewrap pins for transformer connections	× 8	1/4" long
Bent wirewrap pins for oscilloscope taps	× 6	
Socket, pin term. for LD cathode		Tek. 136-0263-03
Wire loop for LD anode	× 1	

A.8. Preliminary Calibration of the Error Link

Power up the error transmitter using the battery pack and the error receiver using external power supplies. With the S-6 unplugged from the error transmitter/feedback receiver unit, apply a sinusoidal signal of 400 mV peak to peak and 100 KHz to the error link input (at C1). Monitor the output (at C7) with an oscilloscope. Adjust R10 to obtain an overall gain of unity for the link. This calibration is not final but is necessary as a first step toward the overall system calibration discussed in Section A.10.

A.9. Preliminary Calibration of the Feedback Link

An important point to be remembered in calibrating this link is that the link can operate with three different settings of transmitter amplification/receiver attenuation as discussed in Section 2.6. The first power-up calibration procedure presented in this section serves to set the transmitter amplification and the receiver attenuation to their proper values in a manner which ensures that the overall link gain is

unity for all settings. The DC level of the output will vary depending on the gain/attenuation setting chosen. The adjustment of this level will be described in the overall system calibration procedure.

To carry out the preliminary calibration of the link the steps below must be followed:

1. With the aid of an ohmeter set R2 and R5 in the transmitter to 47 Kilohms and 11.75 Kilohms, respectively.
2. Power up the link, and using an oscilloscope connected to tap point No. 4 in Figure 2.2, adjust R6 for a quiescent DC level of 2.5 volts at the input of the fiber optic transmitter. This is necessary to ensure that the transmitter operates in its linear region.
3. Set switch S1 in the feedback transmitter to the position marked 1 and S2 in the receiver to position 1 also.
4. Apply a square wave of 100 mV peak to peak voltage and a frequency of 1 KHz to the input of the link at R1.
5. While monitoring the output of the link with an oscilloscope adjust R20 of the receiver to give an overall link gain of unity.
6. Set both S1 and S2 to position 2 and monitor the gain of the link. Bring this gain to unity if necessary by adjusting R2 in the transmitter.
7. Set S1 and S2 to position 3 and repeat the above step by adjusting R5 instead of R2.

In steps 5 to 7 potentiometer R23 in the receiver may have to be adjusted in order to prevent the output of the link from clamping to +15 or -12.2 volts.

A.10. First Time Operation of the Laser Diode Driver

Before attempting to operate the laser driver board it is worthwhile noting that the laser diode employed can be easily damaged by: static, a reverse bias of more than 3 volts, a pulsed forward current in access of 10 amperes, or a continuous current in excess of about 100 mA.

High static voltages can be avoided by properly grounding the body of the operator. To avoid accidental reverse voltages on the diode or large forward continuous currents, it is advisable that no measurement instrument be connected to the diode directly. The tap points provided in the driver board (Figure 2.10) ensure that no damage can occur to the diode by connecting external instruments to monitor the operation of the circuit.

For the first time operation of the circuit the following steps must be followed.

1. Remove the laser diode from the circuit and solder in its place two parallel switching diodes such as the 1N914.
2. Power up the circuit with a stabilized DC source and adjust R8 to give a V_{cc} of 65 to 70 volts at the collectors of the avalanche transistors.

3. Drive the circuit either with the sampling command pulses issued from the 7S12 or an external pulse generator. The repetition frequency must be set to less than 10 KHz.
4. With the aid of an oscilloscope verify that all four transistors in the driver are properly avalanching. For this purpose tap points 1,2,3 and 4 must be used.
5. Connect the ground of a high frequency oscilloscope whose bandwidth is in excess of 100 MHz to tap point 5. Then connect the probe tip to tap point 6 and monitor the voltage developed across R_m by the laser current pulses. From the pulse peak amplitude and the value of R_m. Compute the peak current passing through the two switching diodes which are simulating the laser diode. This current must be less than 10 amperes.
6. Disconnect the power supply from the circuit.
7. Desolder the two switching diodes, and install the laser diode. Utmost care should be taken here to ensure that the laser diode is not connected in a reverse direction.
8. Remove the outer case of the S-6 and install the avalanche transistor which is mated to the end of the laser pigtail as described in Section A.4.
9. Power up the S-6 by plugging it into the error transmitter/feedback receiver assembly.
10. Power up the laser diode driver and trigger it with the sampling command pulses issued by the 7S12.

11. Verify that Q70 in the S-6 sampling head is being driven to avalanche by the laser pulses by monitoring its collector voltage with an oscilloscope.
12. Replace the S-6 into its outer case.

A.11. Overall System Calibration

After carrying out the calibration of the three separate links the optically coupled sampling system can be calibrated by following the procedure outlined below.

1. Remove the 7S12 from the mainframe oscilloscope, and with the aid of a screwdriver turn the "memory gate width" potentiometer (R390, [6]) to the extreme counterclockwise position. This procedure opens the memory gate to its maximum width in order to compensate for the delay introduced into the error signal by the fiber optic error link. Replace the 7S12 in its compartment.
2. Connect the S-6 with an extender cable to the 7S12 sampling unit, turn on the mainframe oscilloscope and leave the system to warm up for at least two hours.
3. Remove the sampling head extender, and plug the S-6 into the error transmitter/feedback receiver assembly. Also connect the error receiver, the feedback transmitter, and the laser diode driver to the 7S12 at the S-6 plug-in socket using the modified extender.

4. Connect a freshly charged battery pack to the sampling head side of the system and leave the system to warm up for an extra half hour. This is necessary in order to avoid the drift caused by the fast drop in the voltage of the battery pack when it is first used.
5. Connect a fast externally triggerable pulse generator to the sampling system as depicted in Figure 3.1. The delay required for the pulse generator trigger is on the order of 40 to 60 ns. The risetime of the pulse generator output must be a small fraction of a nanosecond and its amplitude a few hundred millivolts.
6. At this point the sampling oscilloscope display may still not show any waveform. The reason is that the DC level of the feedback receiver output must be adjusted in order to bring the acquired waveform into the display window. In order to do this begin by setting the DC offset control on the sampling unit at the center position (zero DC offset). With the aid of an oscilloscope connected at tap point No. 4 of the feedback transmitter adjust R6 such that the quiescent DC level at the input of the fiber optic feedback transmitter is 2.5 volts again. Now adjust R23 in the feedback receiver until a waveform appears on the display. If this does not happen or if the DC level at the fiber optic transmitter changes, then iterative adjustment of the three potentiometers should be tried until proper operation is obtained.

7. In order to adjust the sampling loop gain to near unity select the 100 ns/div setting and use the time/distance knob of the 7S12 to bring the rising edge of the test waveform into the display. Adjust R10 in the error receiver such that the first sample point above the 0% level of the pulse is positioned at the 90% level.

This concludes the calibration of the system.

APPENDIX B

SAMPLING OSCILLOSCOPE PRINCIPLES

B.1. Introduction

In this appendix, the basic theory of operation of a sampling system is discussed. Although the discussion will be specialized to the case of the (7S12)-(S-6) system used in this work, the main principles involved are basic to the operation of other sampling systems. For a more complete treatment of this subject, the reader is referred to [5] and [6].

B.2. Real Time and Equivalent Time Oscilloscopes

In real-time oscilloscopes, the horizontal time/division scale of the scope is equal to the time it takes the electron beam to scan one division of the display. One occurance of the event (signal) to be observed is usually sufficient for producing a full account of the event on the scope's screen. Conventional oscilloscopes are of the real-time type. Real-time oscilloscopes are not limited to conventional oscilloscopes only. Some sampling oscilloscopes may be used in the real-time mode in order to observe very slowly varying signals. In this mode, the oscilloscope acquires samples from the slow signal as time progresses and stores them in memory, while generating a display in which the old samples are continuously refreshed and new ones are added as they are obtained. By the time the event ends, the display contains a collection of sample points depicting the waveform associated with it.

In equivalent-time oscilloscopes, however, the time/division scale of the scope can be smaller than the time it takes the beam to traverse

one division by many orders of magnitude. For this type of oscilloscopes several occurances of the same event are required before a complete account or waveform is generated. For each occurance of the event, the oscilloscope acquires one sample of the signal at a different location in time than the previous one, displays it, and possibly stores it in a memory. After a large number of repetitions of the signal, the display will contain a sufficient number of samples which depict the waveform associated with the event.

High frequency oscilloscopes that can handle signals of up to 18 GHz are all of the equivalent-time sampling type. This is mainly due to the unavailability of CRT's that have such a wide bandwidth.

B.3. Sequential and Random Mode Samplers

In sequential mode sampling, the samples acquired from each new occurance of the signal are progressively shifted by small amounts of time on the signal. While in the random sampling mode, samples are obtained at random instants of time on the signal but are displayed at the proper positions on the screen in order to produce a full and coherent picture of the signal.

The (7S12)-(S-6) system is an equivalent-time sequential sampling system. It consists of two sections, namely, the vertical section and the horizontal section. The operation of these sections is presented in what follows.

B.4. Vertical Circuit Functions and Principles

In Figure B.1 a simplified block diagram of the 7S12 vertical section is depicted. Only those functions necessary for understanding the basic principles of operation of the vertical section of a sampling oscilloscope are shown. In Figure B.2 the complete circuit diagram of the S-6 sampling head is shown.

B.4.1. Strobe Generator

The strobe generator is incorporated in the sampling head, as shown in Figure B.2. When the horizontal section of the oscilloscope issues a sampling command pulse, it is received by the primary of the pulse transformer T70. The falling edge of this pulse causes a positive current pulse from the secondary winding to be injected into the base of the reverse biased transistor Q70. This pulse causes Q70 to avalanche suddenly, producing a pair of push-pull pulses (at its collector and emitter sides) with an amplitude of about 35 volts and a risetime of a few nanoseconds. These two pulses are delivered to the usually forward biased snap-off (or step recovery) diode CR56, causing it to be reverse biased. The reverse bias on CR56 causes a reverse current to flow due to the charge stored in the diode. This current stops suddenly (the diode suddenly snaps open) and a pair of very steep push-pull pulses with a risetime on the order of a few tens of picoseconds is developed. These two strobe pulses travel down a transmission line toward the sampling gate, however, a pair of short circuited transmission lines

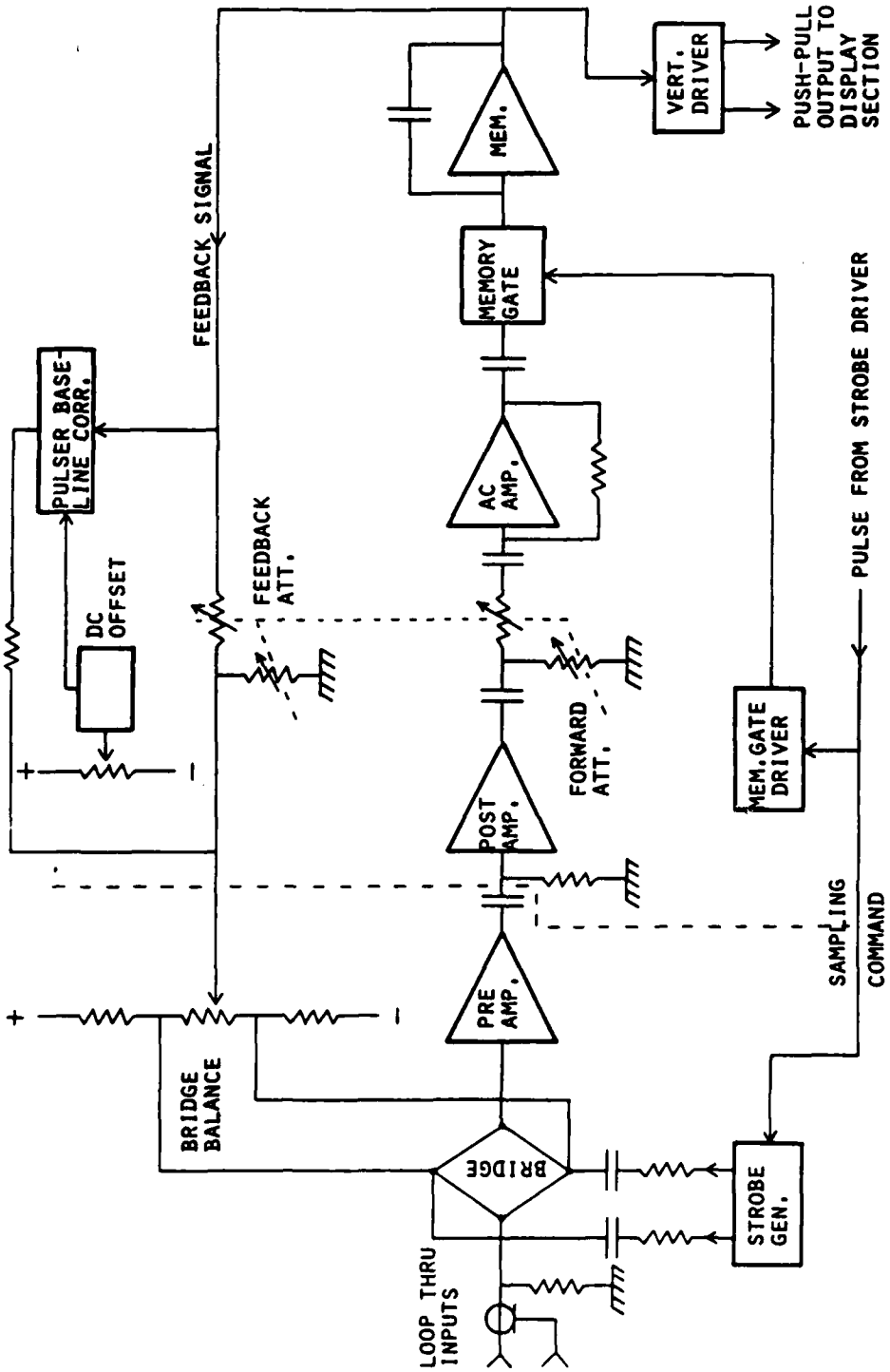

Figure B.1. Simplified block diagram of the 7S12 vertical section.

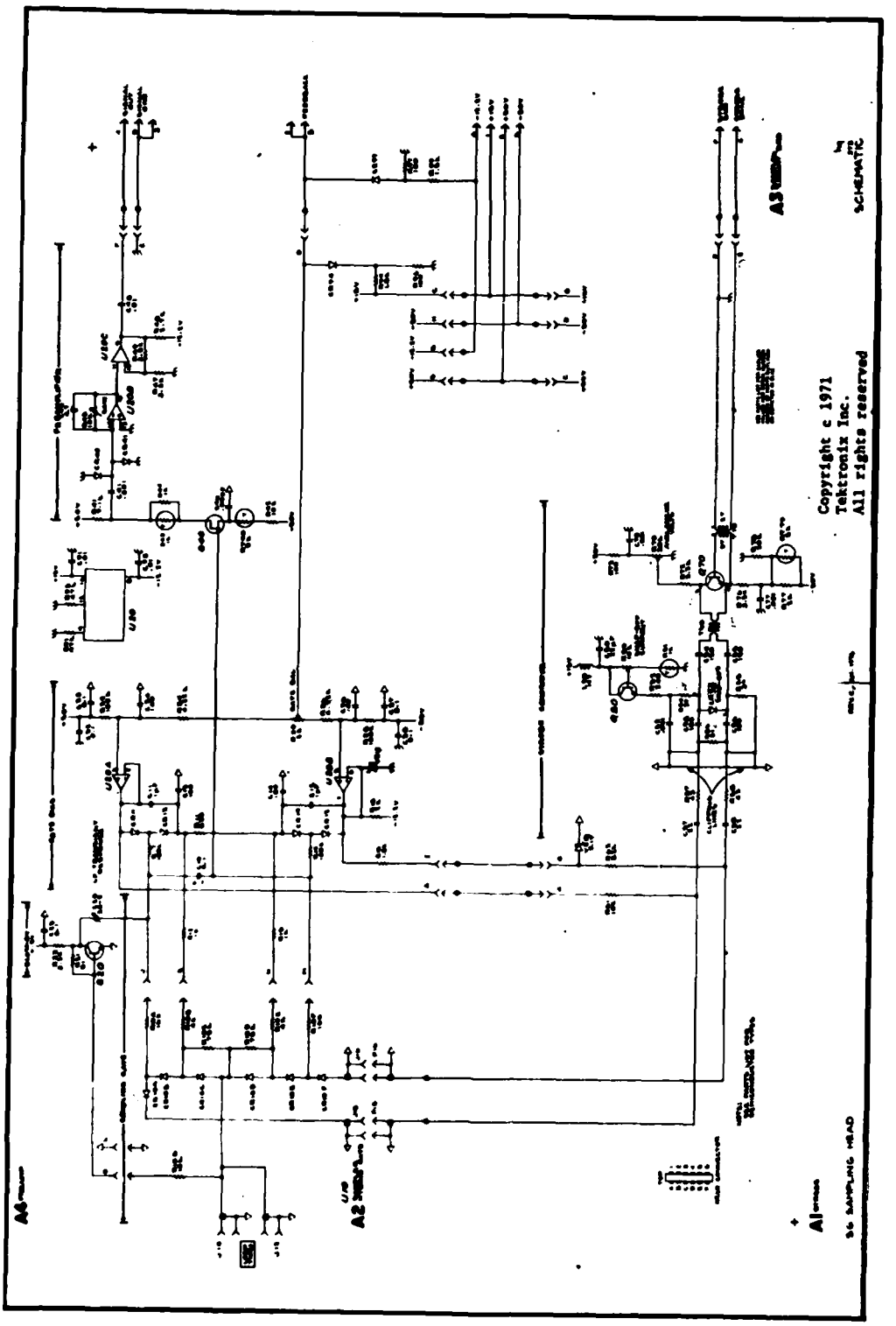

Figure B.2. Circuit diagram of the S-6 sampling head(reproduced with permission from Tektronix Inc.).

which is connected in parallel with the snap-off diode causes the two strobe pulses to be clipped in time, limiting their duration to about 200 ps.

B.4.2. Sampling Gate and Preamplifier

The signal to be observed is connected to the 50 ohm input of the sampling gate in Figure B.2, which consists of 6 very fast, low-storage, Shottky diodes connected in a bridge configuration to makeup a traveling-wave sampling gate. These diodes are usually reverse biased to prevent the input signal from reaching the output of the gate which is connected to the sampling preamplifier input.

When the horizontal section of the 7S12 requests that a sample be taken, the pair of push-pull strobe pulses described in the last subsection are issued. These two pulses travel down the series of 6 diodes causing diodes CR10A and CR10F to be forward biased first, then diodes CR10B and CR10E are forward biased, and finally CR10C and CR10D are also forward biased. After about 200 ps, the strobe pulse end is reached and these diodes are turned off in the same sequence. First CR10A and CR10F are switched off, then CR10B and CR10E, and finally CR10C and CR10D. A sample of the charge associated with the applied voltage is trapped between diode sets CR10A and CR10F, and CR10C and CR10E. This charge is conducted via R10A, C10 and, R10F to the preamplifier input at Q40.

It should be noted here that the step response risetime of the S-6 gate is really controlled by the time it takes a strobe pulse to travel through a certain part of the gate structure. This risetime is $\leq$ 30 ps.

The charge delivered to the preamplifier is stored in the small capacitance associated with its high impedance FET input. This charge resides at the input for a duration of time much longer than the duration the gate was opened. This is aided by the fact that when the gate is closed, it presents a very high impedance to the preamplifier input, thus, making the RC time constant at this input relatively long. This allows the preamplifier time to amplify the sampled voltage for a duration much longer than it took it to appear at its input. This signal stretching lowers, considerably, the bandwidth requirements on the preamplifier circuit and all the following stages. The bandwidth of the preamplifier circuit is on the order of 1.8 MHz.

B.4.3. Memory Circuit

The amplified step at the output of the preamplifier is sent to the 7S12 circuits, where it is further amplified by two stages of AC coupled amplifiers, as shown in Figure B.1. An attenuator between these two stages allows adjustment of the forward gain.

The amplified signal sample is passed on to the memory circuit through an analog gate called the memory gate. This gate is usually closed in the time between two sample acquisitions, but is opened for about 0.4 μs when the sampling command pulse is issued. This duration is sufficient for a sample to be acquired through the gate, pass through the three amplifying stages mentioned previously, and reach the memory circuit. The bandwidth requirement on the forward amplifying stages can be estimated from the gate opening duration.

The memory circuit consists of a very high input impedance inverting amplifier with a feedback capacitor that serves to store the voltage of the last acquired sample until the next sample is taken. When the memory gate is closed, the feedback capacitor retains its voltage. When the memory gate opens, there usually is a new voltage level to which this capacitor charges. Hence, the output of the memory amplifier is essentially constant until another sample is taken. The output of the memory is passed on to the vertical driver which causes a vertical deflection on the screen proportional to the magnitude of the acquired sample.

B.4.4. Feedback Signal

The output of the memory circuit is fed back to the gate bias circuit through the feedback attenuator, as shown in Figure B.1. Superimposed on the feedback signal is an adjustable DC voltage which is injected externally by the DC offset circuit. This voltage is used to adjust the vertical position of the displayed trace, as will be explained later.

The voltage fed back to the bias circuit passes to the output of its unity gain buffer stage and is delivered to the strobe inputs of the sampling gate. The voltage at the output of the gate becomes equal to the voltage of the last sample. This equality is necessary for minimizing strobe signal kick-out (kick-out is defined in footnote of Section 1.1) into the signal source [5].

B.4.5. Error Signal

When the next sample is taken, the voltage at the output of the sampling gate undergoes a step change whose mangitude is the difference between the voltage of the new sample and that of the previous one. This step difference (or error) is amplified starting with the preamplifier and is sent to the memory circuit. This amplified step change corrects the output of the memory to the value of the most recent sample.

B.4.6. Sampling Loop Gain

It is time now to explain the concept of loop gain. This will help understand one of the advantages gained by using this error/feedback technique for sample acquisition.

The percentage of the signal voltage transferred to the output of the sampling gate when the gate opens is called the Sampling Efficiency. This percentage ratio is a function of the strobe width, the source impedance, and the capacitance at the input of the sampling preamplifier. For fast gates like the S-6, the sampling efficiency is usually smaller than 25%.

The concept of sampling loop gain can best be described through a numerical example. Assuming that the first sample taken represents a change at the input of the sampling gate of 0 to 100 mV. The input to the preamplifier will be only 20 mV for a sampling efficiency of 20%. If the total forward gain of the three amplifying stages, the forward attenuator, and the memory amplifier is 200, then the voltage at the

output of the memory will be 4 volts. If the feedback attenuator is set to have a gain of 0.025, then the voltage fed back to the sampling gate will be 100 mV, which is equal to the voltage of the acquired sample. Under these circumstances, the loop gain is said to be unity. Now, if the next sample has a voltage of 110 mV, then only the difference 110 - 100 = 10 mV will be amplified by the sampling preamplifier and sent to the memory circuit to correct its output.

There are several advantages gained by using feedback to acquire signal samples. The first is minimizing strobe signal kick-out as mentioned in B.4.4. The second advantage is to minimize the effect of forward gain error. To understand how this is achieved, assume a step-signal of 100 mV at the input of the sampling gate and a forward gain of 150 instead of 200. The voltage associated with the first sample at the memory output will be 3 volts, and the voltage fed back to the sampling gate will be 75 mV instead of the expected 100 mV. On the occurance of the next strobe, 100 - 75 = 25 mV will be amplified by the preamplifier, causing the memory output to be corrected to 3.75 volts. Continuing in the same manner, the output of the memory circuit will eventually become very close to 4 volts, which is the value that it should have were the forward gain 200 and not the erroneous 150. In other words, a loop gain of less than one will eventually produce the correct deflection on the screen. The only expense paid is that it requires more samples than just one to achieve the correct signal voltage. This self correcting aspect of the sampling loop is quite adequate for visual evaluation of

sampled signals. However, when quantitative analysis is to be carried out on the acquired waveform, this self correcting effect can be a source of error for very fast-rise signals since it causes the rising edge of the signal to be flattened or spread out on a larger number of samples than necessary.

The third advantage gained by using the feedback system is that a system operating on the voltage difference principle allows us to inject an external DC voltage at a certain point in the loop (in this case the feedback attenuator) permitting us to display a small AC signal that has a large DC content without affecting the on/off condition of the sampling gate, [5].

B.5. Horizontal Circuit Functions and Principles

In this section, the basic principles underlying the operation of the horizontal section of the 7S12 sampling system are discussed. The main principles presented are basic to the operation of other sampling systems.

Figure B.3 depicts a simplified block diagram of the horizontal section of the 7S12. In Figure B.4, the sequence of temporal events associated with the following discussion is shown.

Basically, the horizontal section of a sampling oscilloscope performs the task of moving the electron beam horizontally to a specific position on the screen, and then requesting that a sample of the probed signal be taken. The demands on the horizontal section and the

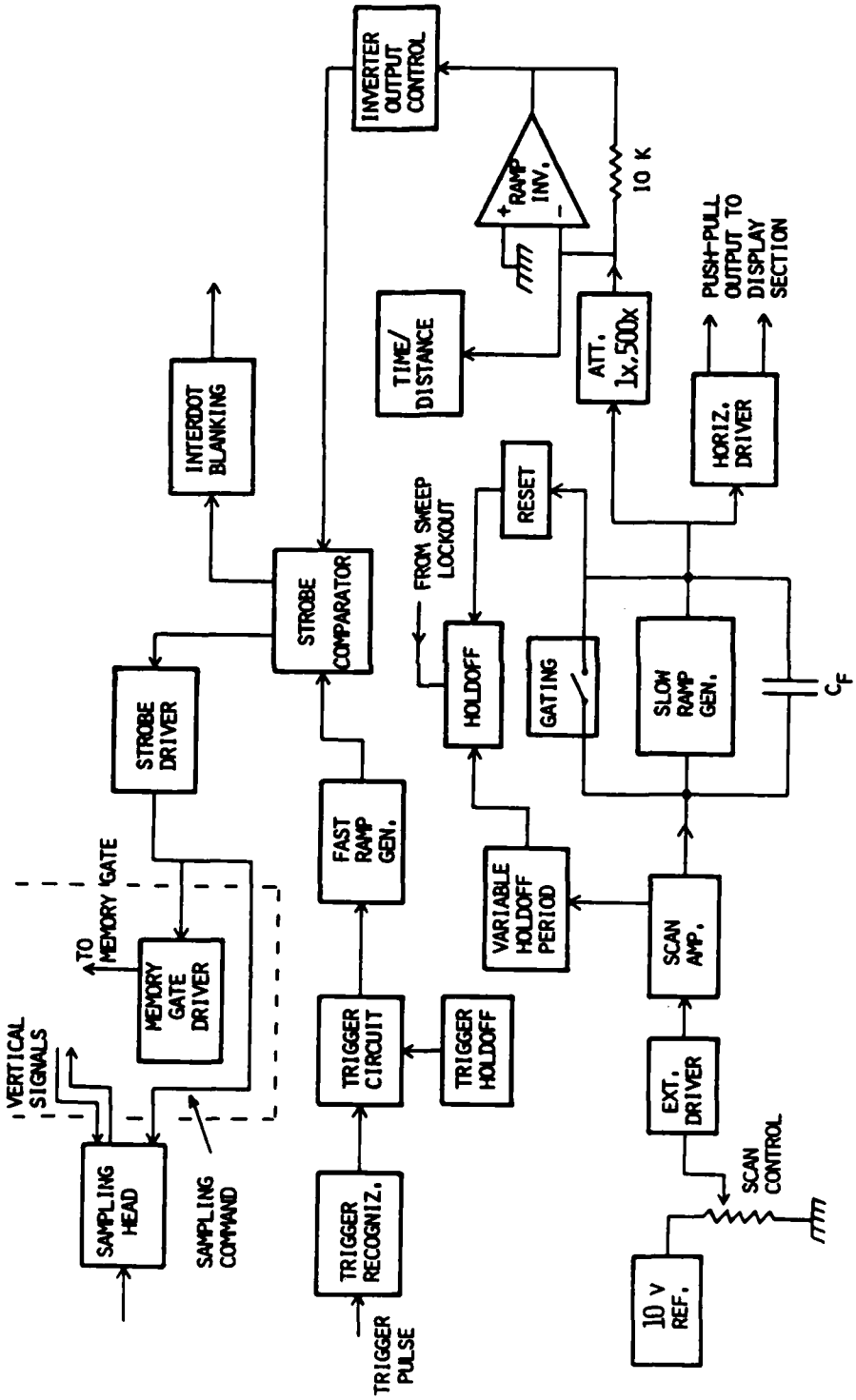

Figure B.3. Simplified block diagram of the 7S12 horizontal section.

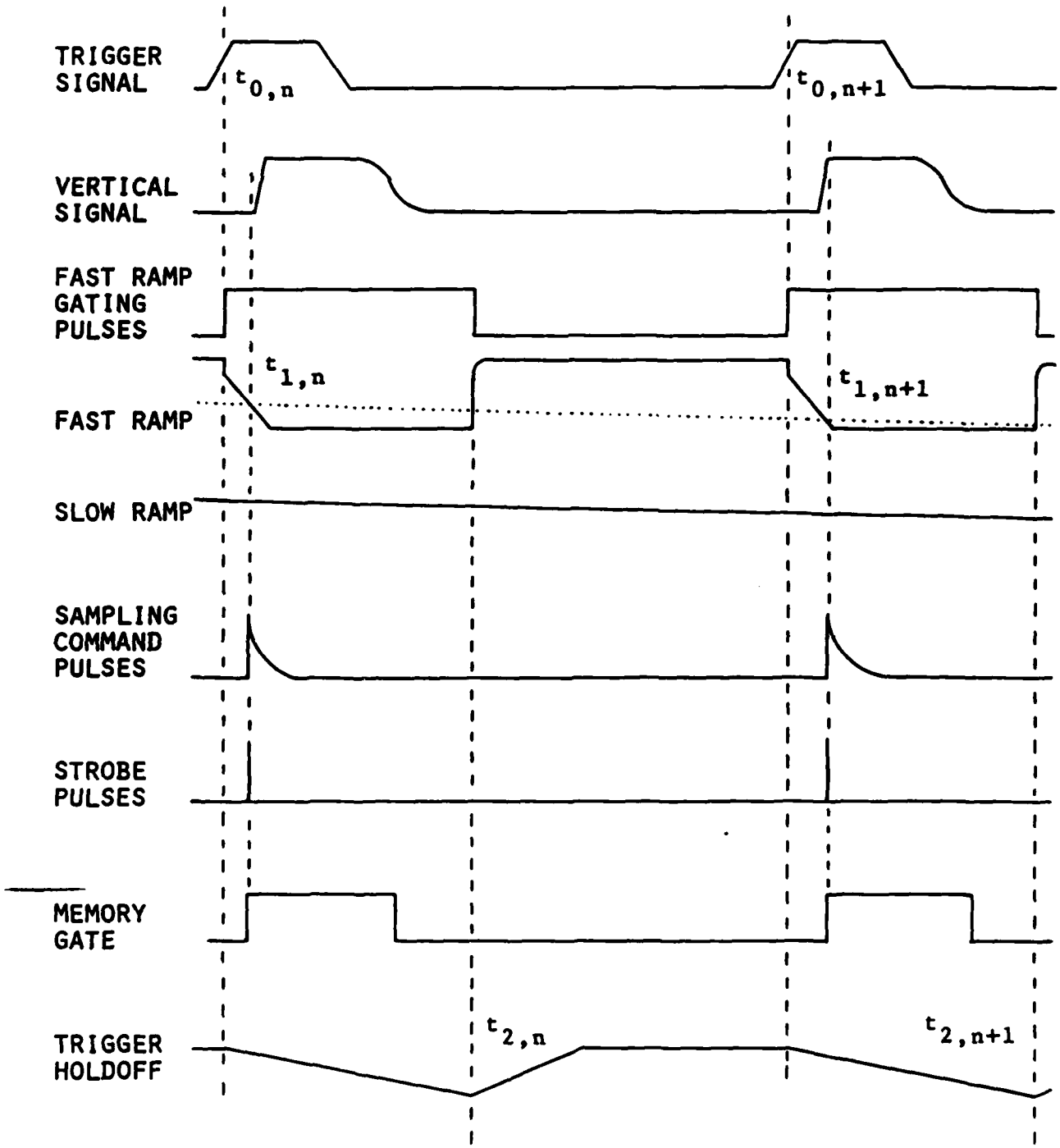

Figure B.4. Sequential-mode horizontal timing diagram

techniques employed to satisfy them can best be appreciated when one considers that, in the case of the 7S12, it has to determine the timing of samples separated from each other by an interval that can range from several nanoseconds down to 195 femtoseconds (0.195 picoseconds).

B.5.1. Trigger

The sequence of timing events in Figure B.4 starts with the trigger pulse issued by the signal generator which produces the signal to be sampled. This trigger pulse is usually issued prior to the generation of the test signal in order to allow time for the oscilloscope's circuits to initiate sample acquisition. The trigger pulse is applied to the trigger recognizer which "recognizes" a point on the pulse having a certain amplitude and slope. Upon detection of this point, the recognizer circuit issues a pulse to the trigger circuit. It is essential for obtaining a coherent display that the recognizer be activated at exactly the same point for every occurance of the trigger pulse.

The trigger holdoff circuit assures that the rest of the system has recovered from the last sampling cycle before allowing the trigger circuit to initiate a new cycle by starting the fast ramp.

B.5.2. Fast Ramp

The trigger circuit initiates a fast negative-going ramp which starts at 0 volts and descends to -10 volts. The time duration of this ramp depends on the time/distance multiplier setting and it can take

either one of the following values, 0.2 μs, 2.0 μs, or 20. μs. This ramp is, also, called the slewing ramp because it is closely associated with producing the progressively delayed (slewed) sampling command pulses. The slope of this ramp, along with the amount of attenuation of the slow ramp (to be presented later), determine the time/division scale of the display.

B.5.3. Slow Ramp

The scan amplifier receives all or a portion of a stabilized 10 DC volts through the scan control potentiometer and the external driver (which serves as a buffer). This amplifier serves as a stabilized constant current source for the integrating circuit which produces the positive going slow ramp. The scan control determines the amount of current supplied to the slow ramp generator and, consequently, the ramp's slope. The slow ramp starts at 0 volts and climbs up to slightly more than 10 volts.

This ramp is responsible for producing horizontal deflection on the screen where 10 volts are required to produce a deflection of 10 divisions. It should be noted that timing accuracy is not affected by the slow ramp's amplitude, only trace length is affected. The position of the scan control determines the full duration of the slow ramp and this ranges from many seconds down to 20 ms.

The full screen is scanned, and all the samples making up a waveform are acquired by the time the slow ramp reaches 10 volts. When the slow

ramp exceeds 10 volts, the reset circuit initiates (through the holdoff and gating circuits) the discharging of the integrating capacitor which produces the slow ramp. The holdoff circuit ensures that enough time elapses for the full recovery of the horizontal and vertical circuits before allowing another display scan to be started.

The slow ramp is, also, fed to an attenuator which reduces its amplitude by a factor of 1 to 500, in a 1,2,5 sequence determined by the time/division setting. The attenuated ramp is then inverted, producing a negative going ramp. The DC content of the inverted ramp is adjusted by the inverter output control circuit before it is led to the strobe comparator.

B.5.4. Strobe Comparator

The negative-going fast ramp is compared to the attenuated and inverted slow ramp at the strobe comparator. When the fast ramp's voltage falls below that of the inverted slow ramp (point $t_{1,n}$, in Figure B.4), the strobe comparator produces an output which causes the strobe driver to produce a fast pulse which is used (after shape standardization) as a sampling command pulse to actuate the strobe generator of the sampling head, and, also, as an input for the memory gate driver which generates the memory gating pulse.

It is important to note that for a full scan of the display, only one slow ramp is generated while the number of fast ramps generated is equal to the number of displayed samples. This is the heart of the

technique used to generate strobe pulses that are slewed by a time interval which can be as small as a fraction of a picosecond. Every new fast ramp reaches the negative level of the slow ramp at a later instant of time compared to the one before. This is due to the fact that the slow ramp had fallen further before the new fast ramp could intersect it. The voltage by which the slow ramp changes between two consecutive fast ramp intersections determines the sampling interval (ΔT) which is depicted in Figure B.5. The more the slow ramp is attenuated, the smaller the time ΔT becomes.

The location of the attenuated and inverted slow ramp's full voltage swing, relative to the fast ramp, determines which part of the probed signal is being looked at through the display's time window. This location can be changed by altering the DC content of the slow ramp and this is achieved by turning the time/distance knob.

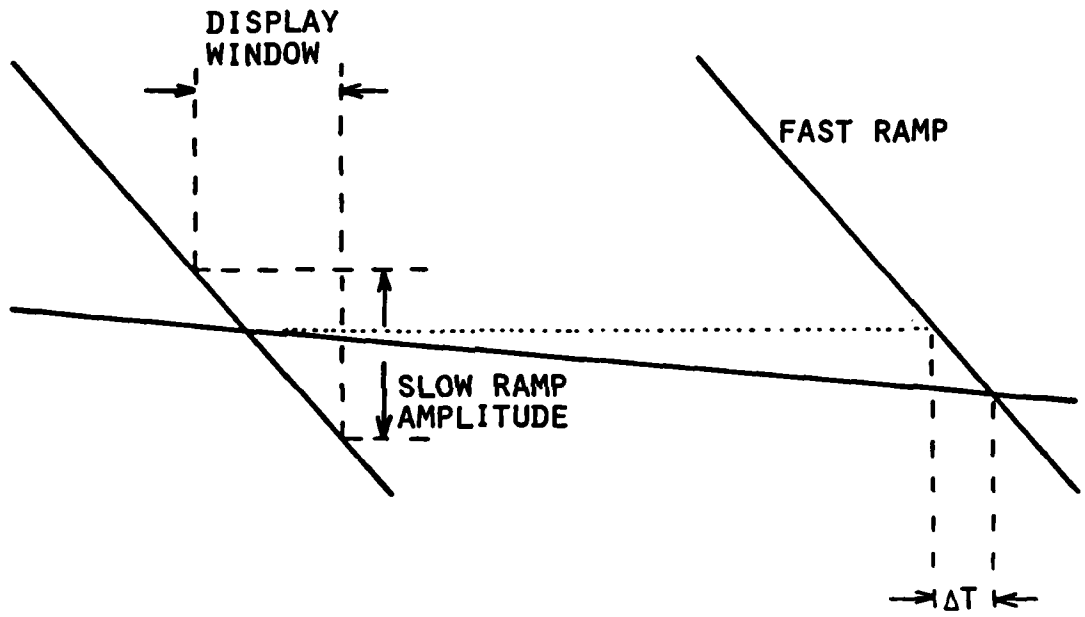

Figure B.5. The time interval between two strobe pulses generated by comparing the fast ramp with the inverted and attenuated slow ramp. (ΔT is exaggerated for clarity).

APPENDIX C

A NOTE ON RANDOM ERRORS IN SAMPLING SYSTEMS

C.1. Introduction

Among the different types of errors in sampling measurements [15], [17] random errors cause the values of the quantities being measured to fluctuate randomly around certain means. Random errors can be subdivided into V (voltage)-axis, and T (time)-axis errors. Fortunately these types of errors represent stationary random processes most of the time, and this facilitates their removal or minimization.

C.2. V-Axis Random Errors

These errors are due to noise superimposed on sample values. When the noise probability distribution function (PDF) has a mean of zero, V-axis random errors can be reduced by acquiring a large number of waveforms, adding them all together, and then dividing by the number of added waveforms. This process is called Additive Signal Averaging, and it takes advantage of the fact that as waveforms are added to each other the random noise tends to cancel out while the signal content is being reinforced. This is expressed by the following formula [15]

$$\lim_{N\to\infty} \left\{ \frac{1}{N} \sum_{j=1}^{N} \left(v_{signal}(t) + v^{j}_{noise}(t) \right) \right\} = v_{signal}(t) \qquad (C.1)$$

$v_{noise}(t)$ is the noise voltage associated with the sample at instant t of the jth acquired waveform, and N is the nubmer of waveforms to be averaged and which is finite in practical cases. This technique improves the signal to noise ratio in proportion to $\sqrt{N}$.

C.3. T-Axis Random Errors

These errors cause the horizontal location of samples to be displaced from their true position in a random fashion. This is especially significant on non-flat parts of acquired waveforms, such as seen in Figure 3.2c. The main cause of these errors is time jitter between a reference point on the sampled pulse and the strobe signal which opens the sampling gate. This jitter is introduced at several locations in a test system, and for our purposes they can be categorized into three sources of jitter. First there is jitter between the trigger pulse and the test pulse at the pulse generator output. Second, jitter is introduced by the sampling scope circuits specialized in recognizing the trigger pulse. The third source of jitter is that between the output of the trigger recognizer and the strobe pulse, this is produced by the scope's horizontal channel electronics, and this is where the fiber optic laser link which delivers the sampling command to the sampling head is introduced.

While additive signal averaging can be used to remove V-axis noise and yield a waveform which can be made arbitrarily close to the ideal noise free waveform, it causes distortion when used in the presence of time jitter.

In a numerical experiment performed by the author, an ideal step "A" of 128 sample points (see Fig. C.1) was time jittered by producing an array "B" whose 128 elements would have a one-to-one correspondence to the elements of A, except for the adding to the index numbers of the B

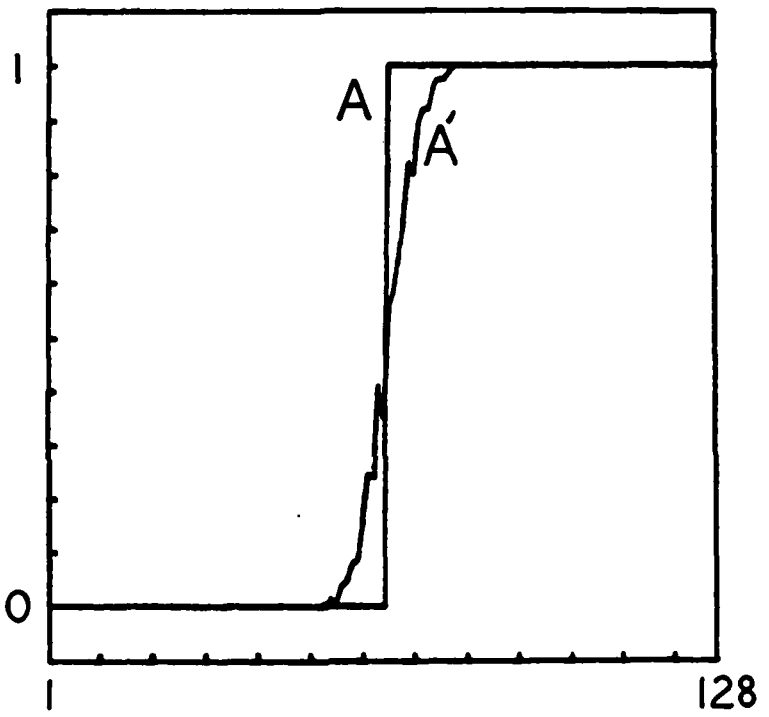

Figure C.1. The result (waveform A') of signal averaging a finite number of acquisitions of an ideal step (waveform A) in the presence of normally distributed random horizontal jitter.

array elments of small randomly generated integers causing the element B(100), for example, to be assigned the value of A(107) instead of A(100). The random integer generator was chosen to have a probability distribution function which is approximately "Gaussian with a mean of zero, and standard deviation of 5." Two hundred such B waveforms were generated, and additive signal averaging was performed, the resulting waveform "A'" is shown superimposed on A. From this it can be seen that the corners of A have been smoothed out, and that "wiggles" have been introduced into the rising edge of the waveform. The wiggles in A' are due to the finite number of averaged waveforms.

Gans [15] (see also [17]) has shown that the effect of additive signal averaging in the limit of an infinite number of acquisitions ($N \to \infty$), and in the presence of normally distributed time jitter, is that of introducing to the system a lowpass filter whose time domain impulse response is a Gaussian function of the form

$$g(t) = K \, EXP \left[- \frac{1}{2} \left(\frac{t}{\sigma_t} \right)^2 \right] \qquad (C.2)$$

where K is a real constant, and σ_t is the standard deviation of the time jitter in the sampling strobe. In arriving at equation C.2 Gans has shown that C.2 is also the PDF of the sampling strobe time jitter.

In the frequency domain, taking the Fourier tranform of C.2 gives for the frequency domain transfer function of the filter:

$$G(f) = C \text{ EXP } \left[-\frac{1}{2} \left(\frac{f}{\sigma_f} \right)^2 \right] \qquad (C.3)$$

where

$$C = K \sigma_t \sqrt{2\pi}$$

and

$$\sigma_f = \frac{1}{2\pi\sigma_t} \qquad (C.4)$$

Hence, normally distributed time jitter in the sample locations has the effect of filtering an additively averaged pulse with a Gaussian lowpass filter which affects the amplitude of the frequency components of the pulse, but leaves their phase intact.

REFERENCES

[1] Holbrook, Lynn R., "An Optically Coupled Sampling System for Transient Electromagnetic Measurements", M.S. Thesis, University of Kentucky, Lexington, KY, 1982.
Also available under the same title as: "Electromagnetics Research Report 82-3", University of Kentucky, Dec. 1982.

[2] Lawton et al., "Waveform Sampler", United States Patent 4,030,840,June 21, 1977.

[3] Lawton, Robert A. and Andrews, James, R., "Optically Strobed Sampling Oscilloscope", IEEE Transactions on Instrumentation and Measurement, Vol. 25, No. 1, March 1976.

[4] Andrews, James R. and Lawton, Robert A., "Electrically Strobed Optical Waveform Sampling Oscilloscope", Review of Scientific Instruments, Vol. 47, No. 3, March 1976.

[5] Tektronix, Inc., Sampling Oscilloscope Circuits, Beaverton, OR, 1970.

[6] Tektronix, Inc., 7S12 TDR/Sampler, Instruction Manual, Beaverton, OR, 1971.

[7] Burr-Brown, Product Data Book, Box 11400, Tucson, Az., 1982.

[8] Thomas, S.W. and Coleman, L.W., "Laser-Triggered Avalanche - Transistor Voltage Generator for a Picosecond Streak Camera", Applied Physics Letters, Vol. 20, No.2, Jan. 1972.

[9] Sze, S.M., Physics of Semiconductor Devices, New York: John Wiley & Sons, Inc., 2nd. ed., 1981.

[10] Millman, Jacob and Taub, Herbert, Pulse Digital and Switching Waveforms, New York: McGraw-Hill, Inc., 1965.

[11] Oppenheim, Alan V. and Schafer Ronald, W., Digital Signal Processing, Englewood Cliffs, NJ: Prentice-Hall, Inc., 1975.

[12] Tektronix, Inc., The FFT Fundamentals and Concepts, Instruction Manual, Beaverton, OR, 1970.

[13] Gans, William L. and Nahman, Norris S., "Continuous and Discrete Fourier Transforms of Steplike Waveforms", IEEE Transactions on Instrumentation and Measurement, Vol. 31, No.2, June 1982.

[14] Tektronix, Inc., 4050 Series R08, Signal Processing ROM Pack No. 2 (FFT), Instruction Manual, Beaverton, OR, June 1979, revised 1982.

[15] Gans, William L., "A Time Domain Automatic Network Analyzer for Microwave Measurements", M.S. Thesis, University of Colorado, Boulder, CO, Spring 1975.

[16] Tektronix, Inc., S-6 Sampling Head, Instruction Manual, Beaverton, OR, 1971.

[17] Gans, William L. and Andrews, James R., "Time Domain Automatic Network Analyzer for Measurement of RF and Microwave Components", NBS Tech. Note 672, Sept. 1975.


FILM